The physics of photoconductive spark gap switching : pushing the frontiers

Please check the document version of this publication:

• A submitted manuscript is the version of the article upon submission and before peer-review. There can be important differences between the submitted version and the official published version of record. People interested in the research are advised to contact the author for the final version of the publication, or visit the DOI to the publisher's website.
• The final author version and the galley proof are versions of the publication after peer review.
• The final published version features the final layout of the paper including the volume, issue and page numbers.

Link to publication

The physics of photoconductive spark gap switching: Pushing the frontiers

PROEFSCHRIFT

ter verkrijging van de graad van doctor
aan de Technische Universiteit Eindhoven,
op gezag van de Rector Magnificus, prof.dr.ir. C.J. van Duijn,
voor een commissie aangewezen door het College voor Promoties
in het openbaar te verdedigen
op maandag 3 juli 2006 om 16.00 uur

door

Jimi Hendriks

geboren te Hoensbroek

Dit proefschrift is goedgekeurd door de promotoren:

prof.dr. M.J. van der Wiel
en
prof.dr.ir. J.H. Blom

Copromotor:
dr.ir. G.J.H. Brussaard

Contents

Chapter 1

Introduction

This thesis describes the development of a photoconductively switched atmospheric gas-filled high-voltage spark gap in the framework of a Technology Foundation program to develop a compact, MV short-pulse transformer and use it to develop a novel compact electron accelerator and its diagnostics.

1.1   History

Breakdown in the form of lightning has fascinated mankind all through history. Actual research on breakdown has been done since electricity was discovered. With the work of Paschen and Townsend at the end of the 19th century, beginning 20th century (sponteneaous) breakdown became a fairly well-understood phenomenon. Paschen described the relationship between breakdown voltage, pressure and dimensions of the breakdown medium and Townsend described breakdown in a low-pressure environment as an ionization process caused by avalanches of electrons. From about 1940 deviations from Townsend's theory were seen in high (atmospheric) pressure experiments. Breakdown occurred much faster than could be deduced from Townsend's avalanche theory. Streamers were discovered and the fundamentals for the theory of breakdown by streamers were developed by Loeb, Meek and Raether [1–3].

The introduction of the laser, especially the high-power Q-switched laser, has rapidly increased the interest in breakdown research. By simply focusing the laser beam a spark in air could be made. It did not take long before the influence of the laser on a high-voltage environment was tested. This research field expanded by the military demand for fast switching of high voltages. These fast switched high-voltage pulses were used to simulate the EMC-effects of nuclear explosions and for (broadband) radar purposes. Pendleton and Guenther [4] were among the first to implement a laser in a spark-gap setup. The laser-triggered spark gap was able to switch high currents and high voltages with nanosecond precision. The laser did not only cause the breakdown to occur faster than spontaneous breakdown, it seemed also possible to use the laser to trigger an under-volted spark gap to switch voltages below the self-breakdown voltage of the gap. In many different laboratories different spark gap geometries and positions and energies of the laser focus were investigated and all kinds of gases and liquids were inserted in the spark gaps. A good review of these research activities up to 1978 is given by Guenther and Bettis [5]. First measurements were done in a simple (two sphere) spark gap that was triggered by a perpendicular incident laser. Voltages up to 100 kV were switched and the effects of different gases as switching medium were investigated. Later the spark gaps became more complicated in structure and spark gaps were developed that were able to switch Megavolts. When new lasers were developed (CO2, UV, Nd:YAG, Ti:Sapphire etc.), they were also tried in spark gaps [6–9]. Detailed studies of the switching plasma were made [10–12] in order to get a better understanding of the switching process.

With the availability of short-pulse lasers (ps-range) a different field, that of optoelectronic switching, took a flight. By using a short pulse laser, it was now possible to create enough charge carriers in a high resistance semiconductor to produce a conductivity of quasimetal-

lic properties. In 1975, Auston [13] made the first photoconductive switch by inserting a silicon substrate in a transmission line structure. By the absorption of a picosecond optical pulse with an energy of a few microjoules, he was able to open and close the switch in a few picoseconds and switch voltages up to 100 V. Adjusting the switch for high-voltage switching purposes led to the photoconductive switching of 1.5 kV with a rise time of approximately 25 ps [14]. Besides silicon, GaAs was under investigation as switching medium. Lee used GaAs to switch 5 kV with a repetition rate of 1 GHz [15] and Mourou and Knox were able to switch voltages up to 8 kV within 40 ps [16]. Recently Loubriel et al. described switching of voltages up to 100 kV with both Si and GaAs switches [17].

1.2   Switching

Different types of closing switches are available for high-voltage switching, like thyratrons, thyristors, transistors, photoconductive semiconductor switches and spark gap switches, either gas or liquid-filled [18]. Irrespective of the type of switch, there are three important parameters when switching high voltages: The amplitude (voltage and/or current) of the switched pulse, the rise time of the switched pulse and the shot-to-shot time stability (time jitter) of the switched pulses. The trend in high-voltage switching is towards switching even higher voltages (and currents) in even shorter times with, preferably, no time jitter. Despite the broad diversity of high-voltage switches, no switch is able yet to push all three parameters. Switches for high voltages and high currents, like laser-triggered spark gaps, are relatively slow and the time jitter is high. For semiconductor photoconductive switches, which are fast and have very little time jitter, the voltages to be switched are limited due to the probability of damaging the switch. Our goal is to develop a switch that combines the benefits of the gas-filled laser-triggered spark gap and the semiconductor photoconductive switch to be able to switch high voltages and high currents very fast (on a ps timescale) with minimal jitter.

1.2.1   Semiconductor photoconductive switch

A semiconductor photoconductive switch consists of two conductors which are separated by a high resistive semiconductor material (Si, GaAs) (figure 1.1). When one conductor is charged, a short-pulsed (ps) laser is used to illuminate the semiconductor completely. When the gap is illuminated, charge carriers (electron-hole pairs) are created nearly instantaneously (on a fs time scale), making the semiconductor material conducting. A current can now start to run, also on the time scale of the laser pulse, from the charged conductor through the semiconductor material to the other conductor.
Depending on the type of semiconductor material, there are two switching modes for semiconductor switches, which depend on the electric field over the medium. The linear mode
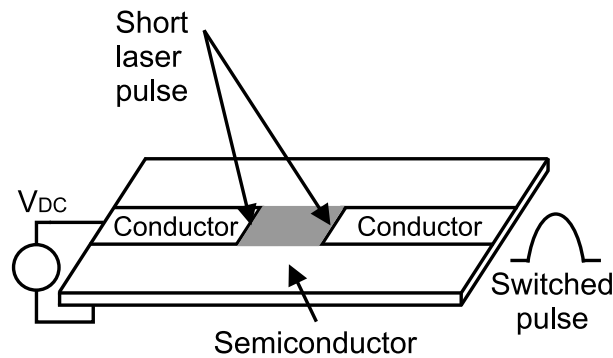
Figure 1.1. *Schematic semiconductor photoconductive switch in a stripline configuration.*

(at relatively low electric fields), where one photon creates one electron-hole pair and the high gain mode (at relatively high electric fields), where a carrier avalanche develops in the semiconductor material after triggering [17, 19, 20].

In the linear mode, the switching process (and thus the switched pulse) is fully controlled by the laser only. When the laser illumination stops, the charge carrier development stops immediately and the recombination time of these charge carriers determines the opening time of the switch. The laser pulse determines the rise time of the output pulse which is limited by the geometry of the switch (see chapter 7). Due to the lack of stochastical switching-processes, the time jitter of the switched pulse is determined by the time jitter of the laser pulse. A drawback of this linear mode is that it requires an impractical amount of laser power when the system is scaled up to higher switching voltages.

A benefit of the high gain mode is that the carrier multiplication lowers the required laser power (5 orders of magnitude are reported [17]) and the rise time is significantly better than in the linear mode. However, this (stochastic) carrier avalanche introduces extra time jitter and also takes away the full control over the switched pulse.

The combination of highest possible voltage and current, fastest possible rise time and minimal time jitter demands a trade-off. The highest voltages can be switched with large switches in the high gain mode. The larger the switch, the slower the rise time and the more jitter. Low jitter means a small switch which is not able to hold off large voltages and conduct large currents. For reasons to be explained in section 1.3, we are interested in picosecond switching with low jitter (less than a ps). In semiconductor switching the voltage amplitude will then be relatively low. To our knowledge the fastest switch was developed by Motet et al. who used GaAs and a femtosecond dye laser to generate 825 V pulses with 1.4 ps rise time [21]. In conclusion, semiconductor photoconductive switches are fast (ps) switches that can create pulses with low time jitter, but the voltage and current that can be switched is limited.

1.2.2 Gas-filled laser-triggered spark gap switch

Spark gap switches, either gas or liquid-filled, are mainly used for creating high-power, high-voltage pulses. Commonly they consist of a coaxial inner and outer conductor (figure 1.2). The inner conductor is interrupted by a spark gap which is filled with an insulating liquid or gas. After one half of the inner conductor has been charged to the self-breakdown voltage of the gap and, subsequently, an arc has developed between the two conductors, a current can start to run, resulting in a switched high-voltage pulse.
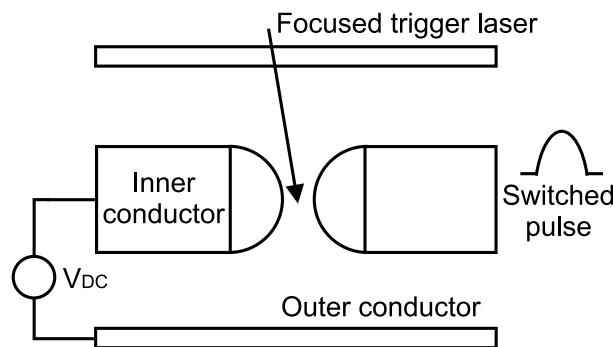
Figure 1.2. *Schematic (cylinder symmetric) coaxial laser-triggered spark gap.*

The benefit of these gas and liquid-filled switches is that they can quickly recover from breakdown. Recombination and diffusion processes will quickly restore the switching medium. Because the switching itself is based on breakdown of the medium, much higher currents can be switched compared to the semiconductor switch where breakdown has to be avoided. A drawback of these spark gap switches is their shot-to-shot timing-instability (jitter). This jitter can be significant, making spark gaps not suitable for accurate timing and synchronization purposes. The large time jitter originates from the stochastic processes that cause the actual breakdown of the spark gap: When an electric field is applied over a gap, at some point in time a free electron will be created (due to (cosmic) background radiation). This free electron is accelerated by the applied electric field, gains energy and, eventually, hits an atom. When the energy of the accelerated electron is high enough, this atom will be ionized and another free electron is created. The two electrons will be accelerated again, additional ionization will take place and this way an electron avalanche in created. Finally, via this avalanche and the additional process of streamer formation a conducting (arc) channel will be formed, spanning the complete gap between the electrodes (a streamer is a narrow filamentary plasma, driven by highly non-linear space charge waves [1]). This breakdown process is a stochastic process. The creation of the first free electrons is stochastic and also the electron avalanche-formation has a stochastic nature, causing the large shot-to-shot time instability and also limiting the rise time of the switched pulse [22]. The time jitter can be reduced if a laser is used to trigger the spark gap. By focusing a

laser in the gap or on one of the electrodes, the first free electrons are created at a well defined time, limiting the stochastic nature of the breakdown process. An even better time stability can be reached if a laser is focused axially into the gap, through one of the conductors. This way, the laser creates some ionization along its entrance axis, predefining a path on which the avalanche and streamer formation process takes place. The result is that the actual breakdown process occurs faster and at a better defined time. The more powerful the laser is, the more free electrons are created initially and the better the timing of the switched pulse will be. The most time-stable switch reported is a Ti:Sapphire laser triggered spark gap. Pulses of 10 kV have been made with sub-ns rise time and 35 ps time jitter [9]. In conclusion, the gas or liquid-filled laser-triggered spark gap is able to switch high power pulses. However, the nature of the breakdown process is stochastic, resulting in a relatively large time jitter. Also the rise time of the switched pulse is relatively large.

1.2.3 Photoconductive switching of an atmospheric gas-filled spark gap

The goal for this PhD project was to develop a switch that is able to make high-voltage pulses (>1 kV and ultimately 2 MV) with ps rise time and (sub-)ps time jitter. The above described switches meet these requirements only partially. We designed a new switch that combines the best of these two switching regimes, photoconductive switching of semiconductors and laser triggering of a high-voltage spark gap. A high-intensity femtosecond Ti:Sapphire laser is used in a gas-filled spark gap. But instead of focusing the laser to a point, we used two cylindrical lenses to create a focus that spans the complete gap. If the laser intensity is high enough, a slab of plasma is formed in the gap, connecting the two conductors. When sufficiently ionized (either by multiphoton or tunneling ionization), this plasma closes the switch, ideally on a femtosecond time scale, comparable to the time scale of photoconductive switching of semiconductor switches. Stochastic breakdown processes like avalanche and streamer formation that cause the breakdown in laser-triggered spark gaps are passed over, which results in a faster rise time and less jitter. On the other hand, it is possible to switch large currents, because gas is the switching medium in our photoconductive switch.

1.3 Applications

High-voltage pulses are used for many applications, for instance extreme ultraviolet light sources, radar technology, nuclear fusion experiments and polluted-gas-treatment. Ultrashort (photoconductively switched) high-voltage pulses with picosecond rise time and time stability will improve synchronization between different high-voltage parts of a setup.

Present applications for high-voltage pulses can be extended and new applications will become feasible. One of the possible new applications is to couple photoconductively switched picosecond high-voltage pulses into an antenna structure to create broadband high-intensity TeraHertz (THz) radiation. Imaging with such 'T-rays' can be a harmless alternative for X-rays for a number of medical and security purposes [23]. Opto-electronic detection of broadband THz-pulses transmitted through a medium enables the determination of the full complex dielectric constant of materials in a frequency range where most chemical compounds show very strong, highly specific frequency-dependent absorption and dispersion. This way, imaging of the chemical composition of unknown objects should become possible, with a spatial resolution of a few tens of microns. Currently, the most intense THz-source is based on optical rectification of femtosecond laser pulses on a semiconductor surface. The THz-intensity that can be generated using MV pulses exceeds that of the laser option by at least a factor of ten.

Another interesting application will be in the field of bioelectrics, where the possibility to control functions and membrane transport processes in biological cells by external pulsed electric fields is investigated (electroporation) [24]. Biomedical material is exposed to short-pulsed, high field strengths that are now limited to the nanosecond time-regime. The availability of ultrashort (ps) high-voltage pulses can extend this research to the regime of higher field-strengths and shorter pulses.

We plan to use ultrashort high-voltage pulses for making compact pulsed DC electron accelerators [25]. This accelerator has to be able to create ultrashort (100 fs) high brightness electron bunches, which are short enough to be used in externally injected laser wakefield accelerators [26]. The creation of very short high-brightness relativistic electron bunches is limited by internal Coulomb forces. Phase-space density is rapidly reduced in the initial acceleration process due to the space-charge explosion. This space-charge explosion can be limited if the distance over which the electrons are accelerated to relativistic energies (~ 10 MeV) is made shorter. State-of-the-art RF injectors are limited to acceleration gradients of approximately 100 MV/m due to vacuum breakdown. Higher gradients can be achieved by applying very short high-voltage pulses in a diode configuration [27]. The target is to produce 10 MeV high-brightness bunches in a compact accelerator. A "table top" 2 MV pulser is operational [28] and can create acceleration gradients of 1 GV/m in a diode of 2 mm. However, the jitter problem in this pulser is still unsolved. In order to accelerate up to 10 MeV, stacking of multiple, rapidly switchable acceleration stages is required. In order to keep the average acceleration field high, the distance between the stacked acceleration stages should not be more than a few mm. High-voltage switching within only a few picoseconds is then required.

1.4   Scope of this thesis

The basis of this thesis consists of published articles on both experimental work and simulations. By way of introduction, the history of switching, for this work two relevant existing switches and the new photoconductive switching principle are treated in **Chapter 1**. Also possible applications for the new photoconductive switch are highlighted. Subsequently, **Chapter 2** describes the different parts of the experimental setup and their characteristics in detail. In **Chapter 3** the first switching experiments are described showing that photoconductive switching in atmospheric air en nitrogen is possible and more elaborate switching experiments, with emphasis on the voltage range, are treated in **Chapter 4**. In **Chapter 5** the feasibility of two diagnostics, one for monitoring the switching plasma and the other for resolving the switched high-voltage pulse with sufficient time resolution is investigated. Together with the results of one of these diagnostics, we describe in **Chapter 6** two possible causes for the observed voltage drop over the gap when lower voltages are switched. To get more insight in the electrodynamic behavior of the spark gap setup and because the measurements of chapter 3 and chapter 4 were limited by the time resolution of the oscilloscope, an electrodynamic model is developed in **Chapter 7**. To improve the pulse shape of the switch, optimization of the switch-geometry is necessary. An optimization procedure, based on the electrodynamic model of chapter 7, is described in **Chapter 8**. In **Chapter 9** the main conclusions are summarized and discussed in general and an outlook for future research is given.

References

[1] Y.P. Raizer, Gas discharge physics, Springer, Berlin (1991)

[2] J.M. Meek and J.D. Craggs, Electrical breakdown of gases, John Wiley and Sons, Chichester (1978)

[3] E.M. van Veldhuizen, Electrical discharges for environmental purposes, fundamentals and applications, Nova Science Publishers, Huntington (2000)

[4] W.K. Pendleton and A.H. Guenther, Rev. Sci. Instrum., 36 (11) p. 1546 (1965)

[5] A.H. Guenther and J.R. Bettis, J. Phys. D, 11 (11) p. 1577 (1978)

[6] J.R. Woodworth, P.J. Hargis, Jr., L.C. Pitchford and R.A. Hamil, J. Appl. Phys. 56, 1382 (1984).

[7] L. Ya. Polonskiy, A. Yu. Goltsov and A.V. Morozov, Phys. Plasmas, 3, 2781 (1996)

[8] S. Soubacq, P. Pignolet and S. Mendonca, J. Phys. D, 35, 1955 (2002)

[9] B.M. Luther, L. Furfaro, A. Klix and J.J. Rocca, Appl. Phys. Lett., 79 (20) p. 3248 (2001)

[10] R.A. Dougal and P.F. Williams, J. Phys. D., 17, 903 (1984)

[11] W.D. Kimura, M.J. Kushner, E.A. Crawford and S.R. Byron, IEEE Trans. Plasma Sci., 14, 246 (1986)

[12] R. Najafzadeh, E.E. Bergmann and R.J. Emrich, J. Appl. Phys., 62, 2261 (1987)

[13] D.H. Auston, Appl. Phys. Lett., 26 (3) 101 (1975)

[14] P. LeFur and D.H. Auston, Appl. Phys. Lett., 28 (1) 21 (1976)

[15] C.H. Lee, Appl. Phys. Lett., 30 (2) 84 (1977)

[16] G. Mourou and W. Knox, Appl. Phys. Lett., 35 (7) 492 (1979)

[17] G.M. Loubriel, F.J. Zutavern, A.G. Baca, H.P. Hjalmarson, T.A. Plut, W.D. Helgeson, M.W. O'Malley, M.H. Ruebush and D.J. Brown, IEEE Trans. Plasma Sci., 25 (2) 124 (1997) and references herein

[18] T.R. Burkes, J.P. Craig, M.O. Hagler, M. Kristiansen and W.M. Portnoy, IEEE Trans. Electron Devices, 26 (10) 1401 (1979)

[19] M.S. Mazzola, K.H. Schoenbach, V.K. Lakdawala, R. Germer, G.M. Loubriel and F.J. Zutavern, Appl. Phys. Lett., 54 (8) 742 (1989)

[20] F.J. Zutavern, G.M. Loubriel, M.W. O'Malley, L.P. Shanwald, W.D. Helgeson, D.L. McLaughlin and B.B. McKenzie, IEEE Trans. on Elec. Devices, 37 (12) 2472 (1990)

[21] T. Motet, J. Nees, S. Williamson and G. Mourou, Appl. Phys. Lett., 59 (12) 1455 (1991)

[22] J.M. Lehr, C.E. Baum, W.D. Prather and R.J. Torres in ultra-wideband, short pulse electromagnetics 4, E. Heyman, Ed. New York: Kluwer Academic/Plenum Publishers, p. 11. (1999)

[23] News feature, Nature 424, 721 (2003)

[24] K.H. Schoenbach, S. Katsuki, R.H. Stark, E.S. Buescher and S.J. Beebe, IEEE Trans. Plasma Sci., 30 (1) 293 (2002)

[25] S.B. van der Geer, M.J. de Loos, G.J.H. Brussaard, O.J. Luiten and M.J. van der Wiel, Proc. Eur. Particle Accelerator Conf. Paris, France, June 3-7, 2002, 989 (2002)

[26] E. Esarey, P. Sprangle, J. Krall and A. Ting, IEEE Trans. Plasma Sci., 24 (2) 252 (1996)

[27] T. Srinivasan-Rao and J. Smedley, Proc. 7th Advanced Accelerator Concepts Workshop, Lake Tahoe, CA (1996)

[28] G.J.H. Brussaard and D.A. Vyuga, IEEE Trans. Plasma Sci., 32 (5) 1993 (2004)

Chapter 2

Experimental setup

This chapter describes the experimental photoconductive switching setup. Figure 2.1 gives a schematic overview. The setup consists of a high-voltage source connected to a spark gap, a Ti:Sapphire laser system with cylindrical lenses to create the switching plasma, and diagnostics to analyze the switched high-voltage pulses. The whole system fits on two optical tables (1.5 x 3 m, each) in a laser-laboratory which is temperature controlled to half a degree (21.0±0.5).
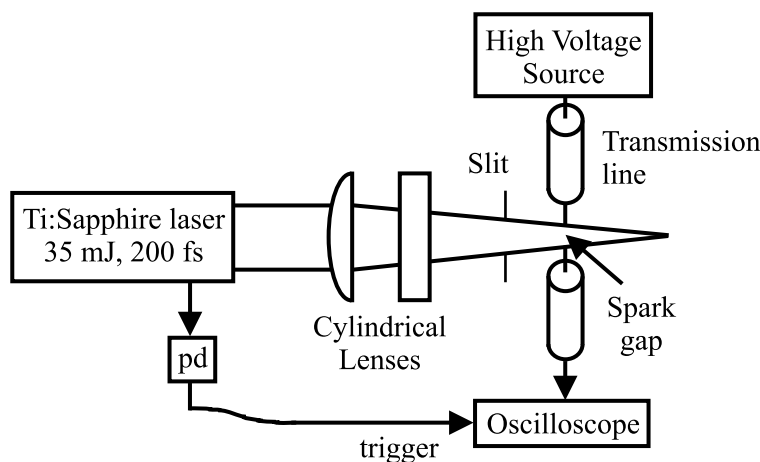
Figure 2.1. *Schematic overview of the experimental setup (pd = photo diode).*

2.1   Laser setup

Photoconductive switching of a gas-filled spark gap requires far greater laser intensity than photoconductive switching of semiconductors. Throughout the gap the laser intensity needs to be high enough to create a plasma over the complete distance between the electrodes.

This plasma has to be sufficiently ionized to pass over stochastical breakdown processes. For a gas-filled gap the intensity has to be above the threshold for tunneling ionization, around 10^{18} Wm^{-2} for most gases [1, 2]. Subsequently, this ionization has to occur on a time scale much smaller than the target for the rise time of the switched high-voltage pulse. A high-power femtosecond Ti:Sapphire laser fulfills both these requirements. Our Ti:Sapphire laser system consists of three parts, a mode-locked Ti:Sapphire laser oscillator and two chirped pulse amplifiers (CPA), producing 200 fs laser pulses with an energy of 35 mJ ($\sim$0.2 TW) at a repetition frequency of 10 Hz.

2.1.1   Oscillator

Short laser pulses are created in an oscillator. In the oscillator, a gain medium is placed in an optical cavity. To be able to produce short pulses (instead of a continuous signal), the oscillator has to be mode-locked (also called phase-locked). At mode-locking, several longitudinal cavity modes with a different frequency oscillate in phase in the cavity. The resulting intensity output is one of repetitive pulses. The frequency of the output signal (the distance between two pulses) depends linearly on the cavity length. The minimum achievable pulse length of a mode-locked pulse is as short as the reciprocal of the bandwidth of the gain medium. This means that the larger the gain medium bandwidth, the shorter the mode-locked pulse can be [3–5].

Titanium doped Sapphire (Al_2O_3) is a solid-state laser material with a broad gain bandwidth (700-1100 nm), a high thermal conductivity and a high energy storage density. When it is placed in an optical cavity and pumped with a high-power laser ($\sim$ 5 W) self-focusing of the emitted broadband light occurs in the Ti:Sapphire. There is an intensity dependent change of the refractive index in the material due to the third order non-linear Kerr effect. This means that the (high-intensity) center of the Gaussian beam is focused more than the (lower-intensity) outer parts. Due to this slight path-length change, a more favorable pulsed mode will dominate over the cw mode and the laser will be mode-locked. This is called passive Kerr lens mode-locking. Now a broadband pulse travels up and down the cavity. One of the end-mirrors is not fully reflective, so every time the pulse arrives at this mirror, a small part of the pulse is transmitted. This transmitted pulse is the output pulse. It's repetition frequency is determined by the cavity length.

A scheme of our mode-locked Ti:Sapphire oscillator (Femtolasers GmbH) is given in figure 2.2. The Ti:Sapphire crystal is placed at the Brewster angle and is cooled by a Peltier element. The crystal is pumped by a frequency doubled Nd:Vanadate (YVO_4) laser at a wavelength of 532 nm (Verdi diode laser, Coherent, Inc.) The pump power is 5 W. Two curved mirrors are used to focus the emitted light in the crystal to stimulate Kerr lensing.
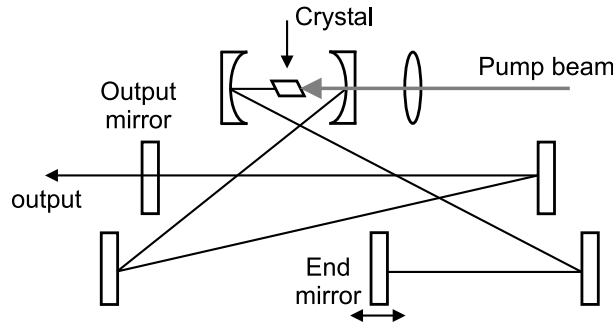
Figure 2.2. *Schematic layout of the Ti:Sapphire oscillator.*

Chirped multilayer dielectric mirrors [6, 7] are used to control dispersion to optimize the shortness of the output pulses. The end-mirror can be shifted in order to adjust the length of the optical cavity and (slightly) change the output frequency. The mode-locked Ti:Sapphire laser oscillator produces broadband laser pulses with an energy of 5 nJ and a duration of 15 fs at a central wavelength of 790 nm ($\Delta\lambda \simeq 116$ nm FWHM). The repetition frequency is 75 MHz.

2.1.2   Amplifiers

After generation of the ultrashort pulses in the oscillator, the pulses have to be amplified. These ultrashort pulses can not be amplified straightforwardly, because the intensities would quickly become much higher than the damage threshold of the amplifying medium. Mourou et al. [8–10] used Chirped Pulse Amplification (CPA) to amplify short pulses to high energies via the scheme of pulse-stretching, amplifying and pulse compression (figure 2.3). First the broadband ultrashort pulse is stretched in time such that the different frequency components are spatially spread out. This way the high-frequency components will precede the low-frequency components in time, increasing the pulse length (chirp). Pulse stretching can be done in several ways. We use both a dispersive medium (glass in CPA 1) and a grating (in CPA 2) for pulse stretching. Amplification of a stretched Ti:Sapphire laser pulse is done by using another Ti:Sapphire crystal. This crystal is pumped by a green pumping laser and its energy is taken out by the stretched pulse that is led through the pumped crystal. We chose a multipass amplifier instead of the more commonly used regenerative amplifier. In a multipass amplifier, the short pulse passes only a few times through the gain medium, which makes it more suitable for keeping the pulses short (less dispersion by the crystal), although a regenerative amplifier is more efficient in amplifying [4]. Finally, the stretched and amplified pulse has to be compressed again. This is the opposite process of stretching; all the different frequencies have to be squeezed back to each other again and possible extra dispersion (introduced by the amplifying crystal) has

to be compensated. This is mostly done by prisms or, when the intensities become too high, by gratings.
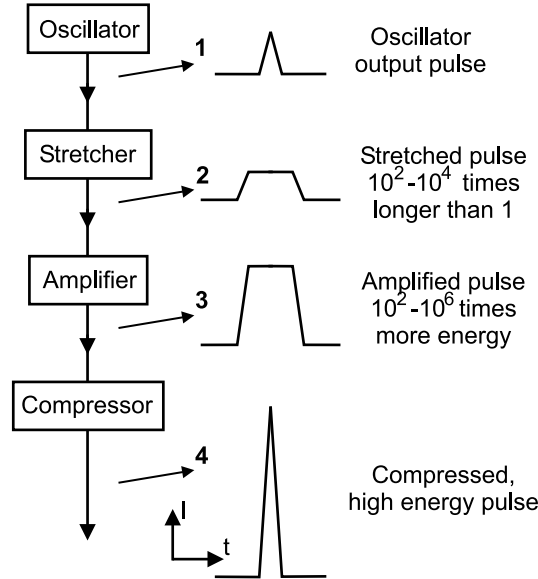
Figure 2.3. *Scheme of Chirped Pulse Amplification. I = intensity, t = time*

In our setup, we have two CPA units behind the oscillator.

The first CPA (CPA 1) is a commercially bought CPA-unit (Omega Pro, Femtolasers Produktions GmbH). It uses 10 cm of glass as (dispersive) stretcher, which stretches the pulse up to 2 ps. This stretched pulse is led through the Ti:Sapphire amplifying crystal. It is pumped by a Nd:YLF laser (621-D, B.M. industries) with an energy of 8 mJ (527 nm) at a repetition rate of 1 kHz. After 4 passes, a Pockel's cell selects from the 75 MHz pulses the most amplified pulse every ms (1 kHz) and these pulses are amplified further in the last 5 passes up to an energy of 1 mJ per pulse. The Pockel's cell can also be used for a 10 Hz selection rate. After amplifying, the pulses are compressed by a prism-compressor down to 25 fs. The total energy per pulse is thus 40 GW.

The output laser light is now split into two parts: the major part is coupled out for other purposes and the remaining light is led into the second, home-built, CPA (CPA 2, see figure 2.4). This second CPA-unit works at 10 Hz. The pulse is first stretched by a grating-based stretcher to a pulse length of about 200 ps and send through a 5 pass amplifier. A Nd:YAG laser (Thales SAGA 230/10) with a pulse-energy of 150 mJ at a wavelength of 532 nm (10 Hz) pumps another Ti:Sapphire crystal. After five amplification passes, pulses of 35 mJ come out of the crystal. The amplified pulse is compressed again down to 200 fs by a grating based compressor. The total energy per pulse is about 0.2 TW at a repetition rate of 10 Hz. Table 2.1 summarizes the properties of each part of the laser system.
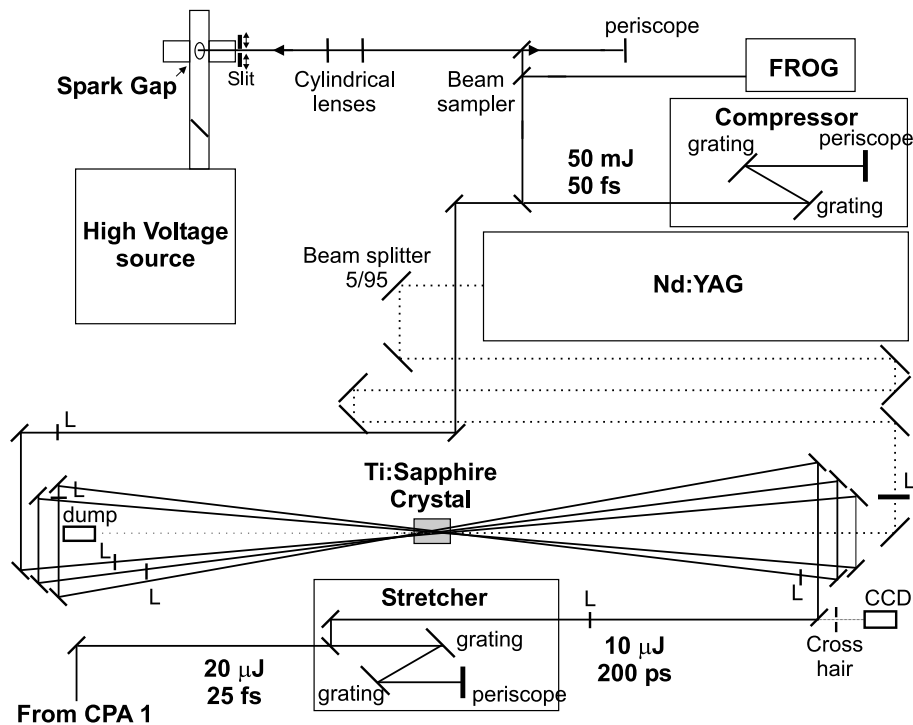
Figure 2.4. *Scheme of the second, home-built CPA unit (CPA 2) The beam is coming in from the bottom. L = lens*

Table 2.1. *Characteristics of the oscillator and the two CPA units.*

	Oscillator	CPA 1	CPA 2
Pump power / energy per pulse	5 W	8 mJ	150 mJ
Pump wavelength	532 nm	527 nm	532 nm
Pump repetition rate	cw	1 kHz	10 Hz
Output pulse energy	5 nJ	1 mJ	35 mJ
Output pulse width (FWHM)	15 fs	25 fs	200 fs
Central wavelength	790 nm	790 nm	790 nm
Spectral width	116 nm	45 nm	20 nm
Repetition rate	75 MHz	1 kHz / 10 Hz	10 Hz

The length of the pulse out of the oscillator is measured by a scanning, dispersion minimized autocorrelator (Femtometer Autocorrelator, Femtolasers GmbH) [11, 12]. The pulse lengths after CPA 1 and CPA 2 are measured using Frequency Resolved Optical Gating (FROG, Coherent Inc.). The FROG method gives both time and frequency information

in a single shot, which makes it also suitable for checking the chirp of the amplified pulses [12]. The FROG is positioned on the optical table permanently, unlike the autocorrelator, which makes a quick analysis of the amplified laser pulse possible.

2.1.3   Switching optics

After two amplifying units, the laser beam has a diameter of 7 mm (FWHM). A small part of it is used to trigger the oscilloscope by a photodiode, the rest of the beam is led through a horizontal and a vertical cylindrical lens (focal distance 150 mm and 200 mm respectively) to create a cylindrical slab of plasma that spans the complete distance between the electrodes (see figure 2.1). A slit in front of the laser entrance port prevents the edges of the laser pulse from hitting and damaging the electrodes. The horizontal cylindrical lens (f = 150 mm) is located at 150 mm from the center of the gap and the vertical lens (f = 200 mm) is located 186 mm from the center of the gap. A CCD camera is used to analyze the laser focus in the spark gap. As mentioned, for photoconductive switching the laser intensity over the entire length of the cylindrical focus in the gap should be above the threshold for tunneling ionization in air ($I_{thr} \approx 10^{18}$ Wm^{-2} for N$_2$). The required laser power (P_{req}) can be calculated if the gap distance (d) and the focus height (h) are known:

$$P_{req} = I_{thr} \times d \times h. \tag{2.1}$$

The gap distance determines the amount of laser power needed. The larger the gap distance, the more laser power is required to create a sufficiently ionized plasma in the gap to be able to switch photoconductively.

At the laser energies we use here (after CPA 2) it is justified to neglect the absorption of laser energy due to ionization in the focus. For this reason, the depth of the focus does not need to be inserted into equation (2.1), because the laser energy will be the same over the complete depth of the focus ($\sim$100 μm).

Even though we can estimate the laser power that is actually used to create the switching plasma, it is difficult to estimate the ionization rate of the gas in the gap. The tunneling ionization rate depends strongly on the laser intensity. A slight difference in laser intensity (for instance 2×10^{18} instead of 1×10^{18} Wm^{-2}) results in an order of magnitude more ionized particles [2, 13]. This makes it hard to estimate the actual ionization rate and thus the actual electron density.

2.2   High-voltage spark gap setup

In figure 2.5 the electrical circuit of the spark gap setup is given. A 30 kV power supply (Lambda EMI 500A) was connected to a grounded, 6 nF capacitor. A high-voltage diode
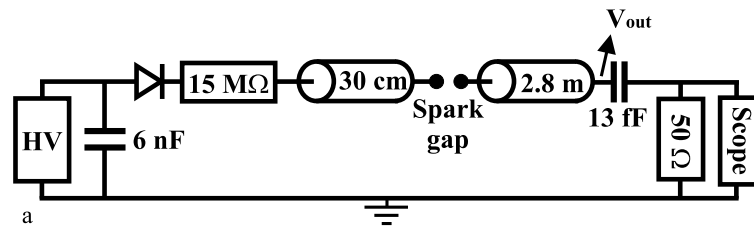
Figure 2.5. *Electrical circuit of the high-voltage spark gap setup.*

prevents reflections back into the HV-source. The high-voltage source charged a 30 cm coaxial transmission line through a 15 MΩ ceramic high-voltage resistor. The spark gap was situated at the end of the 30 cm transmission line. The output side of the spark gap merged into an N-type cable connector. A 2.8 m long coaxial N-type cable was attached to this connector to prevent reflections in the measurement cable from interfering with the signal. A 13 fF capacitor terminated the cable and was connected directly to the 50 Ω input of the oscilloscope. This home-made capacitor was used for measuring the switched high-voltage pulse. The oscilloscope used was a 1.5 GHz, 8 GSa HP Infinium. The capacitively differentiated signal was digitally integrated and scaled by the oscilloscope to represent the signal at the end of the 2.8 m transmission line (V_{out} in figure 2.5).
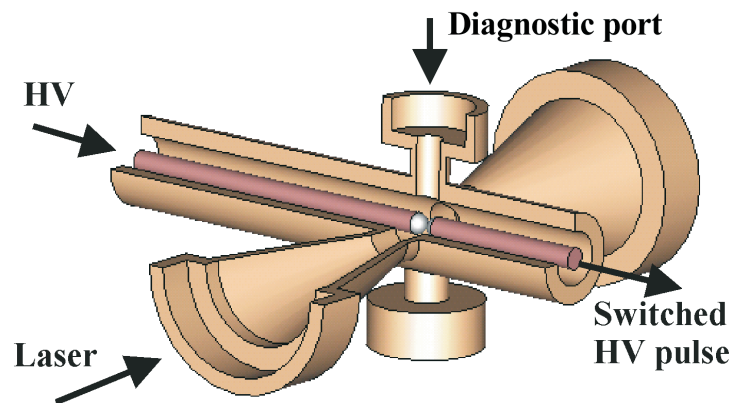
Figure 2.6. *Cut-view drawing of the coaxial spark gap with ports for the switching laser and ports for diagnostic purposes.*

Figure 2.6 shows a cut view of the photoconductive spark gap region. The inner conductor of the transmission line (diameter 6 mm) was made of copper, the outer conductor (diameter 15 mm) was made of brass. The characteristic impedance of the coaxial transmission line is 55 Ω. The tips of the inner conductors were made of copper-tungsten and can be replaced. The gap-distance between the two inner conductors was set to 1 mm, but

can be varied. The gap was filled with atmospheric air, however it is also possible to let nitrogen-gas flow through the gap region (here, typically, with an overpressure of 0.2 bar). Ports for the switching laser and for diagnostic purposes were made to access the gap region.

The spark gap is dimensioned such that it is able to hold off 2 MV pulses with a pulse length of 1 ns [14]. At these short time scales the breakdown process in the gap will start (avalanche and streamer formation), but at the time the actual breakdown can take place (enough free electrons are created over the gap) the high-voltage pulse has already disappeared. As a result no spontaneous breakdown will take place at these short time scales. However, because handling the 2 MV pulser is not trivial, we used a lower DC voltage first to prove the principle of photoconductive switching.

References

[1] S. Augst, D. Strickland, D.D. Meyerhofer, S.L. Chin and J.H. Eberly, Phys. Rev. Lett., 63 (20) 2212 (1989)

[2] C. Guo, M. Li, J. P. Nibarger, and G. N. Gibson, Phys. Rev. A, 58 (6) R4271 (1998)

[3] W.T. Silfvast, Laser fundamentals, second edition, Cambridge University Press, New York, Ch. 13 (2004)

[4] S. Backus, C.G. Durfee III, M.M. Murnane and H.C. Kapteyn, Rev. Sci. Instrum., 69 (3) 1207 (1998)

[5] U. Keller, Nature, 424, 831 (2003)

[6] R. Szipöcs, K. Ferencz, C. Spielmann and F. Krausz, Optics Lett., 19 (3) 201 (1994)

[7] A. Stingl, M. Lenzner, Ch. Spielmann, F. Krausz and R. Szipöcs, Optics Lett., 20 (6) 602 (1995)

[8] D. Strickland and G. Mourou, Opt. Commun., 56 (3) 219 (1985)

[9] M. Pessot, P. Maine and G. Mourou, Opt. Commun., 62 (6) 419 (1987)

[10] P. Maine, D. Strickland, P. Bado, M. Pessot and G. Mourou, IEEE J. Quantum Electron., 24 (2) 398 (1988)

[11] T. van Oudheusden, Technical report on electro-optical detection, Eindhoven University of Technology, (2003)

[12] W. van Harskamp, Technical report on Frequency Resolved Optical Gating, Eindhoven University of Technology, (2004)

[13] A. Talebpour, J. Yang and S.L. Chin, Opt. Comm., 163 (1-3) 29 (1999)

[14] S. Brussaard and D. Vyuga, IEEE Trans. Plasma Sci., 32 (5) 1993 (2004)

Chapter 3

First demonstration of photoconductive switching

Abstract

We have demonstrated photoconductive switching of a gas-filled spark gap. A femtosecond Ti:Sapphire laser was focused in a 1 mm spark gap biased at 4.5 kV. There is a clear transition between triggered operation, when only part of the path between the electrodes is ionized, and photoconductive switching, when the entire length of the gap is ionized directly by the laser. The measured standard deviation of the time fluctuations between the rising edge of the transmitted electrical pulse and the laser was less than 15 ps.

High-voltage applications (above ~ 1 kV) that require accurate timing use laser triggering of gas-filled spark gaps to switch electrical pulses. In these spark gaps, a laser is focused between the electrodes or on one of the electrodes to create a small amount of ionization. The free electrons are accelerated in the gap and cause additional ionization (avalanche, streamer formation) and, eventually, a conducting (arc) channel is formed between the electrodes [1, 2]. Typical rise time and jitter of these switches in the 1-100 kV range is of the order of 100s of picoseconds. A recent improvement in this field was reported by Luther et al. [3] who used a femtosecond Ti:Sapphire laser to trigger the breakdown of a pressurized high-voltage air spark gap at 10 kV and obtained jitter as low as 35 ps. A different technique, namely laser-driven photoconductive switching, has been used to produce pulses with (sub-)picosecond rise time, albeit at lower voltages (below ~ 1 kV). In these switches, a high-resistivity semiconductor separates two electrodes or transmission lines. When a laser pulse illuminates the semiconductor, free carriers are generated and the semiconductor becomes conducting. The switch is closed if a full path between the electrodes is illuminated with sufficient laser intensity. Motet et al. [4] have reported the generation of 825 V pulses with a rise time of 1.4 ps using low-temperature grown GaAs, illuminated by a 150 fs, 2 μJ dye laser at 620 nm wavelength. The basic difference between laser triggering of a spark gap and photoconductive switching is that in the former only part of the path between the electrodes is ionized, whereas in the latter a complete conducting path is created directly by the laser. In this letter we report the first results from a switch designed to combine the benefits of both techniques: The high-voltage, high-current capabilities of a gas-filled spark gap and the fast response of a photoconductive switch.
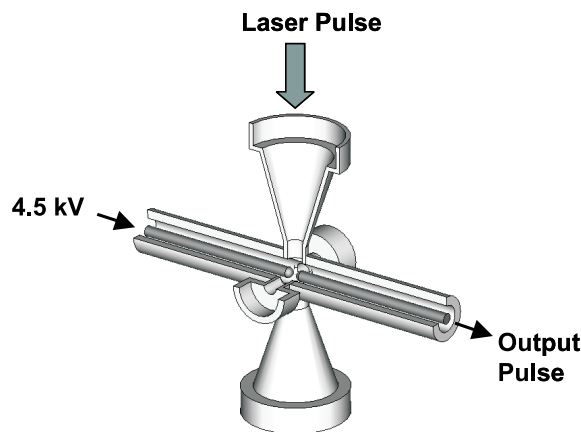
Figure 3.1. *Cut view of the switch*

With today's high power femtosecond lasers it is possible to ionize a complete path be-

tween the electrodes of a gas-filled gap by tunneling ionization [5, 6]. If the intensity of the laser is high enough (around 10^{14} W/cm^2) along the whole path between the electrodes, plasma fills the entire gap and the switch is effectively closed on the time scale of a few femtoseconds. To demonstrate this principle, a spark gap was constructed, shown in figure 3.1, integrated in a coaxial transmission line. The inner conductor of the transmission line has a diameter of 6 mm and the inner diameter of the outer conductor is 15 mm (55 Ω impedance). The transmission line is interrupted by a gap of 1 mm. The laser is focused in the gap using two cylindrical lenses, to create a slab of plasma between the electrodes. The gap is filled with air at 1 atmosphere. Our Ti:Sapphire laser system produces pulses of approximately 200 fs at 800 nm with energy up to 35 mJ at a repetition rate of 10 Hz. The incoming beam has a diameter of 7 mm (full width at half maximum (FWHM)). The two cylindrical lenses have focal distances of 150 mm and 200 mm and are positioned at 150 mm and 186 mm from the center of the gap, respectively. This produces a line focus between the electrodes of the spark gap (in the focal plane of the 150 mm lens) with a width of 20 μm and a length, along the axis of the spark gap of 0.5 mm (both dimensions are FWHM of the intensity). At maximum laser power, the intensity along the axis of the spark gap varies from 10^{15} W/cm^2 at the center to 10^{13} W/cm^2 at the electrode surfaces, comparable to the intensities used by Luther et al. [3] and above the threshold for tunneling ionization (Keldysh parameter [7] $\gamma < 1$) along 80% of the path between the electrodes. A slit is used at the entry port of the spark gap to prevent the edges of the laser pulse from hitting the electrodes.
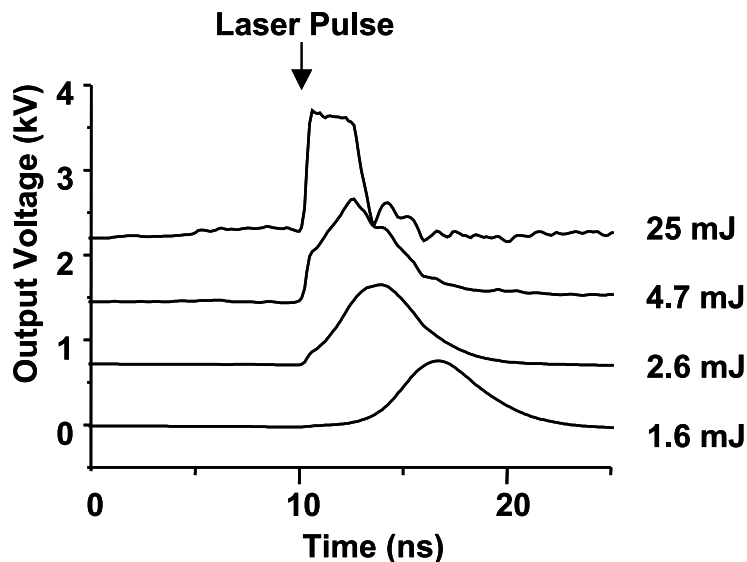
Figure 3.2. *Pulses switched at different laser energy: the measurements at different energy have been offset for clarity. The equivalent arrival time of the laser pulse in the gap has been indicated*

The 30-cm-long transmission line at the primary side of the switch is charged to a maximum of 5 kV (the self-breakdown voltage of the gap). The pulse in the secondary line is measured capacitively through a small gap in the transmission line and the signal is integrated digitally by the oscilloscope (HP Infinium, 1.5 GHz). The absolute value of the measured output pulses is an estimate based on the capacitance measured at 500 MHz ($\approx$13 fF) and losses in the cables ($\approx$10% at 1 GHz).

The results of the switching experiments are shown in figure 3.2 at a charging voltage of the primary line of 4.5 kV (90% of the self-breakdown voltage). At low energy (around 1 mJ) only a small amount of plasma is produced, in the center of the gap. In this case the switch is triggered in the classical sense. The free electrons initiate an avalanche which eventually causes breakdown of the gap and closes the switch. At higher energy (above approximately 2 mJ) a small step appears just after the laser pulse. A narrow plasma channel is created by the laser pulse connecting the electrodes. The stages of avalanche and/or streamer formation are omitted, but the impedance of the plasma is high compared to the transmission lines. As the current starts to run, an arc channel starts to develop, gradually reducing the impedance of the plasma. The same effect, but more pronounced, is visible at even higher energy (5-20 mJ). In this case, a drop off in the transmitted voltage pulse is visible, 2 ns after the initial step. This can be explained by the fact that the closing of the switch causes a voltage drop in the primary transmission line. This wave front travels backwards through the primary transmission line and reflects at the input resistance. The result is the observed decrease in voltage 2 ns, or twice the length of the primary line, after the closing of the switch. True photoconductive switching of the gap is shown in the upper graph of figure 3.2. At laser pulse energies above approximately 20 mJ, the impedance of the initial plasma is low enough to transmit the entire pulse without significant loss. A square pulse is observed in the secondary line with a duration of 2 ns, twice the length of the primary line. The height of the step at the beginning of the transmitted electrical pulse is plotted as a function of laser energy in figure 3.3. At low energy, the initial step is only a fraction of the charging voltage. At higher laser energy, in the photoconductive switching regime, the maximum amplitude of the pulse is reached in the first step. Increasing the laser power further has little effect on the output pulse, which is now completely determined by the length of the primary transmission line and the charging voltage. We have measured similar pulses at charging voltages as low as 10% of the self-breakdown voltage.

The measured rise time of the square pulses (above 20 mJ) is 100 ps, which is limited by the oscilloscope (1.5 GHz). It is expected that the actual rise time of the pulse is much shorter, of the order of the transit time of the pulse through the gap, which is only 3 ps, but this is presently beyond our measuring capabilities. We have attempted to measure the delay
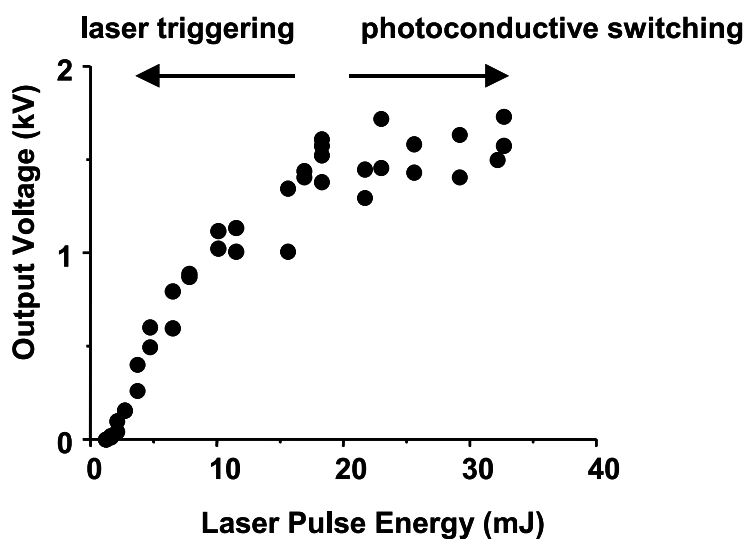
Figure 3.3. *Amplitude of the front edge of the switched pulse as a function of laser pulse energy*
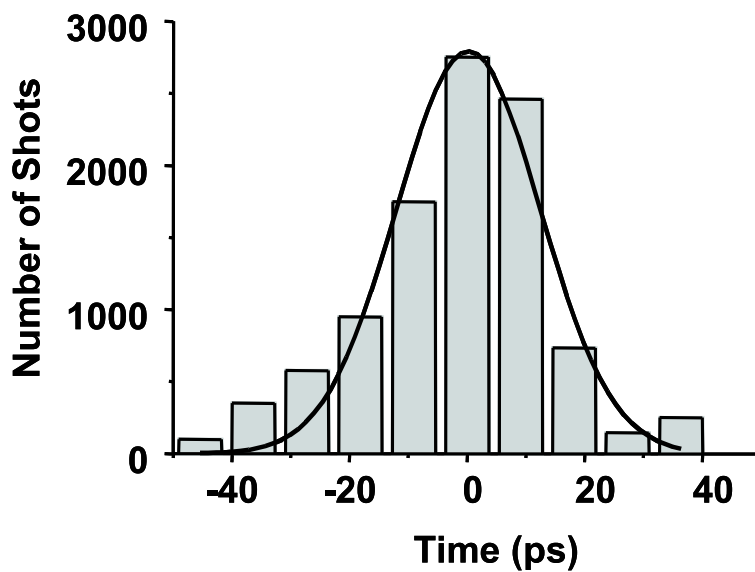
Figure 3.4. *Time variation of the front edge of the high-voltage pulse with respect to the laser pulse. The line is a Gaussian fit to the data, σ=12 ps*

between the arrival of the laser pulse in the gap and the onset of the transmitted pulse. After accounting for the different cable lengths, the measured delay between the laser pulse and the rising edge of the transmitted pulse was less than 200 ps. The corresponding time of arrival of the laser pulse is indicated in figure 3.2. The jitter between the laser pulse and the rising edge of the transmitted pulse was measured at 4.5 kV charging voltage and 25 mJ laser pulse energy. The histogram in figure 3.4 shows the variation of the rising edge as it crosses a fixed level, approximately half the amplitude of the transmitted pulse. Over a period of 15 minutes, at a repetition rate of 10 Hz, the measured jitter (σ) is less than 15 ps. The accuracy of this measurement is determined by the oscilloscope. The limited measurable rise time of 100 ps means that variations in the amplitude of the transmitted pulse are translated directly into a variation in the time at which the rising edge passes through the preset level. A variation of 10% in the output voltage results in a contribution of 10 ps to the measured jitter.

In conclusion, we report the first demonstration of a photoconductively switched gas-filled spark gap. There is a clear transition between triggered and photoconductive operation of the switch. In the photoconductive mode, this technique enables switching far below the self-breakdown voltage, which greatly extends the range of voltages that can be controlled by a single switch.

References

[1] R.A. Dougal and P.F. Williams, J. Phys. D: Appl. Phys., 17, 903 (1984)

[2] M.J. Kushner, R.D. Milroy and W.D. Kimura, J. Appl. Phys., 58 (8) 2988 (1985)

[3] B.M. Luther, L. Furfaro, A. Klix and J.J. Rocca, Appl. Phys. Lett., 79 (20) 3248 (2001)

[4] T. Motet, J. Nees, S. Williamson and G. Mourou, Appl. Phys. Lett., 59 (12) 1455 (1991)

[5] S. Augst, D. Strickland, D.D. Meyerhofer, S.L. Chin and J.H. Eberly, Phys. Rev. Lett., 63 (20) 2212 (1989)

[6] C. Guo, M. Li, J. P. Nibarger, and G. N. Gibson, Phys. Rev. A, 58 (6) R4271 (1998)

[7] L.V. Keldysh, Sov. Phys. JETP 20, 1307 (1965)

Chapter 4

Parameter study of photoconductive switching

Abstract

We report on the experimental investigation of the photoconductively switched gas-filled spark gap. When the laser intensity of a femtosecond laser is high enough (around 10^{18} Wm^{-2}), a plasma can be created that spans the complete distance between the electrodes. The gas-filled spark gap is then closed on a femtosecond time scale, similar to photoconductive switching of a semiconductor switch. Stochastic breakdown processes, such as avalanche and streamer formation that cause the breakdown in laser-triggered spark gaps, are passed over, which results in faster rise time and less jitter. Measurements of the switched pulses as a function of laser energy were performed in a 1 mm gap at an applied voltage of 4.5 kV. A clear transition from triggering to switching was measured with increased laser energy. Measurements of the output pulses with the gap filled with nitrogen at 1 atm showed results very similar to measurements in air in the same gap. In the switching regime, the amplitude of the switched pulse did not depend strongly on the laser energy. Measurements at lower applied voltages but with the same gap distance showed that it was possible to switch voltages as low as 10% of the self-breakdown voltage. At low applied voltages, a significant difference between the applied voltage and the output voltage is measured. A possible explanation is given based on the dynamic behavior of the laser-created plasma. The measured rise time and jitter of the switched pulses were both

below the resolution of the measurement equipment, i.e., better than 100 ps and 15 ps, respectively.

4.1 Introduction

High-voltage pulses are widely used in applications ranging from radar to extreme ultraviolet (EUV) sources and from nuclear fusion experiments to waste-water treatment. Ultrashort high-voltage pulses with picosecond rise time and time stability (jitter) can lead to even more applications. One of these applications is to couple picosecond high-voltage pulses into an antenna structure. This way, broadband high intensity terahertz (THz) radiation is created with intensities an order of magnitude higher than the common laser-semiconductor approach. Higher intensities make THz-radiation more suitable as an alternative for X-rays for medical and security purposes [1]. Another interesting application will be in the field of bioelectrics. Ultrashort high-voltage pulses can be used to explore the influence on biological cells of higher field strengths and shorter pulses [2]. Our own interest is to use ultrashort high-voltage pulses for making compact pulsed DC electron accelerators to create ultrashort electron bunches [3].

High-voltage pulses below 1 kV with rise time and jitter of the order of 1 ps can be made by laser-driven photoconductive switching. In those switches, a high-resistive semiconductor separates two electrodes. When a laser illuminates the semiconductor, free electrons are created and the semiconductor becomes conducting. If a full path between the electrodes is illuminated with sufficient intensity, the switch is closed. Motet et al. [4] used GaAs and a femtosecond dye laser to generate 825 V pulses with 1.4 ps rise time. An important drawback of this method especially for high-power applications is the limited current that can be switched.

High-power, high-voltage pulses are commonly switched using gas-filled or liquid spark gap switches. The main reason for using such switches lies in their capability to recover from breakdown, which allows much higher currents to be switched. One of the main disadvantages of these switches is the timing of the output pulses. To reduce jitter in spark gaps a laser can be used to trigger the switch. The laser pulse is focused in the gap between the two electrodes or on one of the electrodes. This creates free electrons, which are accelerated in the gap by the applied electric field. The accelerated electrons cause additional ionization and after avalanche and streamer formation a conducting (arc) channel is formed between the electrodes. The initial stochastic process of avalanche and streamer formation limits the rise time and time jitter of the switched pulses [5]. Since the first laser-triggered switching experiments in the early 1960s, a wide variety of spark gap geometries and laser

types have been investigated [6]. It turned out that focusing a laser axially through the conductor into the gap gave a better time stability of the switched pulse. Because the laser has already defined a path with some ionization along its entrance axis, the breakdown occurs faster and at a better defined time. Typical rise time and jitter of laser-triggered high-voltage pulses of the order 1-500 kV are in the sub-ns regime [7, 8]. Luther et al. [9] made pulses of 10 kV with time jitter as low as 35 ps, using a femtosecond Ti:Sapphire laser.

In a recent letter [10] we reported on experiments designed to combine these two switching regimes: photoconductive switching of semiconductors and laser triggering of a high-voltage spark gap. In these experiments we used a high-intensity femtosecond Ti:Sapphire laser in a gas-filled spark gap. But instead of focusing the laser to a point, we used two cylindrical lenses to create a slab of plasma between the electrodes. The idea was that, if the plasma completely fills the gap, the switch will be closed on a femtosecond time scale, similar to the photoconductive switching of the semiconductor switches. At the same time, with plasma as the conducting medium it will be possible to switch large currents without permanent damage to the switching medium. In these experiments we were able to switch pulses up to 4.5 kV with the measured rise time and jitter both limited by the time resolution of the measurement equipment, i.e., 100 ps and 15 ps, respectively.

In the present article we elaborate on the experiments reported in the letter. In order to investigate this switching regime we varied a number of parameters, such as applied voltage, gas mixture, gap distance and laser power. The results will illustrate other possibilities created by this switching method.

4.2 Experimental setup

Figure 4.1 gives a schematic overview of the experimental setup. It consists of the following parts: a high-voltage source connected to a spark gap, a Ti:Sapphire laser system with cylindrical lenses to create the switching plasma, and diagnostics to analyze the switched high-voltage pulses.

4.2.1 High-voltage spark gap setup

Figure 4.2(a) depicts the electrical circuit of the spark gap setup. A 30 kV power supply (Lambda EMI 500A) was connected to a grounded, 6 nF capacitor. We incorporated a high-voltage diode to prevent reflections back into the high-voltage source. The high-voltage source charged a 30 cm coaxial transmission line through a 15 MΩ ceramic high-voltage resistor. The transmission line was interrupted by the spark gap. At the output side of the spark gap, the transmission line merged into an N-type cable connector. To prevent
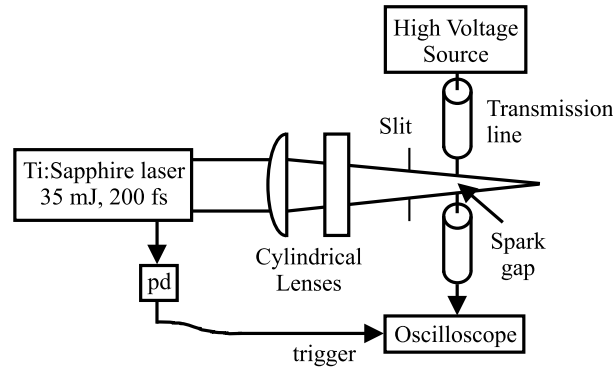
Figure 4.1. *Schematic overview of the experimental setup (pd = photo diode).*
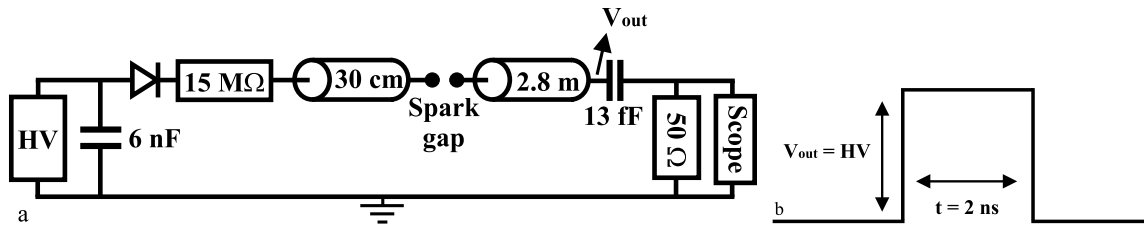
Figure 4.2. *(a) Electrical circuit of the high-voltage spark gap setup. (b) Ideal signal at the indicated position (Vout).*

reflections in the measurement cable from interfering with the signal, a 2.8 m long coaxial N-type cable was attached to this connector. This cable was terminated by a 13 fF capacitor, connected directly to the 50 Ω input of the oscilloscope. The oscilloscope used was a 1.5 GHz, 8 gigasample (GSa) HP Infinium. In order to account for the capacitor and the load, the signal was digitally integrated and scaled to represent the signal at the end of the 2.8 m transmission line.

If the spark gap acts as a perfect switch, with 0 Ω resistance (when closed) and impedance matched to the transmission lines, the signal on the scope will be a square pulse (Figure 4.2(b)). When the switch is closed the applied voltage is divided over the two lines. The resulting pulse in the secondary line, therefore, is twice the length of the primary (charged line). The voltage in the second line is half the applied voltage. This switched pulse is reflected by the 13 fF capacitor, which leads to a doubling of the pulse at the point of reflection. The measured signals on the scope were converted to represent the pulse at the end of this secondary line. For an ideal switch, the output pulse amplitude is then equal to the applied voltage.

Figure 4.3 shows a cut view of the spark gap region. The inner conductor of the trans-
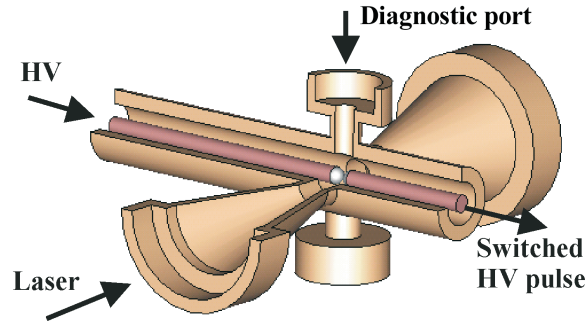
Figure 4.3. *Coaxial spark gap with ports for the switching laser and ports for diagnostic purposes.*

mission line was made of copper, while the outer conductor was made of brass. They have a diameter of 6 mm and 15 mm, respectively, (characteristic impedance 55 Ω). The replaceable tips of the inner conductors were made of copper-tungsten. The gap distance between the two inner conductors was set to 1 mm, but can be varied. The gap was filled with atmospheric air. It is also possible to let nitrogen gas flow through the gap region (here, typically, with an overpressure of 0.2 bar). The ports for the switching laser and for diagnostic purposes were made to access the gap region.

4.2.2   Femtosecond Ti:Sapphire laser system

Compared with semiconductors, the photoconductive switching of a gas-filled spark gap requires far greater laser intensity. The intensity needs to be high enough throughout the gap, to create a plasma over the complete distance between the electrodes. For a gas-filled gap, this means that the intensity has to be above the threshold for tunneling ionization, around 10^{18} Wm^{-2} for most gases [11, 12]. We also require this ionization to occur on a time scale much smaller than the expected rise time. A high-power femtosecond Ti:Sapphire laser fulfills both these criteria.

Our femtosecond Ti:Sapphire laser system consists of three parts. First a mode-locked Ti:Sapphire laser oscillator (Femtolasers GmbH) produces broadband laser pulses with an energy of 5 nJ and a duration of 15 fs at a central wavelength of 800 nm. The repetition frequency is 75 MHz. These pulses were then amplified in the first chirped pulse amplifier (CPA). Here, a Ti:Sapphire crystal was pumped by a Nd:YLF laser (B.M. industries) with an energy of 8 mJ (527 nm) at a repetition rate of 1 kHz. After nine passes, this first CPA produced pulses of 1 mJ and 25 fs (40 GW). A Pockel's cell defines the repetition rate at 10 Hz. Part of the light was coupled out for other purposes while the remaining light was led into the second CPA. Here a Nd:YAG laser (Thales SAGA 230/10) with a pulse energy of 150 mJ at 532 nm (10 Hz) pumped another Ti:Sapphire crystal. After five amplification

passes, pulses of 35 mJ and 200 fs (~ 0.2 TW) at a repetition frequency of 10 Hz were produced. At this point the beam had a diameter of 7 mm (full width at half maximum (FWHM)). A small part of it was coupled out onto a photodiode. This signal was used to trigger the oscilloscope. The rest of the beam was led through a horizontal and a vertical cylindrical lens (focal distance 150 mm and 200 mm, respectively) to create a slab of plasma, spanning the complete distance between the electrodes. A slit was placed in front of the laser entrance port to prevent the edges of the laser pulse from hitting the electrodes.

The incoming laser-beam is 7 mm in diameter (FWHM). The horizontal cylindrical lens ($f = 150$ mm) was located at 150 mm from the center of the gap and the vertical lens ($f = 200$ mm) was located 186 mm from the center of the gap. The laser focus that creates the plasma in the spark gap was imaged on a CCD camera and analyzed. The width of this focus was 949 ± 6 μm and its height was 20 ± 3 μm (both FWHM). At the maximum energy used (34 mJ), the intensity in the center of the gap is almost 10^{19} Wm^{-2}. At the maximum laser energy, the intensity over the entire length of the gap is above the threshold for tunneling ionization in air (10^{18} Wm^{-2}).

4.3   Results and discussion
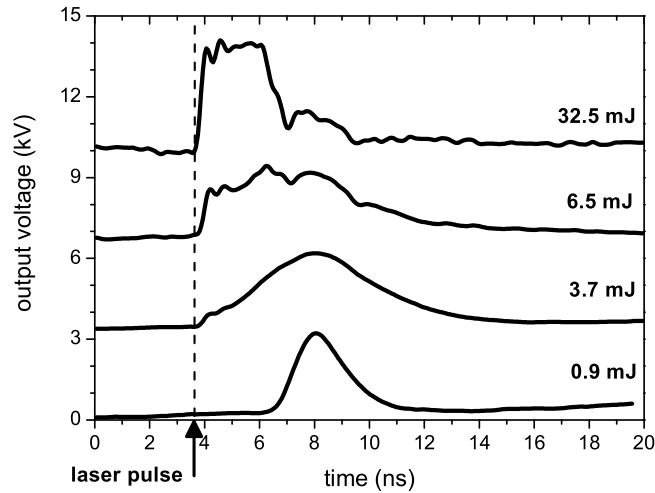
Figure 4.4. *Pulses switched at different laser energies ($V_{applied}$ = 4.5 kV, gap = 1 mm, atmospheric air). The curves are offset for clarity. The arrival time of the switching laser pulse is indicated by the dashed line.*

Figure 4.4 shows output pulses that were switched with different laser energies. The ap-

plied voltage was 4.5 kV (90% of the self-breakdown voltage) and the spark gap distance was 1 mm. The gap was filled with atmospheric air. The evolution of the pulses in order of increasing energy can be understood as follows: At low energy (bottom curve) there is not enough laser energy available to sufficiently ionize the complete gap. The laser creates some ionization, mainly in the center of the gap and subsequently the stochastic processes of avalanche and streamer formation cause the actual breakdown of the gap. Time jitter is of the order of nanoseconds at this laser energy. Increasing the laser energy (3.7 mJ in figure 4.4) results in a small voltage step at the beginning of the pulse, just after the arrival of the laser pulse. In this case, the laser energy is high enough to create a plasma connecting the two conductors. In this initial rise, the stochastic processes of avalanche and streamer formation are passed over and time jitter is reduced to a level well below 100 ps (dedicated time-jitter measurements are presented below). However, due to the resistance of the initial plasma, only a small part of the pulse stored in the charged line is switched in this first step. The charged line discharges completely in 8-10 ns. When the laser energy is increased further (6.5 mJ), the resistance of the initial laser-created plasma is lower and a larger fraction of the pulse is switched immediately. In the upper curve (32.5 mJ) the laser energy is high enough to create a plasma with a resistance low enough to switch nearly the full charge. The pulse now has a rectangular shape and a width of 2 ns (determined by the length of the charged transmission line). A small pulse is visible behind the pulse, also with a width of 2 ns. This trailing pulse is likely to be caused by reflections on the interface between the transmission line and the plasma: When the laser created plasma is formed, a travelling wave from the charged transmission line starts to propagate. Because the laser-created plasma is not matched to the charged inner conductor, reflections will occur at the interface. The reflected part of the pulse propagates in the opposite direction, reflects at the input resistance of the charged line, and returns at the spark gap 2 ns after the initial pulse.

These measurements of varying laser energy were also done in a flow of nitrogen gas with the same applied voltage and the same gap distance. A similar evolution of the switched pulse with increasing laser energy is visible.

The measurements in figure 4.4 suggest a transition from the classical triggered regime, in which the laser initiates a breakdown, to a switching regime where the stochastic processes are passed over and the full amplitude of the output pulse is reached within the first 100 ps (the time resolution of our measuring equipment). This interpretation is also supported if we plot the amplitude of the rising edge of the switched high-voltage pulse as a function of the laser pulse energy. These results are given in figure 4.5 for air (figure 4.5(a)) and nitrogen (figure 4.5(b)). The applied voltage was kept constant at 4.5 kV. Each data point is a single shot measurement. The variation in output voltage at a given setting (input voltage and laser energy) is caused by the method of measuring the output pulse. The
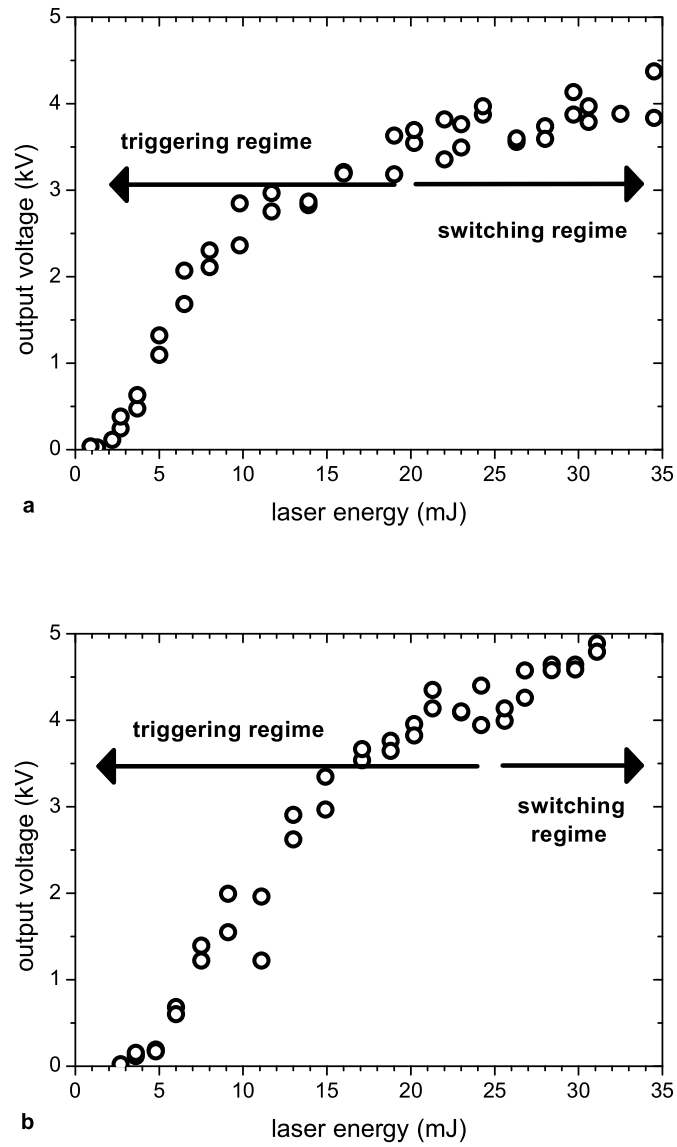
Figure 4.5. *Amplitude of the rising edge of the switched pulse in air (a) and nitrogen (b) as a function of the applied laser energy ($V_{applied} = 4.5$ kV and gap = 1 mm).*

capacitive measurement gives the time derivative of the pulse in the transmission line. Due to the fast onset of the pulse the integration of the capacitive signal relies from four to five data points. The error introduced by the limited sampling speed of the scope is estimated to be around 10% and can account for the variations in the output voltages of figure 4.5.

It can be seen in figure 4.5 that at low laser energy only a small part of the applied voltage is transmitted in the rising edge of the switched pulse. When the laser energy increases, the amplitude of the rising edge of the switched pulse increases until it approaches the value of the applied voltage. Further increase of the laser energy has little effect on the switched pulse. Figure 4.5 shows that there is indeed a transition between two regimes: the triggering regime, when there is not enough laser energy available to initially switch the full amplitude of the pulse, and the switching regime, where the applied laser energy is sufficient to reach the full amplitude in the rising edge of the pulse. The transition between these regimes is somewhat higher for nitrogen (25 mJ for the settings used) than for air (around 20 mJ).
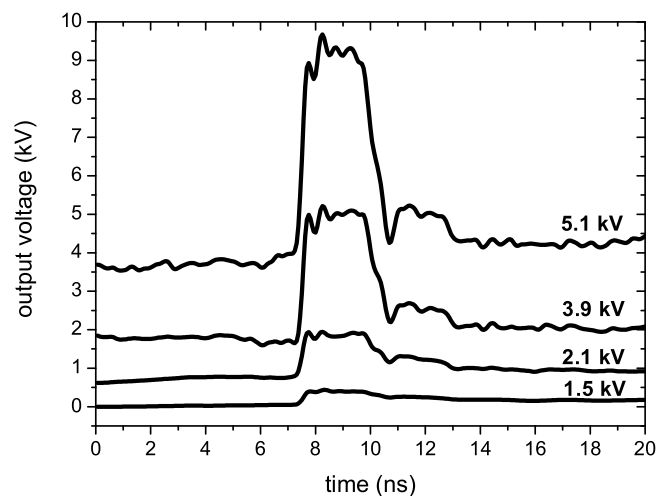
Figure 4.6. *Switched pulses of different applied voltages (E_{laser} = 34 mJ and gap = 1 mm) in atmospheric air. The measurements at different applied voltage are offset vertically for clarity.*

If the pulses at high laser energy are switched photoconductively, similar to photoconductive switching of semiconductors, rather than triggered as in conventional spark gaps, it should be possible to switch pulses far below the self-breakdown voltage of the spark gap. This greatly increases the applicability of gas-filled switches, since laser-triggered gas-filled spark gaps have a rather limited optimum operating range around 80%-90% of the self-

breakdown voltage. To investigate this feature, we measured the output pulses at different applied voltages at a laser energy of 34 mJ, i.e., in the saturated part of figure 4.5. The output pulses are shown in figure 4.6. The highest applied voltage (5.1 kV) was just below self-breakdown of the gap. Figure 4.6 shows that the sharp initial voltage rise and the pulse shape persist at lower voltages. These results also show that it is indeed possible to use this switch far below the self-breakdown voltage of the gap. The amplitude of the lowest output pulse in figure 4.6 is 0.5 kV, less than 10% of the self-breakdown voltage. Output voltages below 0.5 kV were difficult to measure with good accuracy in the present setup due to the use of the capacitor to measure the pulse. Figure 4.7 gives the amplitude of the rising edge of the output pulse as a function of applied voltage. In the high laser-energy regime this is equal to the amplitude of the entire pulse (see figure 4.6). The measurements were performed in atmospheric air and nitrogen with a 1 mm gap and in air with a 0.35 mm gap.
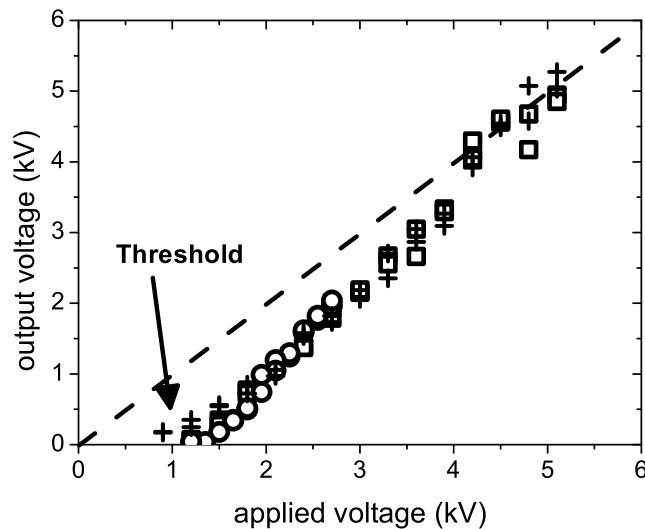
Figure 4.7. *Amplitude of the output voltage as a function of applied voltage at different experimental settings.* □ *gap filled with air, gap distance = 1 mm, laser energy = 34.0 mJ.* ○ *gap filled with air, gap distance = 0.35 mm, laser energy = 32.2 mJ.* + *gap filled with N2, gap distance = 1 mm, laser energy = 28.6 mJ.*

In all three experimental series, the laser energy was high enough to be in the switching regime, i.e., the saturated part of figure 4.5. The laser intensity was comparable in the 0.35 and the 1 mm gap. The energy of the laser was measured before the laser entrance port. For the smaller gap, the focusing lenses were kept in the same position, while the width of the slit at the laser entrance port was decreased to cut a larger part of the laser.

The measurements at 1 mm gap distance in air and nitrogen both show that close to self-breakdown ($\sim$5 kV) the output voltage equals the applied voltage. However, at voltages below 4 kV, a deviation from the dashed line, $V_{applied} = V_{out}$, occurs. There is a trend towards a threshold at approximately 1 kV applied voltage. Measurements done in a smaller gap filled with air (circles in figure 4.7) show the same trend. In fact, the measurements at different settings all overlap, even though the self breakdown voltage was approximately two times smaller in the 0.35 mm gap than in the 1 mm gap.

From a practical point of view, the deviation from the line $V_{applied} = V_{out}$ and the threshold at approximately 1 kV merely imply that at low voltage, in order to reach a certain output pulse, a slightly higher applied voltage must be used. However, a straightforward explanation of the results in figure 4.7 is not readily available. Comparison of the results in a 1 mm gap to those in the 0.35 mm gap shows that the important parameter is not so much the electric field in the gap, but rather the applied voltage. A possible explanation for the results can be given by looking at the initial laser-created plasma. We are not able to determine the ionization degree or electron temperature of the switching plasma. However, we can give a qualitative description of the behavior shown in figure 4.7 if we estimate the initial laser-induced ionization degree to be 1%. This means that the electron density in the laser-created plasma is approximately 10^{23} m^{-3}. The electron temperature for such a plasma will be 1-2 eV (10% of the ionization energy of most constituents). This weakly ionized plasma is dominated by electron-atom collisions and its electrical conductivity is given by Mitchner and Kruger [13]. For the parameters chosen, this initial conductivity is of the order 10^3 Ω^{-1}m^{-1}. Thus, the initial resistance of the plasma is high ($\sim$500 Ω) compared with the impedance of the transmission lines. At high voltages, the current through the plasma will create more ionization which lowers the impedance. This process takes place at time scales of the order of tens of picoseconds and cannot be resolved with our diagnostics. At low voltages the current is not high enough to create sufficient extra ionization and to lower the impedance of the plasma. The output voltage remains significantly lower than the applied voltage. This explanation suggests that photoconductive switching is possible even at low initial ionization (1%), although the output voltage can be significantly lower than the applied voltage. At higher laser intensities, this effect will be less, since the initial resistance of the laser produced plasma will already be low compared to the 50 Ω transmission line impedance.

Another important parameter of laser switching of high voltages is the time jitter of the switched pulses. To determine the jitter, the arrival-time variation of the switched pulses is measured for a large number of shots. The laser pulse is taken as the reference pulse. The arrival time is taken as the time at which the measured signal passes a preset level. A histogram with the time-of-arrival distribution is depicted in figure 4.8 for a measurement
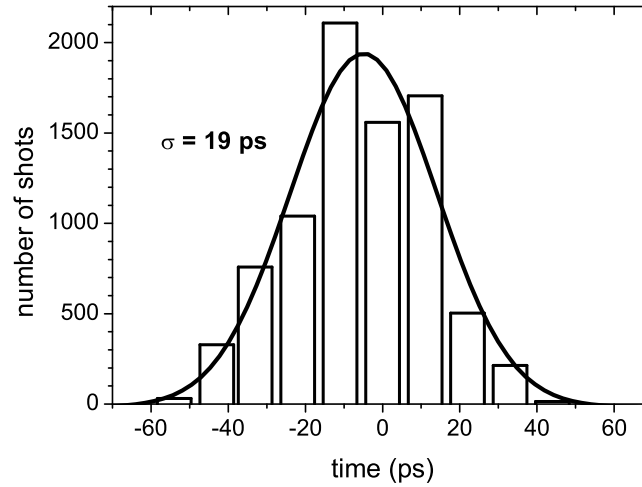
Figure 4.8. *Time-jitter distribution histograms measured at the initial voltage rise flank in the air filled gap.*

series of 15 minutes at 10 Hz repetition frequency. The applied voltage was 4.5 kV and the laser energy was 35 mJ. The solid line is a Gaussian fit to the measured data. Measurements were done for both the air-filled gap and the nitrogen flow through the gap, both at a gap distance of 1 mm. There was no significant difference in the measured time jitter for the two gases. The accuracy of the jitter measurements was limited by the time resolution of the oscilloscope (1.5 GHz and 8 GSa). To determine the resolution of the scope, the output of a pulse generator (Stanford Research Systems DG535) was split and applied to both the trigger and signal input of the scope. For a series of 15 minutes at 10 Hz repetition frequency the measured time jitter was 12 ps. The measurements were also sensitive to amplitude variations in the (capacitively measured) switched pulse. In the present setup, we were not able to measure the time variation at a constant fraction of the amplitude. A variation of the amplitude shifts the time at which the edge of the switched pulse passed the preset measurement level. This way an amplitude variation of 10% resulted in 10 ps apparent time jitter. Together, the resolution of the scope and the amplitude variations in the switched pulse can account for the measured jitter of figure 4.8. The jitter induced by the switching process is therefore expected to be less than 10 ps.

4.4   Conclusions

We report an experimental investigation of the photoconductively switched gas-filled spark gap. At high enough laser intensities (around 10^{18} Wm^{-2}), the amplitude of the output

pulse shows saturation with laser energy. In this regime, the switch operates more like a photoconductive semiconductor switch, rather than a conventionally triggered spark gap. The stochastic breakdown process of avalanche and streamer formation is passed over and does no longer limit the rise time and time jitter of the output pulses. Measurements with nitrogen in a 1 mm gap showed results very similar to measurements in air in the same gap. The switch was also operated far below the self-breakdown voltage. Reducing the gap distance had no significant influence on the output pulse shape. The insensitivity of the output pulse to these parameters implies that such a switch can have great potential in producing stable output pulses in a wide parameter range.

At low applied voltages (or, as it seems, low current through the gap) there is a significant difference between the applied voltage and the output voltage. A possible explanation was offered, based on the assumption that the initial, laser produced plasma was weakly ionized (1% ionization degree). The conductivity of the plasma in that case depends on the current through the switch. At low applied voltage this current is insufficient to lower the resistance of the plasma below the 50 Ω impedance of the transmission lines.

The measured rise time of the switched pulses was better than 100 ps and time jitter was around 15 ps. Both rise time and jitter measurements were limited by the resolution of the measurement equipment.

4.5   Acknowledgements

References

[1] News feature, Nature 424, 721 (2003)

[2] K.H. Schoenbach, S. Katsuki, R.H. Stark, E.S. Buescher and S.J. Beebe, IEEE Trans. Plasma Sci., 30 (1) 293 (2002)

[3] S.B. van der Geer, M.J. de Loos, G.J.H. Brussaard, O.J. Luiten and M.J. van der Wiel, Proc. Eur. Particle Accelerator Conf. Paris, France, June 3-7, 2002, 989 (2002)

[4] T. Motet, J. Nees, S. Williamson and G. Mourou, Appl. Phys. Lett., 59 (12) 1455 (1991)

[5] J.M. Lehr, C.E. Baum, W.D. Prather and R.J. Torres in ultra-wideband, short pulse electromagnetics 4, E. Heyman, Ed. New York: Kluwer Academic/Plenum Publishers, p. 11. (1999)

[6] A.H. Guenther and J.R. Bettis, J. Phys. D, 11 (11) p. 1577 (1978)

[7] J.R. Woodworth, C.A. Frost and T.A. Green, J. Appl. Phys. 53, 4734 (1982)

[8] J.R. Woodworth, P.J. Hargis, Jr., L.C. Pitchford and R.A. Hamil, J. Appl. Phys. 56, 1382 (1984).

[9] B.M. Luther, L. Furfaro, A. Klix and J.J. Rocca, Appl. Phys. Lett., 79 (20) p. 3248 (2001)

[10] G.J.H. Brussaard and J. Hendriks, Appl. Phys. Lett., 86, 081503 (2005)

[11] S. Augst, D. Strickland, D.D. Meyerhofer, S.L. Chin and J.H. Eberly, Phys. Rev. Lett., 63 (20) 2212 (1989)

[12] C. Guo, M. Li, J. P. Nibarger, and G. N. Gibson, Phys. Rev. A, 58 (6) R4271 (1998)

[13] M. Mitchner and C.H. Kruger, Partially Ionized Gases, Wiley, New York (1973)

Chapter 5

Feasibility study of high-voltage and plasma diagnostics

Abstract

This chapter describes the study of the suitability of two diagnostics for the photoconductively switched high-voltage spark gap. First, a plasma interferometer for monitoring the switching-plasma behavior with a time resolution of the order fs is investigated. Because we operate in a new switching regime, photoconductive switching in a gas-filled gap, we want to know how the plasma behaves during switching. Electrodynamic simulations predicted that electrodynamic details are the most important parameters for the shape of the output pulse and plasma simulations showed that the switching happens so fast that no plasma expansion will take place on these short time scales. This can be checked experimentally by using an interferometer.

The other diagnostic is a high-voltage pulse diagnostic based on the electro-optical Pockels effect to achieve a time resolution of the order ps. When measuring the output pulse, we are limited by the time resolution of the oscilloscope (100 ps). Electrodynamic simulations showed that the actual rise time of the switched high-voltage pulse is about 30 ps. In order to resolve this we investigate the suitability of the electro-optical method (time resolution ≤ 1 ps) that has recently been used for electron-bunch length determination.

5.1 Interferometer

The laser-created plasma is the actual switch of the system and its behavior is thus an important parameter for the switched high-voltage pulse. Investigation of the plasma evolution can be done in detail by using the principle of interferometry. By probing the plasma with a (short) laser pulse the electron density and the plasma diameter can be monitored in time. If small time steps for probing are used, the evolution of the plasma can be characterized.

Interferometry is based on measuring the phase difference between two interfering laser beams. A laser beam is split into two beams with one beam probing a medium with a certain index of refraction (n). Due to the difference in index of refraction a phase-difference is induced between the two beams. When these beams are combined again, a modulated intensity distribution of light and dark fringes appears due to constructive and destructive interference [1]. From this interference pattern the phase shift can be calculated and thus the refractive index of the medium. Since the refractive index is linked to, in our case, the plasma electron density, this can then be deduced from the interference pattern.

As mentioned, the phase change of a probed plasma is a function of the electron density. This is derived as follows [1]: Assume one laser beam travels through a plasma with length L and its propagation constant is k_p. The other beam travels through vacuum or air with a propagation constant k_0. The phase difference between these two beams ($\Delta\varphi$) is then given by

$$\Delta\varphi = \int_0^L (k_p - k_0)\, dL = \int_0^L \left(\frac{\omega}{c}\right)(n_p - 1)\, dL, \tag{5.1}$$

with c the speed of light, ω the angular frequency of the light and n_p the refractive index of the plasma. Because the plasma is a dispersive medium there is a frequency dependence in its index of refraction n_p. If we assume the cut-off frequency of the plasma (ω_p = plasma frequency) to be much smaller than the frequency of the probing laser light ($\omega >> \omega_p$) the refractive index is represented by [2–4]

$$n = \sqrt{\frac{\epsilon_r}{\epsilon_0}} \simeq \sqrt{1 - \frac{\omega_p^2}{\omega^2}}. \tag{5.2}$$

Combining (5.1) and (5.2) gives *

$$\Delta\varphi = \frac{\omega}{c} \int_0^L \left(\sqrt{1 - \frac{\omega_p^2}{\omega^2}} - 1\right) dL \simeq \frac{\omega}{c} \int_0^L \frac{1}{2}\frac{\omega_p^2}{\omega^2} dL. \tag{5.3}$$

---

*if $\omega \gg \omega_p$ then $(1\text{-}x)^a \simeq 1\text{+}ax$

The plasma frequency is

$$\omega_p = \sqrt{\frac{n_e e^2}{m_e \epsilon_0}} \tag{5.4}$$

with n_e the electron density of the plasma (m^{-3}) and m_e the mass of an electron (kg). Rewriting c as

$$c = \frac{\lambda \omega}{2\pi} \tag{5.5}$$

and substituting this into (5.3) gives

$$\Delta\varphi = \frac{\pi e^2}{\omega^2 \lambda_0 m_e \epsilon_0} \int_0^L n_e dL, \tag{5.6}$$

which can also be written as

$$N_e = \int_0^L n_e dL = \Delta\varphi \frac{\omega^2 \lambda_0 m_e \epsilon_0}{\pi e^2}. \tag{5.7}$$

The electron density (N_e) given by (5.7) is a chord integrated electron density. We, however, are interested in the local electron density distribution. This local distribution can be resolved from the integrated electron density by assuming that the electron density has a certain profile (here Gaussian) that can be fitted.

We built a Folded Wave Interferometer (FWI) for the analysis of the switching plasma, based on the interferometer described in [5]. It is schematically depicted in figure 5.1. A FWI differs slightly from a conventional interferometer. Not two different laser beams are used here (one reference beam and one probe beams) but only one laser beam that is much larger in diameter than the plasma. Part of this beam probes the plasma, another part does not (visible at position 1 in figure 5.1). By folding these two different regions upon each other and letting them interfere, an interference pattern appears on a CCD camera. The advantage of this configuration is that it is much more stable against vibrations of the optical system.

The evolution of the switching plasma can be monitored because the probe beam is led over a motorized precision delay stage. By changing the delay of the probe beam the plasma is probed at different times. The pulse length of the probe beam is 50 fs; this determines the time resolution of the FWI.

The FWI is computerized in LabVIEW [6]. The system is programmed in such a way that at fixed timesteps pictures of the interference patterns are made. Afterwards, analysis of the interference patterns is done using IDL [7], which directly gives the local electron
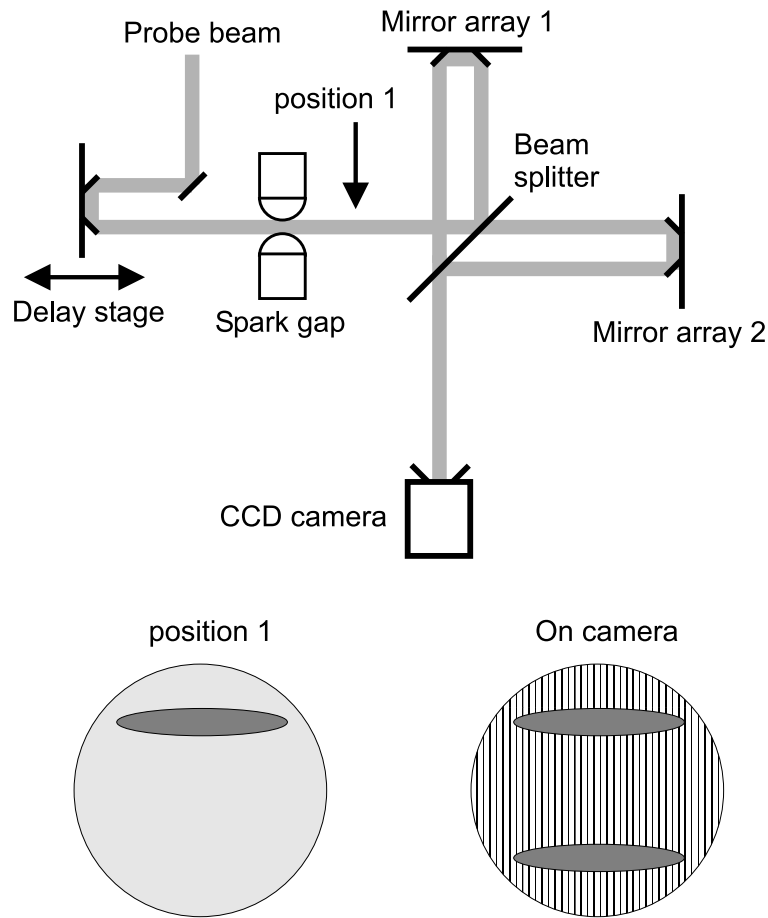
Figure 5.1. *Schematic interferometer setup. The beams also travel upward on the mirror stages. The images just after the plasma is probed (position 1) and the final interference-image are also depicted (on camera).*

density profile [8].

Besides the electron density also the shape of the plasma can be determined from an interferogram by looking at the shape of the different fringes. Several fringes are necessary for a detailed picture of the shape of the plasma. The more fringes the better the shape is represented. On the other hand, the minimal detectable electron density is determined by the minimal detectable phase shift. This phase shift resolution becomes optimal if the number of fringes is minimized. The best electron density resolution will be achieved if there is only one fringe. Because we are interested both in the shape of the plasma and in an accurate electron density a trade-off between the number of fringes and the minimal electron density resolution is necessary. We take 5 fringes as a good trade-off value, but to be complete we will also determine the electron density resolution for 1 and 25 fringes.

The phase shift is imaged on the CCD-camera. This makes the pixel size the determining factor for the actual minimal detectable phase shift. In our setup the effective pixel size is 4.8 μm/pixel. This means that the spark gap (1 mm) is imaged on almost 210 pixels (see figure 5.2). In the case of 5 fringes, each full fringe contains 42 pixels on which a 2π rad phase change is depicted. The resolution per pixel is then 0.15 rad/pixel.
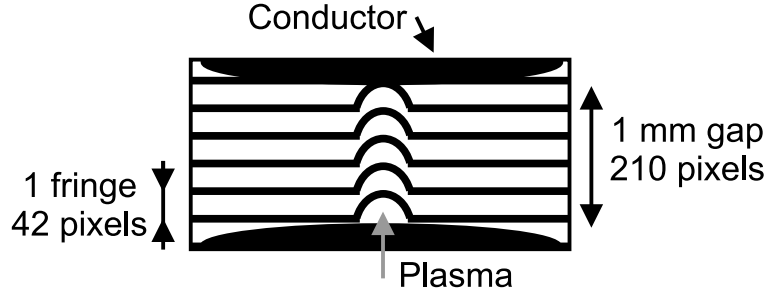
Figure 5.2. *Schematic interference pattern of the switching plasma containing 5 fringes in a 1 mm gap. Also the number of pixels is indicated.*

The electron density for this minimal detectable phase shift is given by (5.7) and can be approximated by replacing the integral by ΔL:

$$\int_0^L n_e dL = \Delta\varphi \frac{\omega^2 \lambda_0 m_e \epsilon_0}{\pi e^2} \rightarrow n_e = \Delta\varphi \frac{\omega^2 \lambda_0 m_e \epsilon_0}{\pi e^2 \Delta L} \tag{5.8}$$

Our plasma is approximately 20 μm (FWHM) in diameter, thus $L = 20$ μm. The minimal resolvable electron density for 5 fringes is then (5.8):

$$n_e = 3.3 * 10^{24} \frac{electrons}{m^3} \tag{5.9}$$

The electron density at full ionization (every atom is ionized once) equals the particle density and is given by

$$n_e = \frac{p}{kT} = 2.5 * 10^{25} \frac{electrons}{m^3}, \tag{5.10}$$

$p = 1$ atm $= 10^5$ Pa, T=295 K and k is Boltzmann's constant.
The minimal ionization degree that can be detected by the interferometer (with 5 fringes) is therefore of the order of 10%.

Table 5.1 gives the minimal resolvable electron density for interferograms with different numbers of fringes. Also the minimal detectable ionization degree (in atmospheric air) is given.

Table 5.1. *Electron density resolution for different interferograms.*

# fringes	electron density (m^{-3})	ionization degree
1	$6.6*10^{23}$	3%
5	$3.3*10^{24}$	13%
25	$1.7*10^{25}$	68%

We were only able to visualize a plasma by its effect on the interference pattern when point-focusing the laser (figure 5.3). Only then the laser power was high enough to ionize the air in the gap sufficiently. We were not able to sufficiently ionize the plasma spanning the complete gap. This means that we do not see a phase change in the interference pattern when photoconductive switching occurs and therefore we can not resolve the electron density of the plasma. If more laser power is used for switching, the electron density should increase to a level that can be visualized by the interferometer. Then this diagnostic is suitable for monitoring the switching plasma density and its shape in time.
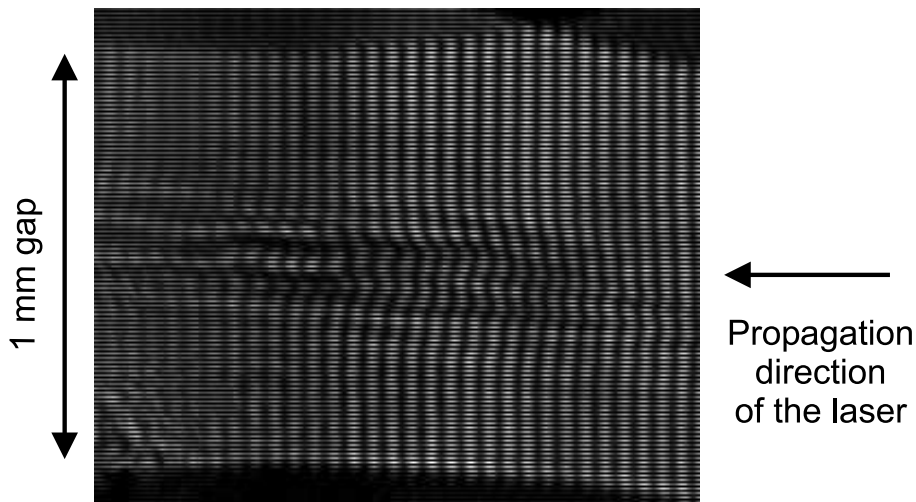
Figure 5.3. *Interference pattern of a (point) focus. Some overlap between the two folded patterns is visible. Laser energy = 32 ± 2 mJ, 1 mm gap. The geometry is the same as in figure 5.2.*

5.2 Electro-optic high-voltage pulse detection

Electro-optic sampling could be a good candidate to improve the time resolution for characterization of the switched high-voltage pulse. It is based on the Pockels effect and this technique has been used for measuring bunch lengths of relativistic electron bunches that

come out of an electron accelerator, with sub-ps resolution [9, 10]. In those experiments, the electric field of a passing electron bunch induces a birefringence in a non-linear optical crystal. Probing this birefringence with a linearly polarized short laser pulse results in a polarization change of the probe laser, which is proportional to the electric field of the electron bunch. There is no difference in the physics between an electron bunch or a high-voltage pulse on a coaxial line passing the crystal. In both cases an electric field travels through the crystal. Therefore, this method could also be suitable to measure the photo-conductively switched high-voltage pulse shape with sub-ps time resolution. We tested a setup almost identical to the one used before in the accelerator group of the Eindhoven University of Technology for measuring electron-bunch lengths [10].

As mentioned, the method is based on the Pockels effect. This is a (second-order) non-linear effect where an external electric field induces a birefringence in the crystal. A detailed description of the processes taking place in the non-linear optical crystal and the effects on the probe beam under the influence of an external applied electric field is given in [10, 11]. When this crystal is probed with a linearly polarized laser in a direction perpendicular to the direction of the applied electric field (taking into account the correct birefringence axes), the polarization becomes elliptical. The phase change is proportional to the applied electric field:

$$\Delta\phi = \frac{\omega}{c}n_0^3 r_{41}E\Delta L = \frac{2\pi}{\lambda_0}n_0^3 r_{41}E\Delta L, \tag{5.11}$$

where λ_0 is the wavelength of the probe beam, E is the applied electric field strength, n_0 the refractive index, r_{41} the electro-optic coefficient and ΔL is the crystal thickness. The crystal we plan to use is ZnTe. This is an optically isotropic crystal with a relatively large electro-optic coefficient, which results in a good interaction with the applied electric field. The crystal is transparant for 800 nm laser light and it is commercially available. The relevant crystal properties are given in table 5.2 [10]:

Table 5.2. *Crystal properties of ZnTe.*

crystal structure	cubic
crystal group	$\bar{4}3m$
electro-optic coefficient	r=r_{41}=r_{52}=r_{63}=4.3 pm/V
refractive index (800 nm)	n_0=n_e=2.85
dielectric constant (DC)	8.4

5.2.1 Setup

The crystal is mounted in the setup as depicted in figure 5.4. The crystal connects the inner conductor with the outer conductor and can be probed by a hole in the outer conductor. The dimensions are given in table 5.3.
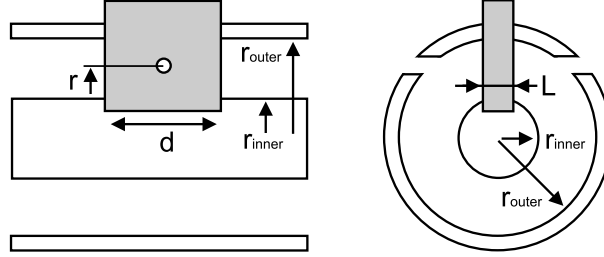
Figure 5.4. *Schematic electro-optical setup with geometrical parameters. The dimensions are given in table 5.3.*

Table 5.3. *Dimensions of electro-optical setup (figure 5.4).*

r_{inner}	1.5 mm
r_{outer}	3.75 mm
r	2.625 mm
d	5 mm
L	1 mm

In order to calculate the amount of phase shift, we need to know the electric field at the probe position in the crystal. This can be calculated by

$$E = \frac{V}{r \ln\left(\frac{r_{outer}}{r_{inner}}\right)}. \tag{5.12}$$

If we use $V = 2.25$ kV (half the applied voltage), then $E = 0.94$ MV/m. This field is of the same order as the field of the electron bunch in [10].

We first tested the setup with a crystal with a thickness of 1 mm, but finally we planned to use a 0.2 mm thick crystal. The phase change (5.11) for these thicknesses are given in table 5.4.

The minimal time resolution depends on the time it takes for the probe beam to travel through the crystal and thus on the thickness of the crystal. For a 0.2 mm crystal the time resolution is

Table 5.4. *Phase changes of two different crystal thicknesses at a voltage of 2.25 kV.*

crystal thickness (mm)	$\Delta\phi$ (rad)	$\Delta\phi$ (deg)
1.0	0.74	42.1
0.2	0.15	8.4

$$t = \frac{L \times n}{c} = \frac{0.2 \times 10^{-3} \times 2.85}{3 \times 10^8} = 1.9 ps. \tag{5.13}$$

In order to measure the induced polarization change accurately, the following components, are necessary (see figure 5.5 [10]):
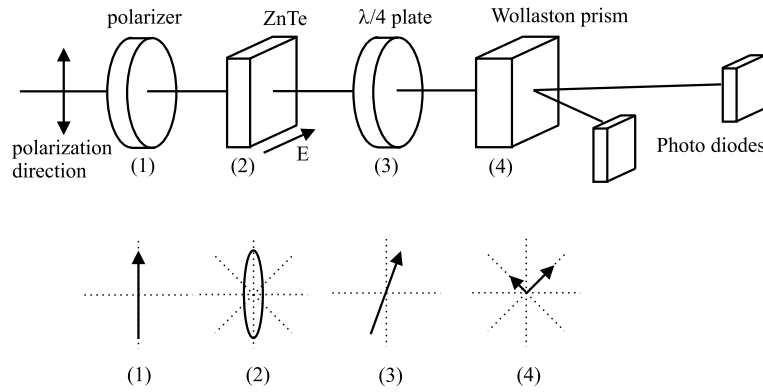
Figure 5.5. *Schematic electro-optical measurement setup with all the components. Also the polarization of the probe beam is given after it has passed the different components.*

First a linear polarizer makes sure that the probe beam is linearly polarized. The ZnTe crystal (INGCRYS laser systems Ltd), cut in the [110] direction, will make the polarization elliptical when the external electric field is applied. A quarter wave plate converts the elliptical polarization to linear again, and a polarizing beam splitter (Wollaston prism) resolves it into two linearly polarized pulses. Measuring the difference between the two linearly polarized components with photodiodes gives the phase change. For small angles this phase change ($\Delta\varphi$) is proportional to the intensity and thus the applied electric field:

$$|I_{pd1} - I_{pd2}| = I_0 \sin(\Delta\phi). \tag{5.14}$$

By using this configuration, the quarter wave plate can easily be used to calibrate the system and to make a $\Delta I/I_0$ graph: A rotation of the wave plate over θ is equivalent to an induced ellipticity of $0.5\Delta\phi$.

5.2.2   Pulse transmission simulations

In order to check whether the crystal does not ruin the high-voltage pulse while it traverses the crystal, we used Microwave Studio [12] (see also chapter 7) to simulate the traversing pulse through the coaxial setup, including the crystal. The simulated setup is given in figure 5.4. The crystal connects the inner conductor to the outer conductor. The rest of the space between the inner and outer conductor is filled with air (vacuum in the simulation). The probe ports in the outer conductor are also depicted. A pulse with a smooth rise time (20 ps) and a flat top is coupled into the coaxial setup and starts to travel to the other side (same pulse as the "ideal pulse" in chapter 8). The local electric field is monitored in time, in the crystal at the spot where the laser will probe it, as well as in air. The position in the crystal is indicated in figure 5.4 as r, the position in air is symmetrically below the inner conductor. The results are depicted in figure 5.6.
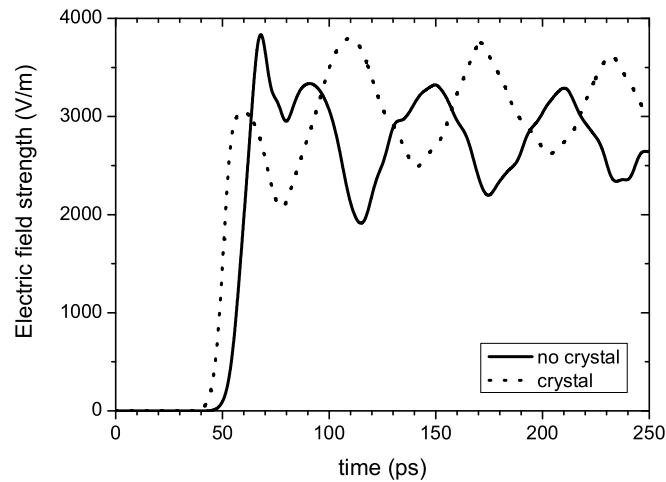
Figure 5.6. *Simulated electric field strength in the crystal (dotted line) and in air (solid line).*

The pulse does not have the "ideal" shape anymore. This is caused by the probe ports and the groove in the inner conductor in which the crystal is mounted. However, the rise time is sustained and because this is the parameter we are interested in, this setup should be able to give the correct rise time of the switched pulse. Notice that the signal from the crystal is induced later in time than the signal in air, although their axial position is the same. This is caused by the difference in dielectric constant. The crystal has a dielectric constant which is around 8 times higher than the one for air.

5.2.3 Measurements

We built a test setup, which incorporated the crystal setup of figure 5.4, the optical setup of figure 5.5 and a pulsed high-voltage source. The pulsed high-voltage source can produce pulses up to 1 kV with a pulse length that can be varied between 200 ns and 5 μs. The pulses are flat top with a rise and fall time of several ns. This source is used to simulate the photoconductively switched pulses that, eventually, are to be measured. In this test setup, we use a 780 nm diode laser (Thorlabs CPS192, cw, 4 mW) for probing the crystal. The test setup is used for different pulse lengths, all with a maximum voltage of 1 kV. The absolute difference of the signals of the two photodiodes was measured.

No sensible pulses, comparable to the simulated pulses, were measured electro-optically. When the high-voltage pulses were applied, breakdown could be heard clearly. The crystal showed signs of breakdown (black spots) after applying the pulses, making the crystal not suitable for probing anymore. Due to this effect, this setup is not suitable for electro-optically measuring high-voltage pulses.

It is possible that the conductor and the crystal are not attached to each other completely. A small open space filled with air could be present and cause the breakdown. However, it is not possible to mount the crystal more tightly (and thus isolated) into the conductors. Mechanical strain will also induce a birefringence [13], which complicates the analysis. To glue the crystal on the conductor could be an option, but this makes the setup permanent, because the crystal breaks easily. The problems of breakdown over the crystal were not encountered when the method was used for measuring electron-bunch lengths [10]. However, in the electron-bunch length case, the crystal was mounted on an insulator while here the crystal connects a high-voltage conductor to a grounded one. This difference makes that the method can not simply be copied and used for high-voltage pulse measurements.

5.3 Conclusions

We tested the feasibility of two diagnostics, a folded wave interferometer and an electro-optical high-voltage pulse detection system.
The folded wave interferometer should be able to visualize the evolution of the electron density of the switching plasma with a time resolution limited to the probe beam pulse length (here 50 fs). We were not able to resolve the electron density of the switching plasma, because the ionization degree was not high enough. If the ionization degree of the switching plasma would be around 10% the electron density distribution can be resolved and also spatial changes of the plasma shape can be followed in time. This means that more laser power is required to create a switching plasma with a higher degree of ionization.

The electro-optical high-voltage pulse detection setup would be able to measure the switched high-voltage pulse with ps resolution. A test setup was made where pulses of 1 kV and variable pulse lengths were used. After applying the high-voltage pulses, signs of breakdown were visible on the crystal making the crystal non-transparant for the probing laser. Unfortunately, this made it impossible to measure the high-voltage pulses electro-optically.

References

[1] I.H. Hutchinson, Principles of plasma diagnostics, Cambridge University Press, New York, Ch. 4 (1987)

[2] J.D. Jackson, "Classical Electrodynamics, 3rd ed.", John Wiley and Sons, Inc., New York, Ch. 7 (1999)

[3] M. Mitchner and C.H. Kruger, Partially Ionized Gases, Wiley, New York (1973)

[4] F.L. Pedrotti and L.S. Pedrotti, Introduction to Optics, Prentice-Hall, Inc., New Jersey, CH. 27 (1993)

[5] W.P. Leemans, D. Rodgers, P.E. Catravas, G. Fubiani, C.G.R. Geddes, E. Esarey, B.A. Shadwick, J. van Tilborg, S. Chattopadhyay, J.S. Wurtele, L. Archambault, M.R. Dickinson, S. DiMaggio, R. Short, K.L. Barat, R. Donahue, J. Floyd, A. Smith and E. Wong, Proceedings XX Int. Linac Conf., Monterey, California, USA, p. 701 (2000)

[6] National Instruments LabVIEW Express, Version 7.0 (2003)

[7] Research Systems Inc. IDL, Version 5.5 (2001)

[8] P.K. Tiwari, Technical report on Folded Wave Interferometry, Eindhoven University of Technology, (2004)

[9] X. Yan, A.M. MacLeod, W.A. Gillespie, G.M.H. Knippels, D. Oepts, A.F.G. van der Meer and W. Seidel, Phys. Rev. Lett., 85 (16) 3404 (2000)

[10] F.B. Kiewiet, PhD thesis Eindhoven University of Technology, Eindhoven, The Netherlands (2003)

[11] T. van Oudheusden, Technical report on electro-optical detection, Eindhoven University of Technology, (2003)

[12] CST Microwave Studio Version 5, CST GmbH, Germany (2003)

[13] F.L. Pedrotti and L.S. Pedrotti, Introduction to Optics, Prentice-Hall, Inc., New Jersey, CH. 26 (1993)

Chapter 6

Plasma simulations

Abstract

In this chapter the plasma physical behavior of the switching plasma of the photoconductively switched high-voltage spark gap is investigated. Experiments showed that when voltages close to the self-breakdown voltage of the gap were applied, almost 100% of the voltage was switched, while at low applied voltages there was a significant difference between the applied voltage and the output voltage. We investigated two possible causes of this voltage drop, the cathode fall in the switching plasma and the resistance of the plasma arc.

The cathode fall voltage was estimated to be of the order 1-10 V, which is much smaller than the experimentally observed voltage drop over the gap (∼1 kV). The cathode fall formation time is 300 fs which is much shorter than the typical rise time of the switched pulse (10s of ps). Hence, the cathode fall can be excluded as a cause of the observed voltage drop.

The switching plasma, with an emphasis on the evolution of the conductivity, was investigated. We give an analytical description of the important plasma processes that take place in the first couple of ps, together with the results of the simulations done by a one-dimensional, time-dependent non-LTE fluid model of the arc plasma. A good qualitative match between the experimentally observed and simulated voltage drop over the gap was found for a range of applied voltages, taking into account the poorly known initial plasma condition. This indicates that the finite arc resistance caused the voltage drop over the

gap. Based on these findings, suggestions for improvements of the switching efficiency are given.

6.1   Introduction

In chapter 3 ([1]) and 4 ([2]) photoconductive switching experiments were described. In these experiments a high-power femtosecond laser was used to photoconductively switch voltages up to 5 kV in a 1 mm spark gap. The switched pulses had a rise time and time jitter below the resolution of the measurement equipment, i.e., better than 100 and 15 ps respectively. By switching photoconductively, we were able to switch voltages as low as 10% of the self-breakdown voltage, which is not possible with conventional laser-triggered spark gaps. However, we observed a significant voltage drop over the spark gap when switching these lower voltages. At voltages close to the self-breakdown voltage of the gap this drop of voltage was not observed (see figure 6.1).
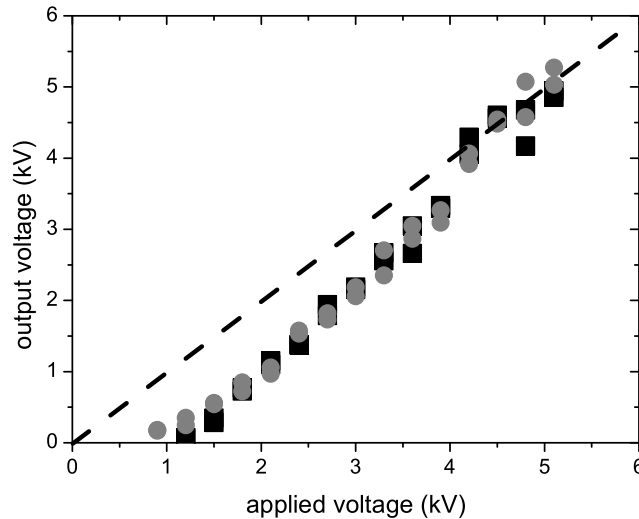
Figure 6.1. *Amplitude of the switched output voltage as a function of the applied voltage at a 1 mm gap. Black squares: gap filled with air, grey bullets: gap filled with N_2 [2]. For high voltages almost all the voltage is switched and a small part of the voltage is lost over the gap. With decreasing voltage an increasing part of the voltage is lost over the gap.*

By using theoretical models, we investigated two possible (plasma physical) causes of the observed voltage drop over the discharge in detail, i.e., the cathode fall and the plasma arc resistance. First we will describe the experimental switching plasma and the important parameters that are necessary for the models. A simplified analytical model of the cathode

fall formation in the laser-produced plasma is treated and its relevance to the observed switching behavior is discussed. Next, an analytical description of the important plasma processes in the first couple of ps is given, together with the results of the detailed plasma simulations. Finally, suggestions to improve the switching efficiency are given.

6.2   Setup

The experimental photoconductive switching setup is described in detail in chapter 2, 3 and 4 ([1, 2]). Only the essential parts for modelling are described here.

The coaxial transmission line was interrupted by a 1 mm gap (for a figure see paragraph 2.2). The radius of the inner conductor was 3 mm, the radius of the outer conductor 7.5 mm. This makes the characteristic impedance of the coaxial part 55 Ω. A Ti:Sapphire laser (35 mJ, 200 fs per pulse) was shot perpendicular into the gap and cylindrically focused such that the focus connected the two conductors. The laser intensity over the entire gap was above the threshold for tunneling ionization. Voltages up to 5 kV were switched. The block-shaped switched pulses had a rise time better than 100 ps and a pulse length of 2 ns (determined by the length of the charged transmission line). Because the geometrical impedance is 55 Ω and the voltage over the gap is half the applied voltage when switching occurs, the maximum current (I) that can run through the gap is 45 A. Experiments were done with a gap filled with either air or nitrogen. Since there was little experimental difference between the switching behavior of the gases [2], we only model the nitrogen plasma here. The initial laser-created plasma composition and its size were not measured. Therefore an estimate of its composition was made based on the size of the laser focus and the laser-power density in the focus (see chapter 2 and 4). The estimated initial electron density (n_{e0}) is 5×10^{23} m^{-3} (2% ionization). The modelled plasma is schematically depicted in figure 6.2. Since the radius of curvature of the conductors is 3 mm, they are considered as infinite planes here.
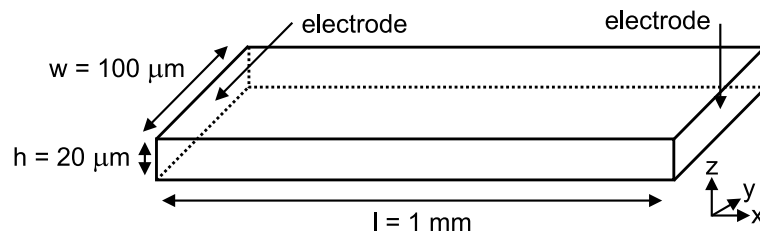

Figure 6.2. *Schematic representation of the modelled switching plasma. The sizes are derived from the size of the laser focus (FWHM-values). The width (w) is estimated.*

6.3   Cathode fall

A possible cause of the observed voltage drop is the voltage over the cathode fall of the switching plasma. From the experiments we know that a current runs through the plasma, just after the plasma is created by the laser. However, a mechanism is required that supplies enough electrons from the cathode to the plasma to sustain the current. Unlike in a conventional arc, our electrodes are not heated up sufficiently during the 2 ns pulse and thermionic emission can not provide enough electrons. For this very short discharge time (2 ns), field emission from the cathode is the only likely supplier of the necessary electrons. In order to have significant field emission, a cathode fall has to be present near the cathode (the cathode fall is the region of positive space charge in front of the cathode). Due to the region of space charge near the cathode, an electric field is present in this cathode fall which can extract electrons from the cathode by field emission if this electric field is high enough. Also secondary emission can take place when ions, accelerated by the field in the cathode fall, hit the cathode and liberate more electrons.

The cathode fall formation is schematically depicted in figure 6.3. The femtosecond laser produces a plasma almost instantaneously compared to the time scale of the other plasma processes under investigation here. The top graph shows the laser produced plasma density and the applied voltage over the spark gap on a small part of the cathode side of the gap. Due to the applied voltage, electrons will move away from the cathode creating a cathode fall in which the electric field is enhanced (bottom graph). This electric field facilitates electron emission from the cathode through field emission. The contribution to the transport of charge (current) and energy by the heavier ions is negligible compared to that of the electrons. The ions can therefore be considered motionless during switching (2 ns).

6.3.1   Cathode fall voltage

We assume that the current through the plasma is delivered by field emission only. The influence of secondary emission is neglected here. This field-emission current (I_{field}) as a function of the electric field at the cathode E_{cath} is given by the Fowler-Nordheim equation [3, 4]

$$I_{field} = K_4 E_{cath}^2 A \exp\left(\frac{-K_5}{E_{cath}}\right), \tag{6.1}$$

where $K_{4,5}$ are emission coefficients and A is the cathode area. Taking into account the local electric field enhancement due to surface roughness of the cathode we have to multiply E_{cath} with a correction factor β, which is typically 50. Incorporating this field enhancement factor and substituting the emission coefficients following [5], we get
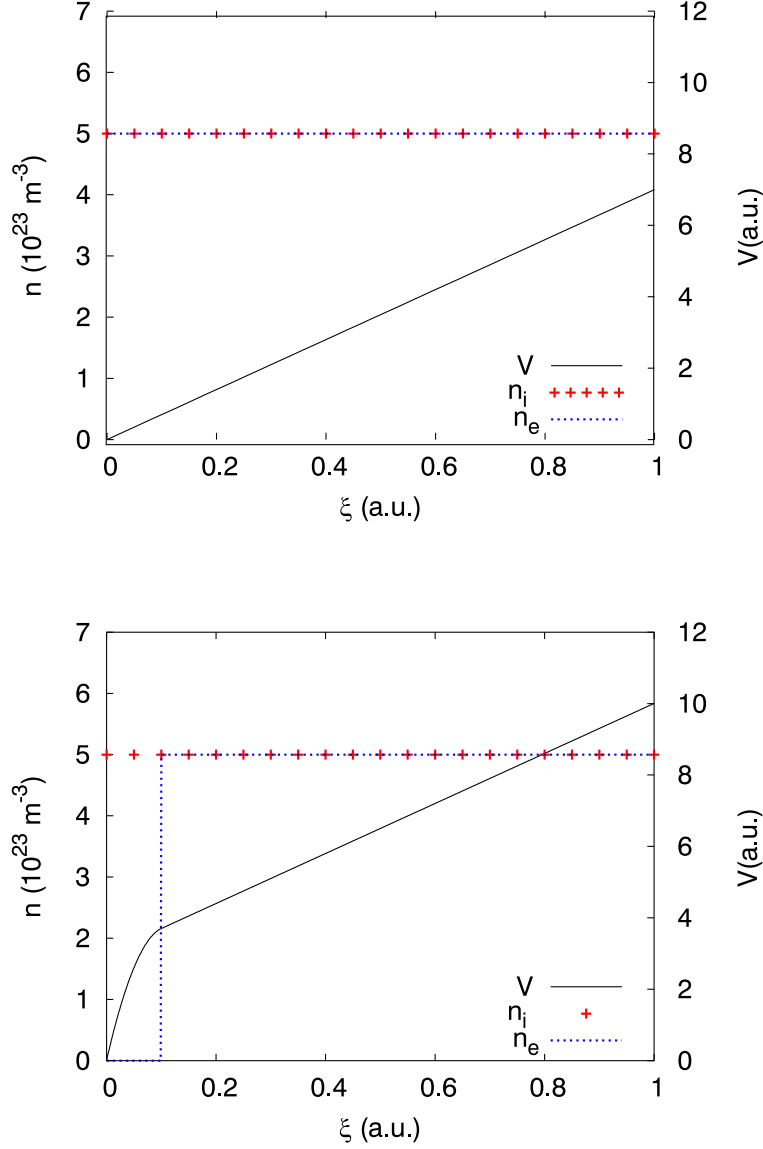
Figure 6.3. *Schematic representation of the cathode fall formation in the switching plasma. The cathode is situated at $\xi = 0$, the anode at $\xi \gg 1$. n_i is the ion density, n_e is the electron density and V is the voltage over this plasma region. The top graph depicts the situation when the laser has just created the switching plasma, the bottom graph gives the situation somewhat later (> 300 fs) when the cathode fall has appeared.*

$$I_{field} = \frac{1.54 \times 10^{-6} \times 10^{4.52\phi^{-0.5}} (\beta E_{cath})^2 A}{\phi} exp\left(\frac{-6.53 \times 10^9 \phi^{1.5}}{\beta E_{cath}}\right), \qquad (6.2)$$

with E_{cath} in $\mathrm{Vm^{-1}}$, ϕ (workfunction) in eV, A in $\mathrm{m^2}$ and I_{field} in A. The cathode and anode tips are made of a tungsten-copper alloy. The work function of tungsten (ϕ_W) is

4.54 eV [6] and that of copper (ϕ_{Cu}) is 4.65 eV [7]. The value of the work function of an alloy is assumed here to be typically between the values of its constituents [8]. Substituting our electrode area ($A = 2 \times 10^{-9}$ m^2) into (6.2) gives I_{field} as a function of E_{cath}. This has been plotted for W and Cu in figure 6.4.
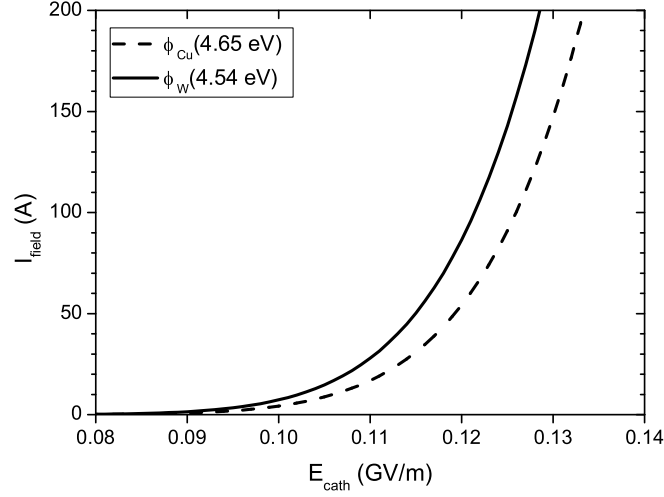
Figure 6.4. *Field emission current as a function of the electric field at the cathode surface (β = 50) for values of the work function corresponding to copper and tungsten. The field emission current of the actual cathode material (WCu) lies between the two curves of this graph.*

Figure 6.4 shows that the field emission current is negligible for values of E_{cath} lower than 0.09 GV m^{-1} and increases rapidly with increasing E_{cath}. The maximum switched current of 45 A in the switching experiments can be supplied by field emission if the electric field is 0.12 GV m^{-1}. Note again that this is an upper-bound value for the actual E_{cath} needed because secondary emission is neglected here.

The cathode fall can be described by Poisson's equation

$$\overrightarrow{\nabla}^2 V_{cath} = -\frac{\rho}{\epsilon}, \tag{6.3}$$

with $\rho = n_e e$ the charge density and ϵ the permittivity of the plasma (approximated by ϵ_0 here), and

$$\overrightarrow{E}_{cath} = -\overrightarrow{\nabla} V_{cath}. \tag{6.4}$$

We approximate $\overrightarrow{\nabla}$ with the inverse of the typical length scale of the cathode fall (L^{-1}) and, subsequently, substitute the initial electron density and the electric field necessary for field emission. This gives, at $I = 45$ A, a calculated cathode fall length of 1.3×10^{-8} m

and an accompanying voltage of 1.6 V over the cathode fall.

Compared to the applied voltage, a voltage over the cathode fall of the order 1-10 V (at 2% ionization) is negligible, eliminating this as a cause of the observed voltage drop over the spark gap when lower voltages are switched.

6.3.2   Cathode fall formation time

The formation of the cathode fall is not an instantaneous process. If the formation time is long, it could contribute to the rise time of the switched pulse. In order to estimate the cathode fall formation time, we calculate the time an electron needs to travel over the distance of the cathode fall (10^{-8} m). For this we use

$$eE_{gap} = m_e a \rightarrow a = \frac{V_{gap}e}{m_e l} \tag{6.5}$$

and

$$L = \frac{1}{2}at^2 \rightarrow t = \sqrt{\frac{2L}{a}}, \tag{6.6}$$

where e is the charge of the electron, E_{gap} is the initial electric field over the whole gap, V_{gap} is the voltage over the whole gap, l is the length of the gap, a the acceleration, m_e the electron mass and t is the time. Substituting for L the previously calculated cathode fall length ($\sim 10^{-8}$ m) and for V_{gap} 1 kV (the lowest switched voltage) we find that t is about 300 fs. This calculated cathode fall formation time is much shorter than the electrodynamically simulated rise time ($\sim$ 30 ps) [9]. From this we conclude that the cathode fall formation time has no significant influence on the rise time of the switched high-voltage pulse.

6.4   Arc plasma

Since the cathode fall is not the cause of the voltage drop over the gap, the resistivity of the laser created plasma is a good candidate. In order to investigate the plasma in more detail than in chapter 4 ([2]), a numerical model of the arc plasma that connects the electrodes was made to study the time behavior of its most important parameters for switching, such as conductivity, electron density, electron temperature etc.. Details of this model can be found in [10]. Since we are interested in the influence of the plasma on the switching behavior and not so much in the plasma-physical details, we will first give a simplified analytical description of the dominant processes in the plasma, which are important for photoconductive switching. This description will make use of some of the

simulation results. Finally, we will use the conclusions from the plasma simulations to see whether the plasma resistance is causing the experimentally observed voltage drop.

6.4.1 Analytical description of the switching plasma

In section 4.3 we estimated the electron temperature of the initial laser created plasma (T_{e0}) to be relatively low, 1-2 eV (10% of the ionization energy). The initial electron density (n_{e0}) is estimated to be 2% (5×10^{23} m^{-3}). When this plasma is created by the laser in the gap, the electrons are accelerated by the field of the applied voltage. Due to this acceleration they gain energy. When T_e has reached a value of approximately 5 eV (according to the simulations), ionization of N_2 starts to dominate. More electrons are created by ionization which lower T_e and, in turn, lower the ionization again. The result is a decrease in T_e and a slower increase in n_e.

We will now make an estimate of the time constants of these two processes, heating of the electrons and ionization, respectively. First the behavior of the electron temperature (T_e) in time is analyzed. Suppose that the laser creates a homogeneous plasma between the conductors with length l, area A, T_{e0} and n_{e0}. We assume here that the electrons are heated homogeneously in the whole plasma. The electrical resistance of the plasma can then be used to calculate the dissipated power (P):

$$P = \frac{V^2}{R} = \frac{V^2\sigma A}{l}. \tag{6.7}$$

This dissipated power leads to a temperature increase given by

$$\frac{d\hat{T}_e}{dt} = \frac{\hat{P}}{n_e A l} = \frac{V^2\sigma}{l^2 n_e e}, \tag{6.8}$$

with $\hat{P}$ the power in eV s^{-1}, $\hat{T}_e$ the electron temperature in eV and e the electron charge. Solving this gives

$$\hat{T}_e = \hat{T}_{e0} + \frac{V^2\sigma}{l^2 n_e e}t. \tag{6.9}$$

The conductivity can not be estimated easily. For the present analysis we will take the conductivity from the detailed model [10] at the initial conditions given there. Substitution of $\sigma_0 = 10^3$ Ω^{-1} m^{-1}, our estimated initial values ($n_{e0} = 5\times10^{23}$ m^{-3}, $l = 10^{-3}$ m) and a voltage of 5 kV results in

$$\hat{T}_e \simeq \hat{T}_{e0} + 3 \times 10^{11}t, \tag{6.10}$$

where 3×10^{-12} (1 over 3×10^{11}) is the time constant that causes T_e to reach a certain value for the temperature (with these initial conditions). This also resulted from the simulation

where a value of 5 eV for T_e is reached in the first couple of ps.

When the temperature rises, also ionization will increase. Electron impact ionization, described by

$$N_2 + e \rightarrow N_2^+ + 2e \tag{6.11}$$

will take place first. The rate coefficient of this reaction is given (in SI-units) in the simulation paper [10] as

$$k_{MI} = 3 \times 10^{-18}(T_e)^2 exp\left(\frac{-E_{MI}}{k_B T_e}\right), \tag{6.12}$$

with E_{MI} is the ionization energy of this reaction (15.6 eV) and k_B Boltzmann's constant. The change in electron density in time can be written as

$$\frac{dn_e}{dt} = n_e n_{N_2} k_{MI}, \tag{6.13}$$

where the density of N_2 is atmospheric. Solving this and substituting our initial values (T_e= 5 eV) gives

$$n_e = n_{e0} exp\left(n_{N_2} kt\right) = n_{e0} exp\left(10^{16} t\right), \tag{6.14}$$

where 10^{-16} is the time constant that causes the ionization increase well within a ps. Note that the rate coefficient and thus also $n_e(t)$ is very sensitive to T_e (due to the exponential term). This means that only when T_e is sufficiently high, significant ionization can take place.

The calculated time constants for heating and ionization (3×10^{-12} and 10^{-16}, respectively) show that these processes take place within the first couple of ps. This is much faster than we were able to resolve experimentally.

We did not take recombination into account yet. After ionization has taken place, also (dissociative) recombination of electrons with N_2^+ happens. Eventually (after $\sim$10 ps according to the numerical model), N^+ becomes the dominant ion. In that regime a more or less stable situation is reached where no rapid processes are to be expected anymore. The temperature continues to decrease slowly ($\sim$20% in 2 ns) and the electron density increases steadily (factor of 2 in 2 ns).

We mentioned already that we do not know the initial plasma condition exactly. The electron density was estimated, but can vary two orders of magnitude (roughly between 0.2% and 20%). Also the low initial electron temperature (T_{e0}) was estimated. Suppose we

would have more laser power available to create a plasma with a T_{e0} that is much higher than the estimated 1-2 eV mentioned above. This would not change the outcome after a few ps. When T_{e0} is high, immediate ionization will occur which lowers T_e rapidly. In that case, both T_e and ionization decrease and the same fairly stable situation is reached within the first couple of ps. A lower or higher n_{e0} will only linearly change the final n_e, but the processes involved are essentially the same.

We are interested in the conductivity as a function of the applied current. Because our plasma is not in the Spitzer-Härm conductivity limit, this can not be derived analytically. Qualitatively, the conductivity increases with temperature and electron density. Therefore, a stable value of the conductivity is reached within the first couple of ps and this value is not expected to change rapidly anymore after these first couple of ps.

The main conclusion from this analytical derivation is that the major plasma processes take place in the first couple of ps, much faster than we were able to measure. This is what we expected and the experiments were designed for: the rise time is only limited by the geometry of the spark gap, not by plasma processes.

6.4.2   Simulated voltage drop for various switching currents

As mentioned in the introduction of this chapter, we are interested in the influence of the plasma on the switched voltage. We want to know whether the plasma resistance depends on the applied voltage and if this causes the observed voltage drop. This was verified by running simulations for various values of the applied current (I) with the initial plasma conditions of section 6.2. The results for the simulated voltage drop and the resistance of the plasma (at $t = 2$ ns) are depicted in figure 6.5, together with the experimentally determined voltage drop [2]. Note that the experimental values are determined after 100 ps and the simulated values after 2 ns. After the fast plasma processes have taken place, the conductivity rises by a factor of two or less (depending on the chosen initial conditions) to its final value after 2 ns.

Figure 6.5 shows that the resistance of the plasma is high when a small current is switched ($\sim 800\ \Omega$) while it is only 20 Ω for high currents. This resistance at a high current is smaller than the geometrical impedance of the transmission lines of the spark gap (55 Ω). From the ratio of the resistances at the highest current ($I = 50$ A) it was calculated that 73% of the voltage is switched and 27% is lost over the gap. At the lowest current (highest plasma resistance) only 6% of the applied voltage is switched while 94% is lost. Figure 6.5 also shows that the resistance (and thus the switched voltage ratio) is strongly non-linear with the applied voltage.
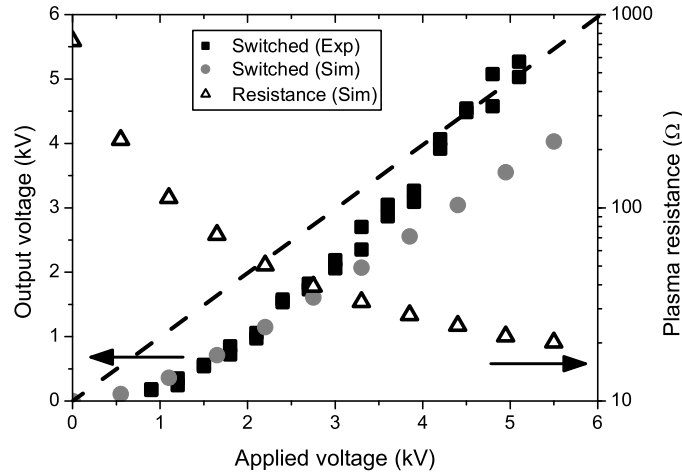
Figure 6.5. *Right axis: total resistance R of the switching plasma at t = 2 ns as a function of*
$V_{applied}$. *Left axis: the simulated (at t = 2 ns) and measured (at t = 100 ps) [2] fraction of the
applied voltage that is switched over the spark gap.*

As mentioned, we do not know the exact starting condition of the plasma. The initial
electron temperature does not play a significant role after the first couple of ps anymore,
because it has stabilized. However, there could be a 2 orders of magnitude difference in the
initial electron density, resulting in a different starting conductivity and therefore also in a
different final conductivity (after 2 ns). This makes it plausible that the resistance-curve
could just as well be somewhat higher or lower. Within this margin, we can conclude that,
at least qualitatively, the plasma simulation results match the experimental results.

6.5   Conclusions

When switching a spark gap photoconductively we observed a voltage drop over the gap,
which became more pronounced when lower voltages were switched. We investigated two
possible causes for this voltage drop, namely the cathode fall in the switching plasma and
the resistance of the plasma arc.
Based on an analytical model, we showed that the cathode fall formation time has a neg-
ligible influence on the rise time of the switched high-voltage pulse. The voltage drop
over the cathode fall is typically three orders of magnitude lower than the experimentally
observed voltage drop (1-10 V vs 1 kV). This means that the cathode fall can not be the
cause of the observed voltage drop over the spark gap.
We gave an analytical description of the most important plasma processes that take place

in the switching plasma in the first couple of ps. Together with a one-dimensional, time-dependent non-LTE fluid model of the (nitrogen) arc plasma we showed that the plasma processes stabilize within the first couple of ps to a more or less stable value. No rapid changes are to be expected after this stabilization period. The time scale of these processes (ps) can not yet be resolved experimentally. They do not significantly influence the measured rise time of the switched pulse, as expected for photoconductive switching and observed in the experiments. A range of switching currents was used to simulate the resistance of the plasma. The result is a qualitative match between the measured voltage drop and the simulated voltage drop, taking into account the poorly known initial plasma parameters. From this we can conclude that the finite resistance of the switching plasma is a function of the applied voltage and is likely the cause of the observed voltage drop over the gap.

This insight shows where improvements can be made to increase the efficiency for switching voltages far below self-breakdown. We saw that the initial electron density has only a limited effect on the plasma resistance. A straightforward increase in laser power to create a plasma with the same size but with a higher n_{e0} will therefore still result in a significant voltage drop. A better solution would be to create a larger switching plasma with the same n_{e0}. This will lead to a lower plasma resistance and a higher switching efficiency when switching lower voltages.

References

[1] G.J.H. Brussaard and J. Hendriks, Appl. Phys. Lett., 86, 081503 (2005)

[2] J. Hendriks, B.H.P. Broks, J.J.A.M. van der Mullen and G.J.H. Brussaard, J. Appl. Phys., 98, 043309 (2005)

[3] R.H. Fowler and L. Nordheim, Proc. Roy. Soc. A, 119 (781) p. 173 (1928)

[4] R. Hawley, High-voltage technology, L.L. Alston (Ed.), Oxford University Press, London, Ch. 5 (1968)

[5] G.A. Loew and J.W. Wang, Handbook of accelerator physics and engineering, A.W. Chao and M. Tigner (Ed.), World Scientific, Singapore, Ch. 6 (1998)

[6] B.J. Hopkins and J.C. Riviera, Proc. Phys. Soc., 81, 590 (1963)

[7] M.D. Lang and W. Kohn, Phys. Rev. B, 3 (4) 1215 (1971)

[8] S.C. Fain, jr. and J.M. BcDavid, Phys. Rev. B, 9 (12) 5099 (1974)

[9] J. Hendriks, S.B. van der Geer and G.J.H. Brussaard, J. Phys. D: Appl. Phys., 38, 2798 (2005)

[10] B.H.P. Broks, J. Hendriks, W.J.M. Brok, G.J.H. Brussaard and J.J.A.M. van der Mullen, accepted for publication in J. Appl. Phys. (2006)

Chapter 7

Electrodynamic simulations

Abstract

We present a full three-dimensional electrodynamic model to simulate a photoconductively switched high-voltage spark gap. This model describes the electromagnetic field-propagation in a coaxial spark gap setup, which determines the rise time of the switched pulse and reveals the influence of discontinuities, such as view ports, on the pulse shape and the rise time. Existing inductive lumped element and transmission line models, used to model laser-triggered spark gaps, are compared with our electrodynamic model. The rise time of the switched pulses in the different models does not differ significantly. In the electrodynamic simulation, a curvature of the electric field wave front is visible, resulting from the presence of non-TEM modes near the gap. Furthermore oscillations on the output signal are revealed. These oscillations are caused by internal reflections on the inner and outer conductors. Our electrodynamic model is able to visualize the rise time evolution by monitoring the electric field propagation in the gap region. The presence of view ports in the setup increases the rise time at the output significantly and induces, owing to internal reflections, extra oscillations in the signal.

7.1   Introduction

Spark gap switches are widely used to create high-voltage, high-power pulses. By using a laser to trigger a spark gap, shot-to-shot time variation (jitter) is minimized and voltages below the actual self-breakdown voltage can be switched.

Since the introduction of the laser in the 1960s, laser-triggered spark gap characteristics have been studied extensively. Guenther and Bettis [1] gave a detailed review on spark gap research done up to 1978. The influence of different lasers to trigger the spark gap was investigated elaborately [2–5] and detailed studies of the switching plasma were made [6, 7]. Several models have been proposed to describe the spark gap behavior. Levinson et al. [8] reported on a model that describes the inductive and electromagnetic effects of triggered spark gaps. Kushner et al. modeled the arc resistance and developed a laser-triggered spark gap plasma model [9, 10]. Persephonis et al. [11] gave an induction model for the spark gap discharge. Recently, Lehr et al. [12] gave an overview of the fundamental physical considerations for ultrafast spark gap switching.

In laser-triggered spark gaps, the rise time and time jitter of the switched pulses are important parameters. Avalanche and streamer formation, initiated by the trigger laser, cause the actual breakdown and close the spark gap switch. The rise time of the switched pulse is comparable with this breakdown time. Because of the stochastic nature of avalanche and streamer formation, time jitter of the switched pulse is significant. Most laser-triggered spark gap models are based on lumped element or transmission line theory, where the plasma is represented as a part of a lumped element electrical scheme or as a transmission line. These models give a good approximation for the behavior and the rise time for laser-triggered spark gaps that create (sub) ns high-voltage pulses. Recently, we demonstrated photoconductive switching of a spark gap with a femtosecond, high-power laser [13]. Photoconductive switching omits the stochastic breakdown processes of avalanche and streamer formation because the spark gap switch is closed almost instantaneously. Time jitter is reduced enormously while the rise time is no longer comparable to the plasma formation time. Electrodynamic details of the switching process, negligible in the laser-triggered case, become important now. Lumped element and transmission line models are not able to describe these electrodynamic effects in great detail.

We have developed a full three-dimensional electromagnetic spark gap model which is implemented in CST Microwave Studio [14]. This model simulates complete electromagnetic field-propagation in the switched spark gap and is able to predict rise times for different spark gap geometries. The inductive lumped element and the transmission line model are compared with our electrodynamic simulation results, on the basis of our experimental

setup parameters [13]. Finally, we show that our model is able to simulate the influence on the rise time and the pulse shape of discontinuities in the spark gap structure, like entrance ports for the laser or ports for (plasma) diagnostic purposes.

7.2   Different models

A schematic representation of a typical spark gap is given in Figure 7.1.
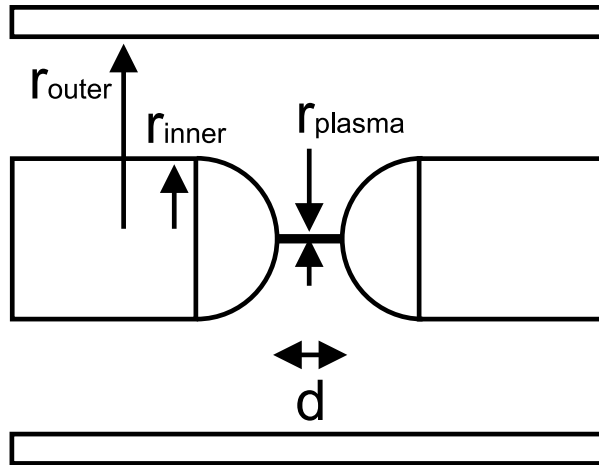
Figure 7.1. *Schematic spark gap setup with geometrical parameters.*

Table 7.1. *Setup properties of photoconductively switched spark gap setup.*

Inner conductor radius (r_{inner})	3 mm
Outer conductor radius (r_{outer})	7.5 mm
Coaxial impedance (Z_0)	54.9 Ω
Plasma radius (r_{plasma})	10 μm
Gap distance (d)	1 mm
Spark gap inductance (L')	1.33×10^{-6} Hm^{-1}
Spark gap capacitance (C')	8.40×10^{-12} Fm^{-1}
Spark gap characteristic impedance ($Z_{gap} = \sqrt{\frac{L}{C}}$)	398 Ω
Estimated spark resistance (R)	1000 Ω

In this coaxial spark gap setup, the inner conductor has a radius r_{inner} and the outer conductor has an inner radius r_{outer}. The gap distance is given by d and the created plasma has a radius r_{plasma}. Initially, one of the conductors is charged to a high voltage (> 1 kV)

while the other is not. At $t = 0$, a laser is focused in the gap. Owing to the laser-induced plasma formation, the charged conductor can discharge and a high-voltage pulse is created.

Lumped element, transmission line and two-dimensional cylindrical-symmetric electrodynamic simulations are compared. We use the experimental parameters of the photoconductively switched spark gap setup [13] for comparison. These parameters are given in table 7.1.

7.2.1 Inductive lumped element model

An often used model to simulate spark gaps uses an inductor to model the plasma [8, 10, 12]. This is a zero-dimensional model where propagation times of signals in the different elements are not taken into account. The result is a purely inductive circuit with two resistors. Figure 7.2 shows the circuit for this model.
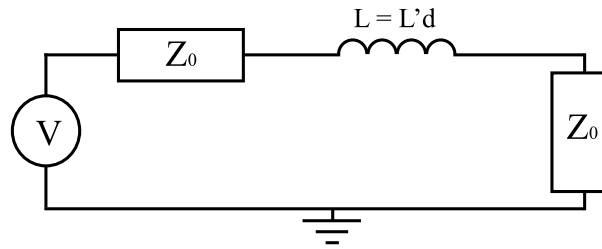
Figure 7.2. *Lumped element scheme of the spark gap setup with our experimental parameters (see table 7.1).*

For this scheme, the voltage as a function of time is given by

$$V(t) = \frac{V}{2}\left(1 - \exp\left(-\frac{2Z_0}{L}t\right)\right), \qquad (7.1)$$

in which Z_0 is the impedance of the coaxial lines and L is the inductance of the spark gap. Following Levinson et al. [8], we define the rise time as the time it takes to reach 90% of the amplitude:

$$t_{rise} = 2.2\frac{L}{2Z_0}. \qquad (7.2)$$

The inductance is given by

$$L = \frac{\mu_0 d}{2\pi} \ln\left(\frac{r_{outer}}{r_{plasma}}\right). \qquad (7.3)$$

The minimum achievable rise time is limited by the inductance. The inductance is determined by the plasma radius, the radial spark gap geometry and the gap distance. The gap distance limits the maximum applicable voltage over the spark gap.

7.2.2   Transmission line model

If the spark gap setup is treated as a composition of transmission lines, the following scheme is used (figure 7.3):
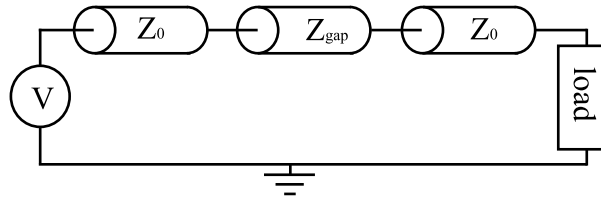
Figure 7.3. *Transmission line scheme of spark gap.*

A lossy transmission line with an inductance, capacitance, resistance and a certain length represents the plasma. Transmission lines with characteristic impedances Z_0 represent the coaxial parts of the setup before and after the gap.

With the transmission line approximation, travelling waves in one dimension (propagation direction) in the transmission line setup are modelled. Only one propagating mode (TEM) is considered. These travelling waves encounter (partial) reflection at a transition in the setup where characteristic impedances are not matched. If the load (and source)-impedance is equal to the plasma-impedance, no reflections occur at the plasma-conductor-boundary and the rise time of the pulse is infinitely fast. In practice, however, the plasma-impedance is not matched to the input and output impedance. In our setup, two such impedance boundaries are present: the conductor-plasma boundary and the plasma-conductor boundary. Because of this mismatch, the pulse is transmitted only partially at each boundary and multiple reflections occur in the plasma part, between the two boundaries. The result at the output is a signal that converges stepwise and asymptotically to its end-value ($V/2$). The height and the length of these steps depend on the mismatch and the length of the plasma, respectively.

Because the characteristic impedance in our setup is similar at the input and the output side, the same reflection-coefficient can be used for both boundaries.

Assuming no losses, the reflection-(Γ) and transmission-coefficient (T) are given by [15]:

$$|\Gamma| = \left| \frac{Z_{gap} - Z_0}{Z_{gap} + Z_0} \right| \tag{7.4}$$

$$T = 1 - |\Gamma| \tag{7.5}$$

The output voltage is a summation of all the transmitted parts of the signal:

$$V = \sum_n VT|\Gamma|^{2n} \left(|\Gamma| + 1 \right) \tag{7.6}$$

The signal increases stepwise with each reflection at the plasma-conductor interfaces. The first step at the output (n=0) starts at 3.3 ps after the arrival of the laser pulse, i.e. the time it takes to cross the gap of 1 mm in our setup geometry. All the following steps take twice this time, i.e. the time it takes for the reflected part to travel back to the first boundary and forward again to the output. In this transmission line model, the rise time is limited by matching only. L and C of the plasma determine the matching and these, in turn, depend on the plasma and spark gap dimensions.

7.2.3   Electrodynamic model

To calculate the full electrodynamic behaviour of the spark gap, we need to take into account all propagation delay times and all electromagnetic field orientations (thus also non-TEM modes). For this purpose, we numerically solve Maxwell's equations in time-domain by means of the finite integration technique (FIT). This brute-force method, introduced in 1977 by Weiland [16], has been proven to provide accurate and stable results [17] for a variety of applications.

The FIT technique discretizes both Maxwell's equations and the geometry under investigation to a rectangular (hexagonal) grid. Subsequently, the full three-dimensional field-propagation is calculated in time-domain with a leap-frog method. Spatial discretization can be significantly improved by taking into account the 'filling factor' of each cell, optionally combined with the use of a non-equidistant mesh to refine the calculation at the position of small features. It should be noted that the latter is at the cost of a global decrease in the maximum stable time step hereby slowing down the simulation. The best known application for the FIT technique are the calculations of reflection- and transmission-coefficients for waveguide structures. In these simulations, the system is typically fed with an eigenmode of an attached port to obtain the reflected and transmitted amplitudes of selected eigenmodes of all ports in the system. Fourier analysis is the obvious final step to determine the frequency response based on the time-domain signals. The FIT technique forms the core of a variety of public-domain and commercial electromagnetic solvers. We

use one of them, CST Microwave Studio [14], to simulate the electrodynamic behavior of the spark gap.

To compare the lumped element and transmission line approaches with the electrodynamic model, described earlier, we use the (two-dimensional) cylindrical-symmetric setup of figure 7.1. The photoconductive switching situation can be divided into two parts: first, we have a static situation where one conductor is charged. This is the static starting situation. Next the laser is fired and almost instantaneously a current starts to run through the laser-induced plasma and the rest of the setup. This is the dynamic situation where electromagnetic fields propagate in the spark gap setup. To our knowledge, no commercially available electromagnetic field simulator is able to simulate the transition from a static situation into a dynamic pulse directly. We therefore need to approximate the static starting situation (one conductor charged, the other not and no plasma present yet) in a dynamic simulation model.
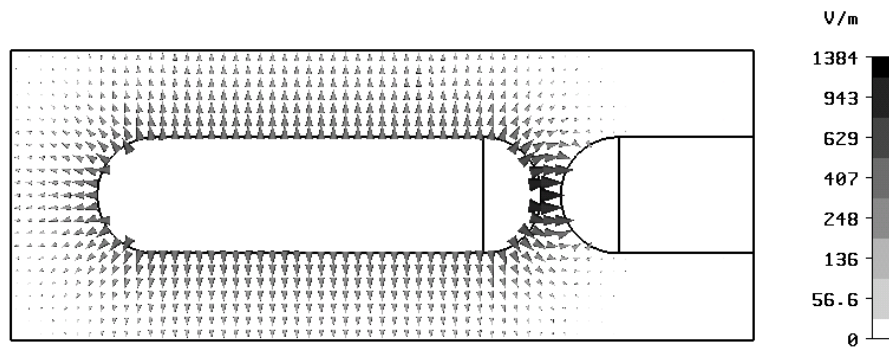
Figure 7.4. *Electric field (amplitude and direction) in the simulated setup at the static starting situation of the switching process.*

In the starting situation, a static electric field is present in the gap region. We apply a potential difference between the two inner conductors, comparable with the field present in the static situation. This starting-field can be simulated in Microwave Studio by putting a thin wire with ideal voltage sources in the gap. Some time, after the voltage sources are switched on, the static situation is reached. Now the left conductor is charged but the right one is not. The electric field-map at this time is shown in figure 7.4. Although, obtained less efficient, it is identical to a field-map created with an electrostatic solver. This electrostatic field-pattern is the starting situation of the switching process.

When we, subsequently, switch off the voltage sources, the left charged conductor can discharge through the thin wire in the gap and the switched pulse can travel to the right (output side). Thus, by switching off the voltage sources in the gap, the (instantaneous)

creation of the plasma channel by the laser in the gap is simulated. In this electrodynamic model, the plasma is represented by an infinitely thin, ideal conducting wire. These assumptions are no limitations of the simulation model: A non-equidistant mesh can be used to model a relatively small plasma channel inside the spark gap. Plasma channels with a certain thickness and dielectric constant can be implemented and also a finite creation time of the plasma can be defined.
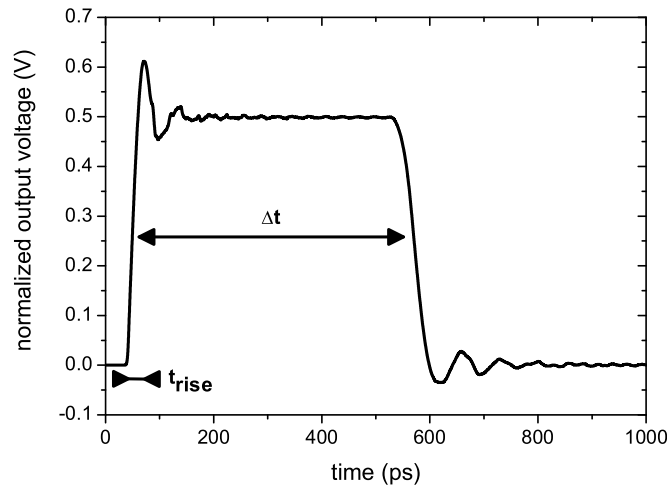
Figure 7.5. *TEM output signal at output side of the spark gap setup; Δt = pulse width, t_{rise} = rise time.*

The signal at the output side of the spark gap is given in figure 7.5. This is the signal of the TEM mode that has propagated through the setup. At $t = 0$ ps, the source signals are turned off instantaneously and the charged conductor can discharge. It takes 40 ps for the pulse to reach the output port. The pulse width (Δt) is 520 ps and is determined by the length of the charged conductor (78 mm). There is an overshoot of the signal, followed by some oscillations, which are caused by internal reflections in the setup. To ease the comparison with the other models, we chose to only investigate the time-domain output and not the frequency analysis, that typically goes hand-in-hand with the FIT integration technique.

In order to get more insight in the electrodynamics of the switching process, the electromagnetic field-propagation is monitored in time. Figure 7.6 shows the electric field variation (isolines of electric field amplitude) in time [1].

---

[1]For clarity the situation after switching the voltage sources on is given here. Due to symmetry, this is exactly the same situation as after switching the voltage sources off.
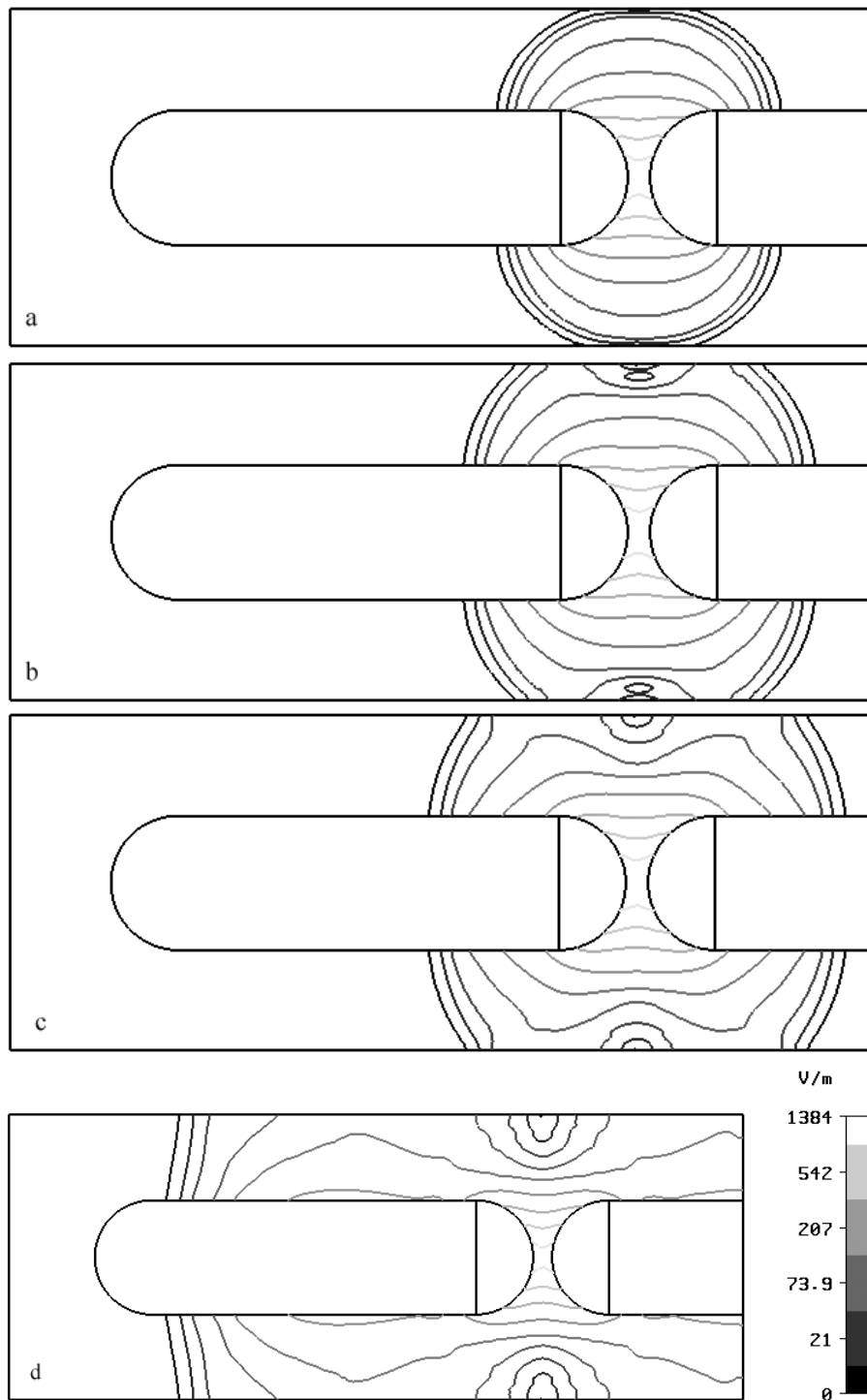
Figure 7.6. *Electric field maps (isolines) to show the shape of the wave fronts at t = 30 ps (a), t = 35 ps (b), t = 40 ps (c) and t = 75 ps (d).*

From figure 7.6 can be seen that electric (and magnetic) fields propagate almost spherically from the center (the plasma) to the outer conductor (figure 7.6(a)). When the outer conductor is reached, the electromagnetic field propagates further through the coaxial setup with a curved wave front (7.6(b) and 7.6(c)). This curved wave front is caused by the presence of TE and TM modes (in addition to the TEM mode), which also propagate through the setup. While the TEM-mode propagates undisturbed through the coaxial part, the non-TEM modes experience dispersion [18]. Because of this dispersion, the influence of these non-TEM modes on the rise time at the output is negligible (only 1% of the total signal). Dispersion of the non-TEM modes is visible when comparing the curvature of the wave fronts in figure 7.6(b) and 7.6(d).

7.2.4 Comparison of the different models

The results of the three models are compared using the experimental parameters of [13] (table 7.1).
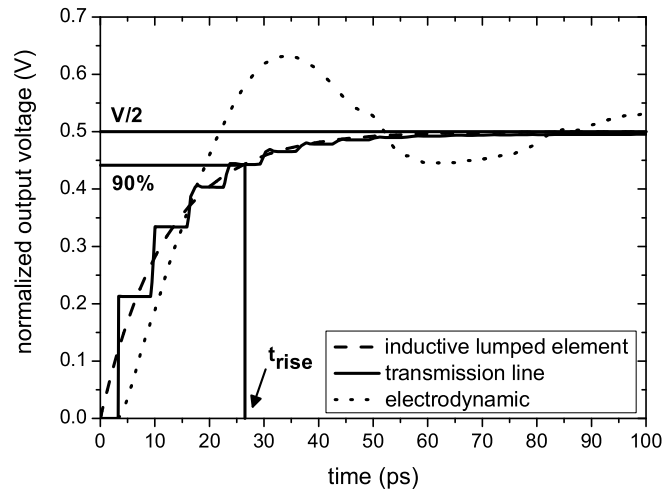
Figure 7.7. *Comparison of three simulation models, inductive lumped element (dashed), transmission line (solid) and electrodynamic (dotted).*

The inductive lumped element model, equation (7.1), and its rise time, equation (7.2), are depicted as the dashed line in figure 7.7. The rise time to 90% of the output voltage is 26.6 ps. The lumped element model does not take into account the delay of the transmission lines. In this model, $t = 0$ is the time at which the switch is closed and coincides with the onset of the signal. In the other two models, the transmission line model and the electrodynamical model, there is a delay between the arrival of the laser pulse, i.e. the

closing of the switch and the voltage pulse at the end of the transmission line. For better comparison, we have subtracted this delay. Both these signals then start at 3.3 ps after the arrival of the laser pulse. 3.3 ps is the transmission time of the pulse through the 1 mm gap. The transmission line model (the solid line in figure 7.7) shows the stepwise increase of the signal, caused by the multiple reflections on the plasma-conductor boundaries. Each step is delayed by 6.7 ps, which is the time for the reflected pulse to travel back through the gap, reflect at the first boundary and travel forward again. The resulting rise time to 90% of the output voltage is 23.3 ps, comparable to the rise time of the lumped element model.

The electrodynamic model is shown as the dotted line in figure 7.7. The rise time to 90% of the final output voltage is 19 ps. This model, however, shows a clear overshoot and oscillations. These oscillations are significant (up to 20% of the total signal) and are caused by reflections on the outer conductor. This effect is not visible in the lumped element and transmission line models, since they do not take the radial size of the setup into account. In the electrodynamic model, the rise time at some distance from the gap region is mainly determined by the buildup time of a stable TEM-mode. This time is comparable to the time needed for the electromagnetic field disturbance in the center of the gap to propagate to the outer conductor. Thus, the spark gap geometry determines the rise time, just as in the lumped element and the transmission line model. The rise time to 90% of the final output voltage, calculated using the different models, is summarized in table 7.2.

Table 7.2. *Rise time to 90% of the output voltage for different models.*

Model	Rise time (ps)
Lumped elements	27
Transmission lines	23
Electrodynamics, without ports	19
Electrodynamics, with ports	24

7.3 Three-dimensional electrodynamic simulation of a spark gap setup with discontinuities in the outer conductor

In the previous section we verified that the electrodynamic model is able to simulate the switching behavior of a cylindrical-symmetric spark gap. However, an experimental setup is generally not cylindrical-symmetric. We use our experimental setup [13], which is depicted
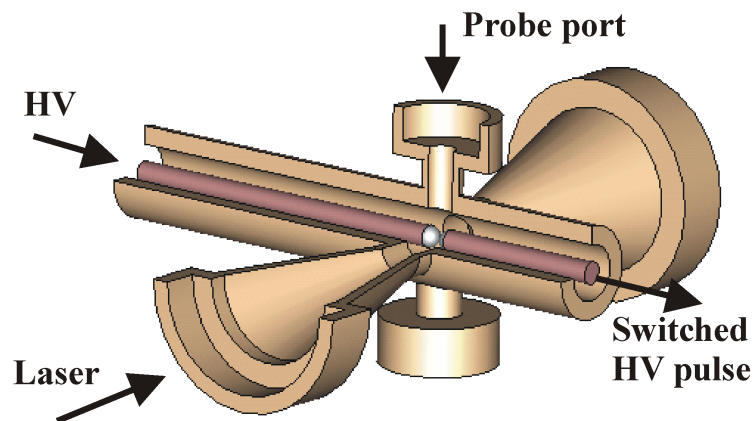
Figure 7.8. *Simulated setup with laser and probe ports.*

in figure 7.8. It contains ports to couple in the switching-laser and ports for diagnostic purposes. We want to know how the presence of these openings influences the shape of the output signal, especially the rise time. This is impossible to simulate with a lumped element or transmission line approach, but can be done with the electrodynamic model. The electrodynamic model is able to simulate electromagnetic field-propagation in full three dimensions. The influence of discontinuities in the coaxial spark gap setup on the electromagnetic field-propagation and thus on the rise time of the output pulse can be monitored.

Electric field maps of the three-dimensional simulation are given in figure 7.9. The discontinuities of the ports in the coaxial structure cause a complex field distribution. For these simulations, the ports were treated as open boundaries, operating like free space with minimal reflections. In figure 7.10, the output signals of simulations with and without ports are given. The rise time in the setup with ports is about 5 ps longer than in the setup without ports. It takes more time to build up the stable TEM-mode because of the ports. Also, more oscillations are present. These originate from the presence of the ports causing more internal reflections.
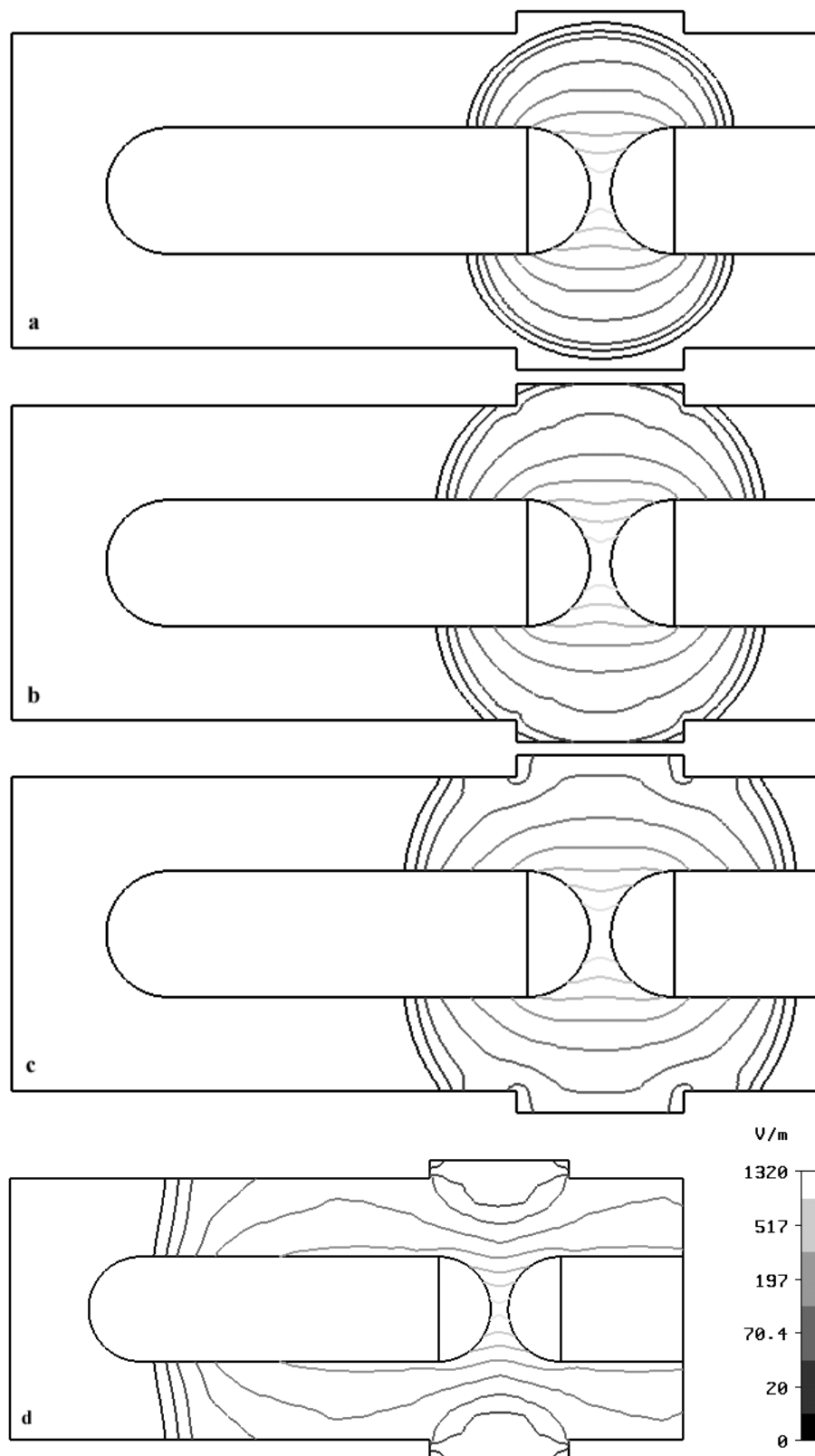
Figure 7.9. *Electric field map (isolines) to show the complex shape of the wave fronts in the setup
with ports at t = 30 ps (a), t = 35 ps (b), t = 40 ps (c) and t = 75 ps (d).*
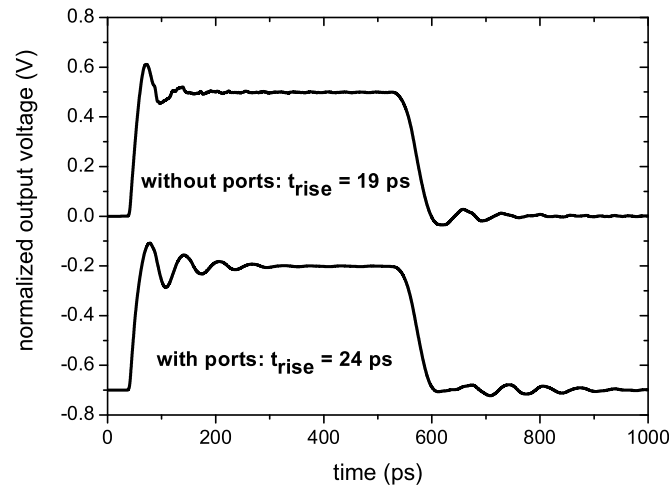
Figure 7.10. *Comparison of output signals of simulations with and without ports.*

7.4   Conclusions

We compared different existing spark gap models with a new developed electrodynamic model. This model simulates the electromagnetic field-propagation in coaxial spark gap structures, determines the rise time of switched pulses and reveals the influence of discontinuities in the gap. The rise times determined with a zero-dimensional lumped element approach and a one-dimensional transmission line approach are comparable with the two-dimensional cylindrical-symmetric electrodynamic simulation. In the two-dimensional case, a curvature of the electric field wave front is visible, indicating the presence of non-TEM modes near the electrodes. These non-TEM modes do not influence the rise time significantly due to dispersion. Also, oscillations in the signal of the two-dimensional simulation are present. The oscillations are caused by internal reflections on the inner and outer conductors.

The lumped element and the transmission line models are limited to spark gap geometries without ports. The influence of port-discontinuities in the geometry on the rise time can be determined with the three-dimensional electrodynamic model. These ports significantly increase the rise time at the output.

7.5   Acknowledgements

References

[1] A.H. Guenther and J.R. Bettis, J. Phys. D, 11 (11) p. 1577 (1978)

[2] J.R. Woodworth, P.J. Hargis, Jr., L.C. Pitchford and R.A. Hamil, J. Appl. Phys. 56, 1382 (1984).

[3] L. Ya. Polonskiy, A. Yu. Goltsov and A.V. Morozov, Phys. Plasmas, 3, 2781 (1996)

[4] S. Soubacq, P. Pignolet and S. Mendonca, J. Phys. D, 35, 1955 (2002)

[5] B.M. Luther, L. Furfaro, A. Klix and J.J. Rocca, Appl. Phys. Lett., 79 (20) p. 3248 (2001)

[6] W.D. Kimura, M.J. Kushner, E.A. Crawford and S.R. Byron, IEEE Trans. Plasma Sci., 14, 246 (1986)

[7] R. Najafzadeh, E.E. Bergmann and R.J. Emrich, J. Appl. Phys., 62, 2261 (1987)

[8] S. Levinson, E.E. Kunhardt, M. Kristiansen and A.H. Guenther, Proc. 2nd IEEE Pulsed Power Conference, Lubbock, Texas, USA, p. 433 (1979)

[9] M.J. Kushner, W.D. Kimura and S.R. Byron, J. Appl. Phys., 58 (5) 1744 (1985)

[10] M.J. Kushner, R.D. Milroy and W.D. Kimura, J. Appl. Phys., 58 (8) 2988 (1985)

[11] P. Persephonis, K. Vlachos, C. Georgiades and J. Parthenios, J. Appl. Phys., 71 (10) 4755 (1992)

[12] J.M. Lehr, C.E. Baum, W.D. Prather and R.J. Torres in ultra-wideband, short pulse electromagnetics 4, E. Heyman, Ed. New York: Kluwer Academic/Plenum Publishers, p. 11. (1999)

[13] G.J.H. Brussaard and J. Hendriks, Appl. Phys. Lett., 86, 081503 (2005)

[14] CST Microwave Studio Version 5, CST GmbH, Germany (2003)

[15] G. Metzger and J. Vabre, "Transmission lines with pulse excitation", Academic Press, Inc., New York, p. 51 (1969)

[16] T. Weiland, Electronics and Communication (AE), 31 p. 116 (1977)

[17] R. Schuhmann and T. Weiland in Geometrical Methods in Computational Electromagnetics, volume 32 of Progress in Electromagnetic Research (PIER), EMW Publishing, Cambridge, Massachusetts, USA, p. 301 (2001)

[18] J.D. Jackson, "Classical Electrodynamics, 3rd ed.", John Wiley and Sons, Inc., New York, p. 356 (1999)

Chapter 8

Spark gap optimization by electrodynamic simulations

Abstract

When switching times are no longer dominated by the plasma formation time, such as for photoconductive switching of high-voltage spark gaps, electrodynamic details of the switching process determine the rise time and pulse shape of the switched pulse. We show that the commonly used zero-dimensional lumped element and one-dimensional transmission line theory are no longer sufficient for optimizing such fast-switching devices, because important electromagnetic-field propagation in three dimensions is neglected. In order to improve the output of the photoconductively switched spark gap, we developed an optimization procedure for spark gap geometries based on full three-dimensional electrodynamic simulations. By monitoring the electromagnetic-field propagation in time, it will be shown that the initial electromagnetic-field disturbance in the gap reflects at the outer conductor and interferes with the initial field. The reflection and interference are essential for the shape of the output signal. We propose the following optimization procedure to improve the output of the photoconductively switched coaxial spark gap. Initially, the reflection and interference can be influenced by reshaping the inner conductor. The outer conductor can be used to fine-tune the system to get an output pulse with a sharp rising edge and no significant oscillations. We also present the optimal spark gap geometry that gives the best output signal at photoconductive switching.

8.1   Introduction

A widely used device to create high-voltage, high-power pulses is the spark gap switch. By using a laser to trigger a spark gap switch, it is possible to switch voltages below the self-breakdown voltage of the gap and to minimize the shot-to-shot time variation (jitter), allowing for better synchronization between different high-voltage devices.

After the discovery of the laser in the early 1960s, extensive research on laser-triggered spark gaps began. A wide variety of laser types and spark gap geometries have been investigated [1–6] and the switching plasma was also studied in detail [7, 8]. The rise time of the switched pulse and the time jitter between different pulses are important parameters in the field of high-voltage switching. Although a laser improves the time jitter significantly, the breakdown and closure of the gap are still dominated by stochastic plasma processes. The laser initiates free electrons in the gap and via avalanche and streamer formation the switch finally closes at breakdown (arc formation) of the gap. The rise time of the switched high-voltage pulse is comparable with the time it takes for this breakdown process to occur. However, this process of avalanche and streamer formation is stochastic and the time jitter of the switched pulse will be significant.

Recently, we demonstrated photoconductive switching of an (atmospheric) air-filled spark gap with a femtosecond high-power laser [9, 10]. At photoconductive switching the complete gap is ionized and closed almost instantaneously by the high-power laser, omitting the stochastic breakdown processes of avalanche and streamer formation. The time jitter is reduced enormously and the rise time of the switched pulse is no longer comparable to the plasma formation time. Because plasma processes are no longer determining the rise time at photoconductive switching, we needed a model that was able to visualize the effects of the electrodynamic details of the switching process. For this we developed a full three-dimensional electromagnetic spark gap model that simulates complete electromagnetic field-propagation in the switched gap and is able to predict rise times for different spark gap geometries [11].

In this paper we will show that we can use this numerical model to optimize the geometry of the photoconductively switched spark gap to achieve an even better output pulse. In the literature, an optimal spark gap configuration is derived based on lumped element and transmission line theory. We will first show that this theory is not sufficient for optimizing the photoconductively switched spark gap. Then, after a brief description of the model we will describe in detail the electrodynamic processes and the influence of the geometry on the switched pulse. Finally, we will give a recipe for the design of the optimal spark gap geometry and propose a configuration for the optimal output signal at photoconductive

switching.

8.2   Three-dimensional electrodynamic spark gap model

When the switching time is no longer dominated by the plasma formation time in the spark gap, such as for photoconductive switching, electrodynamic details of the switching process determine the rise time and pulse shape of the switched pulse. To describe these details we developed a full three-dimensional electromagnetic spark gap model [11], implemented in Microwave Studio [12]. This model is able to simulate rise times for different spark gap geometries and to visualize the complete electromagnetic field-propagation in a photoconductively switched spark gap by solving Maxwell's equations in time-domain. We will describe the model briefly here. A more detailed description can be found in [11].
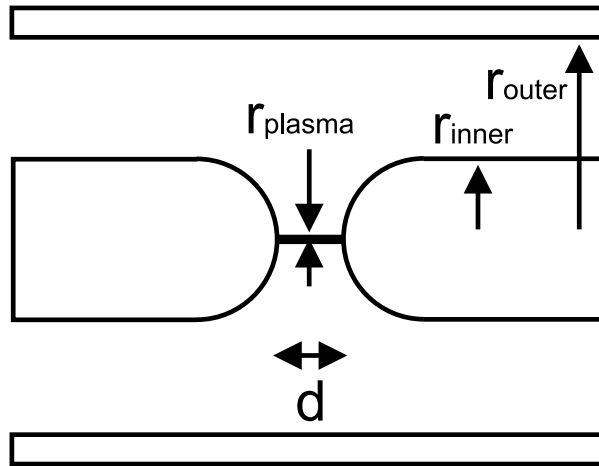
Figure 8.1. *Schematic spark gap setup with geometrical parameters.*

A schematic spark gap is depicted in figure 8.1. It consists of a coaxial transmission line with inner conductor radius r_{inner} and outer conductor radius r_{outer}, interrupted by the spark gap (width d). r_{outer}/r_{inner} is chosen such that the impedance at the output is around 50 Ω, d is smaller than r_{outer} and $r_{plasma} \ll r_{inner}$. The photoconductive switching process consists of two parts: First, a static electric field is present in the gap. One conductor is charged, the other is not and no switching plasma is present yet. This is the static starting situation of the switching process. Subsequently, the laser is fired and a current starts to run, almost instantaneously, through the laser created plasma (spanning the whole gap) and the rest of the setup. This is the dynamic situation where electromagnetic fields propagate through the setup.

We were able to simulate this static-dynamic transition by using a thin wire with an array of voltage sources in the gap. First a potential difference is applied over this wire, resulting in the static situation where one conductor is charged and the other is not. Subsequently the voltage sources are switched off and the charged conductor can discharge through the thin wire in the gap. A pulse starts to travel to the output side. Thus, switching off the voltage sources simulates the (instantaneous) creation of the plasma channel in the gap by the femtosecond laser, approaching the photoconductive switching process.

This (transient) model is capable of monitoring the electrodynamic field-propagation in time. From this we concluded that the rise time of the output pulse is determined by the time it takes for a stable TEM-mode to build up in the gap region [11].

8.3   Spark gap optimization according to the literature

The geometry depicted in figure 8.1 is the geometry of our experimental photoconductively switched spark gap (see table 8.1 and references [9, 10]). In order to improve the rise time of the switched pulse we want to optimize this geometry.

Optimization in the literature is often based on lumped element and transmission line theory. A spark gap is often modelled as a lumped element system where the switching plasma is represented by an inductor L and the coaxial part of the setup as an impedance Z. The rise time of the switched pulse is then proportional to the inductance and inversely proportional to the impedance of the coaxial part:

$$t_{rise} \propto \frac{L}{Z}, \tag{8.1}$$

where L, in turn, is proportional to the outer conductor radius and the plasma radius by

$$L \propto \left(\frac{r_{outer}}{r_{plasma}} \right). \tag{8.2}$$

This implies that the rise time can be minimized if the inductance (and thus r_{outer}) in the gap region is minimized. Rise time enhancement by induction minimization is proposed in several articles [13–15].

From a transmission line point of view, the impedance through the whole setup has to be as constant as possible. An abrupt change in impedance results in reflections of the

transmitted signal and thus in a decrease of output efficiency [11]. This means that the transmission line part of the setup has to be smoothly matched to the gap part. Taking these considerations into account, the optimal spark gap geometry proposed in the literature [14, 15] is shown in figure 8.2. This biconical gap minimizes the intrinsic inductance of the spark channel (and thus enhances the rise time) and maintains a quasi-constant impedance throughout the setup to avoid major power loss.
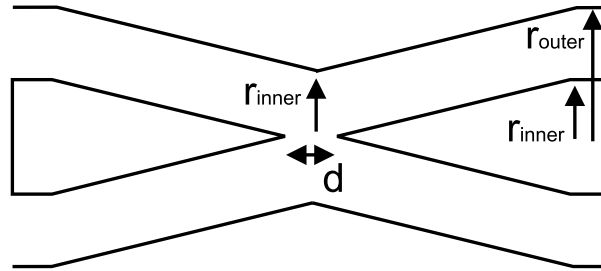
Figure 8.2. *Biconical spark gap with quasi-constant impedance for optimal rise time and power transmission proposed in the literature.*

The optimal spark gap configuration as proposed in the literature (figure 8.2) can be simulated with our electrodynamic model. We used our experimental dimensions, listed in table 8.1. For comparison, we included the simulation result of the geometry of figure 8.1. The simulation results for both configurations are shown in figure 8.3.

Table 8.1. *Geometry parameters of the experimental photoconductively switched spark gap [9, 10].*

r_{inner}	3 mm
r_{outer}	7.5 mm
d	1 mm
r_{plasma}	10 μm

The signal from the biconical spark gap turns out to be far from optimal. Initially, there is a fast rising edge, comparable to the rising edge of the non-tapered gap, but it stops about halfway to its final value. From here it oscillates slowly to its final value. It seems to behave like an over-damped system. The non-tapered gap looks like an under-damped system. Its rise time to the final value is much better. Thus, the suggested optimal configuration does not give an optimal result in our three-dimensional electrodynamic model. This can be explained by the difference between laser triggering, where the lumped element and transmission line models suffice, and photoconductive switching where electrodynamic details
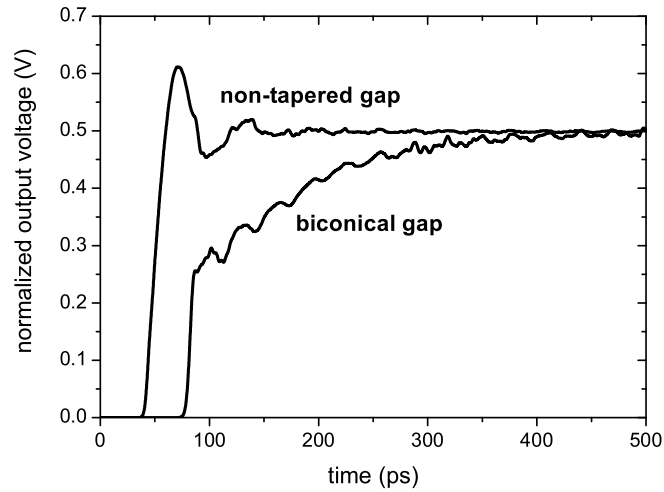
Figure 8.3. *Simulated output TEM signal of the optimal spark gap configuration as proposed in the literature (biconical gap, figure 8.2) and the non-tapered spark gap configuration (figure 8.1, [11]). An offset in time is generated for clarity.*

are important. At laser triggering the actual breakdown and switching are dominated by plasma processes which take place at (sub-)ns time scales. Electrodynamic details are not significant on these time scales and the zero and one-dimensional theories give a sufficient description. However, at photoconductive switching these plasma processes are omitted and electrodynamic details at ps time scales are dominant for the switching process. The rise time is determined by the time it takes for a stable TEM-mode to build up in the gap region [11]. This three-dimensional phenomenon makes lumped element and transmission line theory insufficient for an accurate description of the switching processes and, therefore, also insufficient for optimization.

8.4 Electrodynamic optimization of the spark gap configuration

The optimal spark gap should be able to transfer a pulse with a smooth rising edge and a flat top. No oscillations should be present in the signal. Such an ideal pulse on a coaxial line is given in figure 8.4.

The pulse consists of a smoothly-shaped rising edge and a flat top. In this example the rise time is 20 ps, close to our target value. The distribution of lines of constant electric
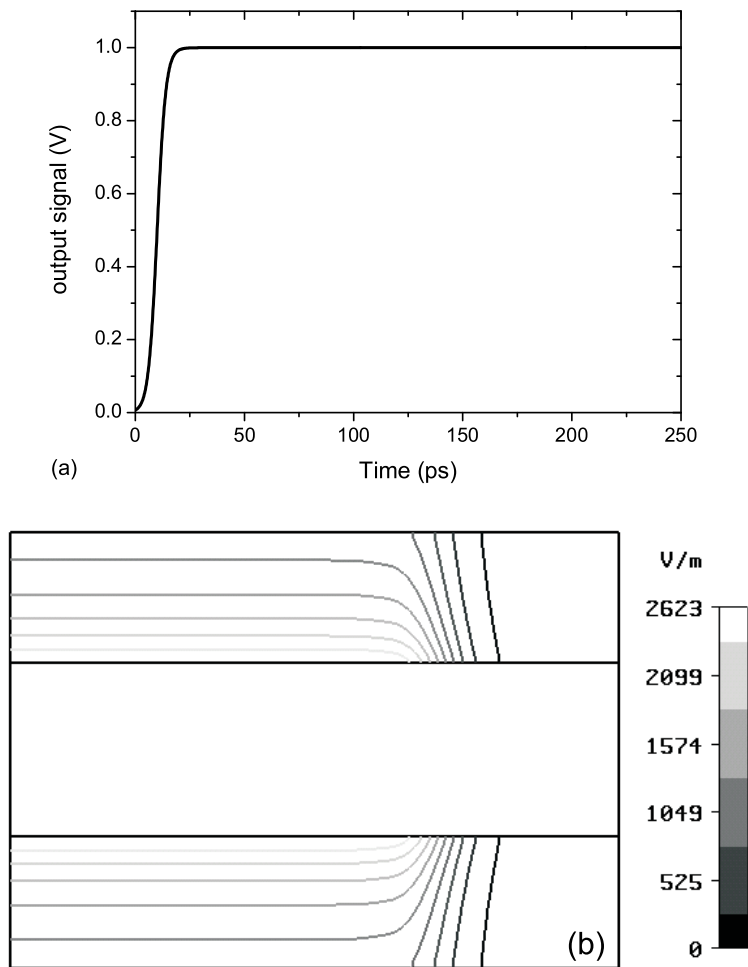
Figure 8.4. *"Ideal pulse" (a) and the corresponding electric field-strength distribution (b).*

field-strength is also given. The front of the pulse consists of lines almost perpendicular to the conductors. The flat top part of the pulse consists of lines parallel to the conductor, indicating that a stable TEM-mode has formed. The transition between the front and the flat top part is smooth. This is the field line distribution that results in an "ideal output pulse": the one we want to have after switching.

As mentioned, with the spark gap model we are able to monitor the electromagnetic field-propagation in time after switching. For clarity we will monitor only the electric field-propagation here. When the spark gap is switched, an (initial) electric field starts to propagate spherically from the middle of the gap to the outer conductor. This is visualized in figure 8.5.
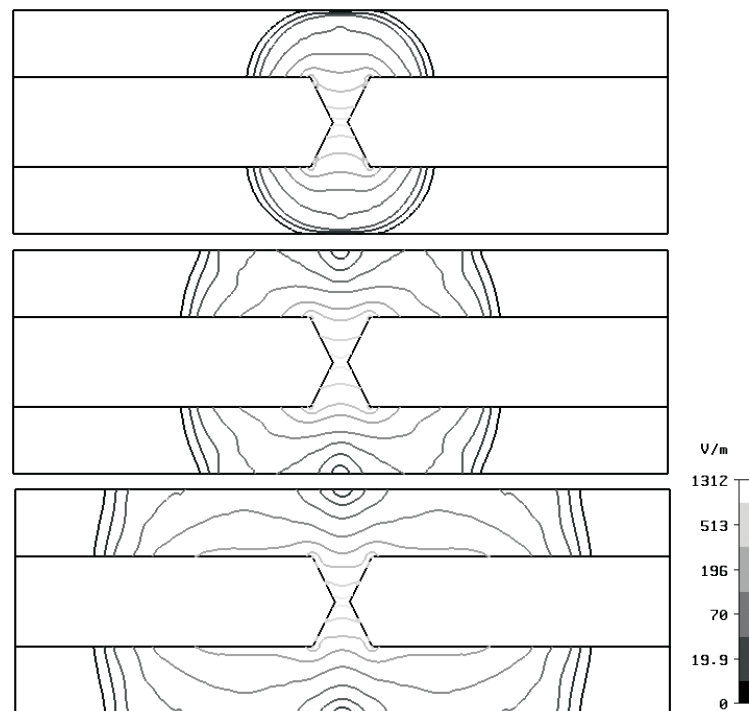
Figure 8.5. *Pulse propagation after switching. Lines of constant electric field strength are depicted.*

When the field reaches the outer conductor, it reflects on the outer conductor and is transmitted (spherically) back into the gap region again. This reflected field interferes with the initial field, resulting in a reshaping of the orientation of the electric-field strength lines. While the first field-front has already propagated into the coaxial part of the structure, the reshaped part follows this initial part. The idea is now to reshape the conductors in such a way that, with the help of the field-interference, the field gets the distribution of the ideal pulse as depicted in figure 8.4.

8.4.1 Optimization procedure

In order to mould the field two parameters can be varied, namely the shape of the inner and outer conductor. We investigate first the influence of the inner conductor. As a start we will use tapered inner conductors with sharp (not rounded off) edges. Although these sharp edges are not practical, because of field enhancements, they give a clearer insight into the physics of the system. Later on we will suggest a more practical solution. Figure 8.6 shows the TEM output signal for four different inner conductors, from the sharp (right) to the blunt (left). The time of arrival of the signal at the output is offset for clarity. In figure 8.7 the accompanying electric-field strength pictures of the different geometries are

depicted, just before the field reaches the output.
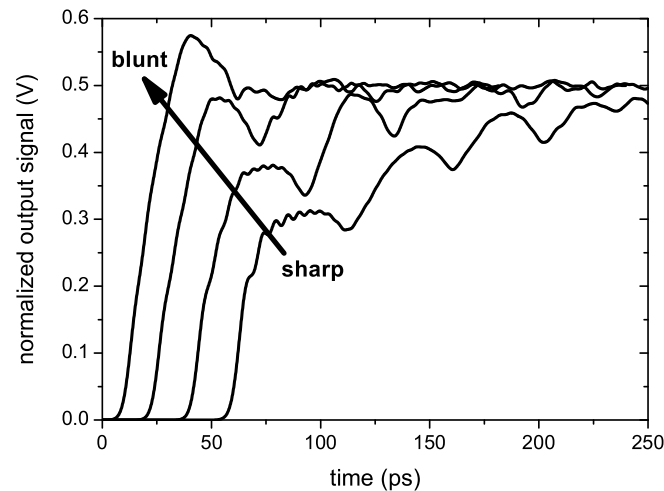
Figure 8.6. *TEM output signals of geometries with different sharpness of the inner conductor. The curves are offset in time for clarity.*

At the sharpest tip (right curve in figure 8.6) the output signal is an over-damped signal. The first rising edge does not go all the way to the final value, but stops halfway. From here the signal oscillates slowly to its final value, resulting in a bad rise time. When the inner conductor gets more blunt the over-damping of the output signal decreases and turns to an under-damped signal at very blunt conductors (left curve in figure 8.6). Here a slight overshoot in the output signal is visible.

When the conductors are made more blunt the electric-field strength figure becomes comparable with the "ideal pulse" field strength distribution (up to a certain optimal bluntness). At the sharp tip (figure 8.7(a)) the influence of the reflected electric field at the outer conductor is severe and the fields keep oscillating in the gap region for a long time. The electric field strength lines in the gap region are constricted so much that an over-damped signal reaches the output. The more blunt the conductor is, the less is the influence of the reflected signal on the final output signal.

The second parameter that can be varied is the amount of constriction of the outer conductor. Two different constriction radii are shown in figure 8.8.
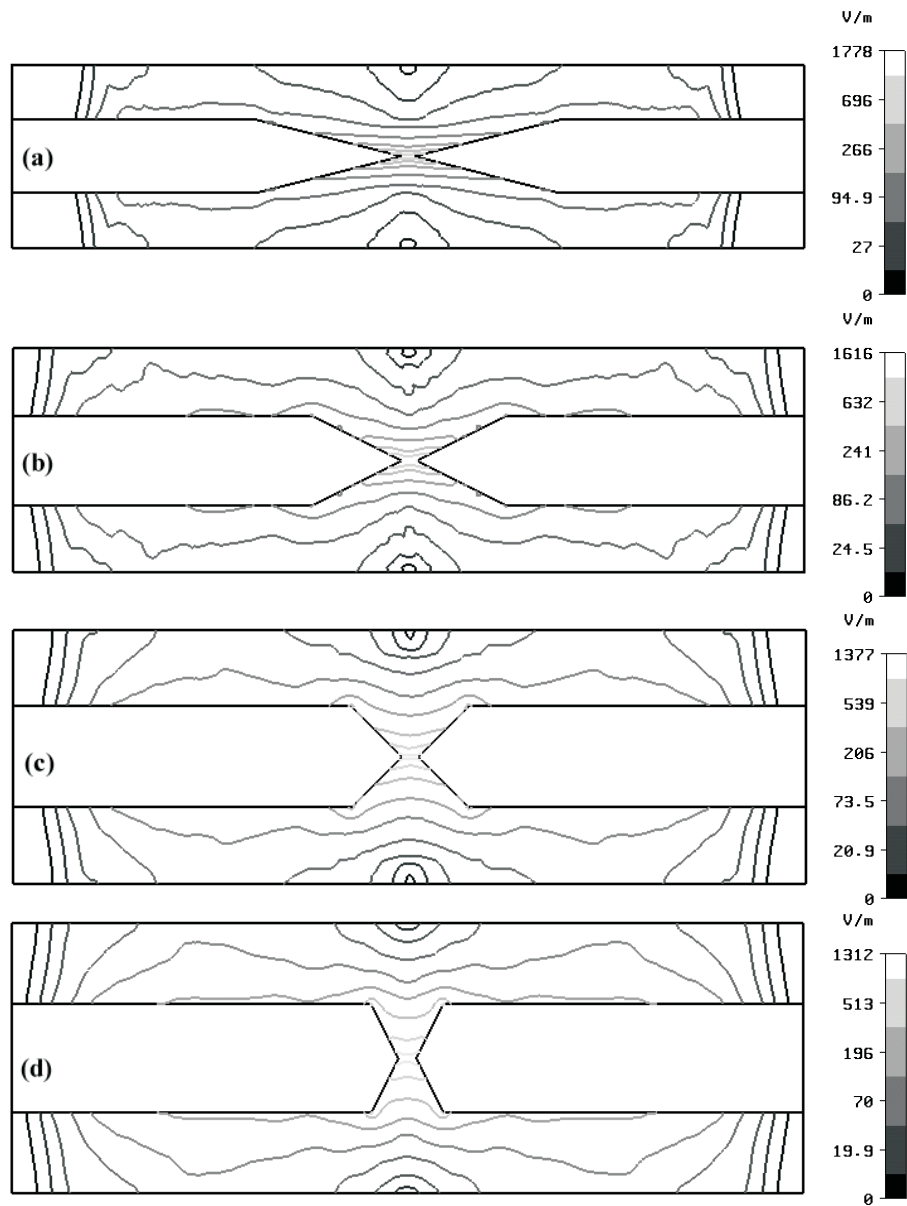
Figure 8.7. *Electric field strength distribution of geometries with different sharpnesses of the inner conductor, just before the field reaches the output.*
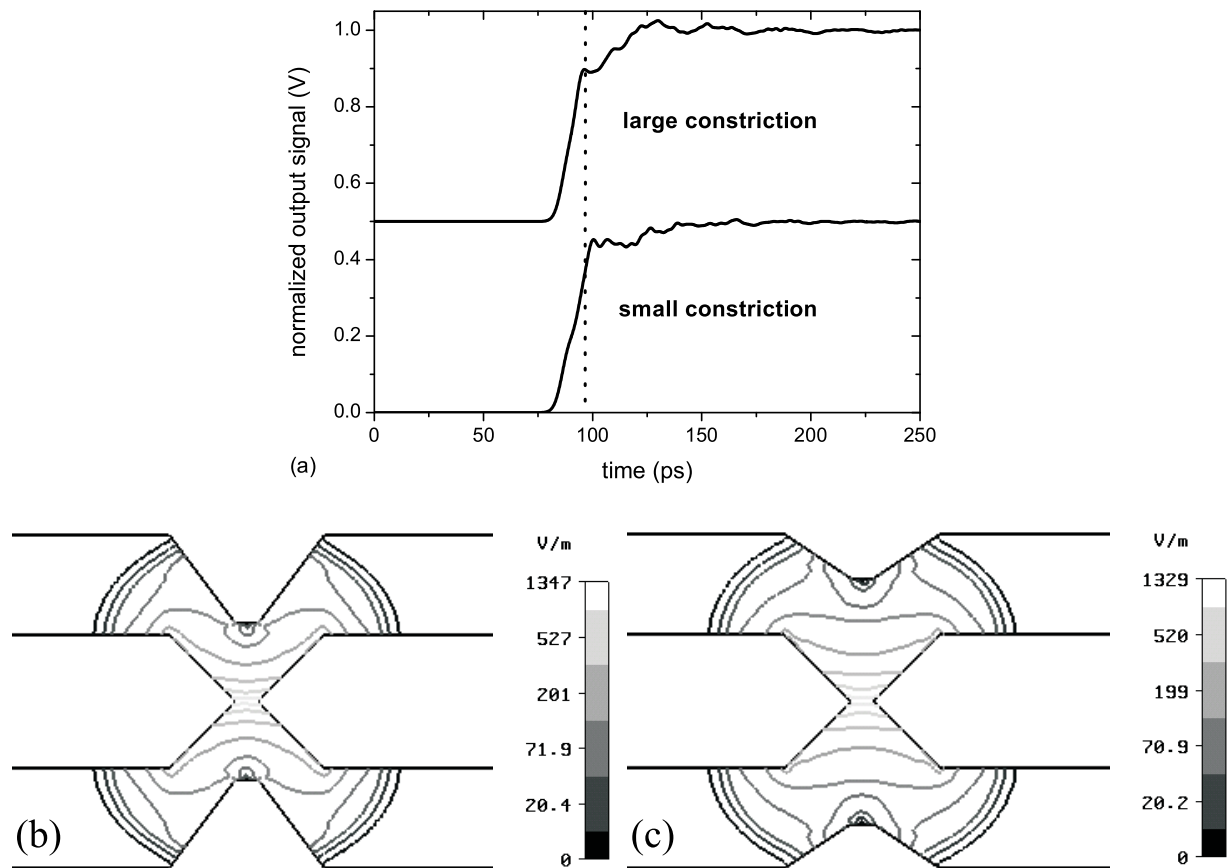
Figure 8.8. *TEM output signals (a) and electric-field strength distributions (at t=30 ps) (b, c) of two spark gaps with different constriction radii.*

By changing the constriction radius, the time when the reflection occurs at the outer conductor can be varied. A large constriction results in an earlier reflection of the initial field at the outer conductor and thus an earlier damping of the signal. A small constriction lets the damping occur somewhat later. This way slight over and under-damped configurations can be influenced such that the output signal becomes more "ideal".

We found that the influence of the shape of the inner conductor is the most significant factor for getting the desired output signal. The constriction of the outer conductor can be used only for fine-tuning of the output signal. No rise time enhancement takes place at larger constriction radii, although this was predicted by lumped element theory. This is because the rise time is determined only by the time it takes to build up a stable TEM-mode in the gap region. This build up time is not affected by the constriction but is

determined by the position of the outer conductor in the region where the TEM-mode will start to propagate.

8.4.2   The ideal spark gap configuration

We showed that by choosing the correct inner and outer conductor geometry it is possible to get a spark gap configuration that produces nice square-shaped output pulses with minimal oscillations. However, as mentioned, a practical geometry can not have sharp edges. Sharp edges can result in field enhancement regions and thus in unwanted, spontaneous breakdown in the setup. To prevent this, round and smooth surfaces have to be used. In figure 8.9 the optimal practical spark gap geometry together with its output signal and electric-field strength distribution is depicted.

The sizes of the different components (in mm) are also included. The output signal is a critically damped signal. No significant overshoot or over-damping is present anymore. Oscillations are minimized and the electric-field strength distribution is comparable to the "ideal signal" distribution of figure 8.4.

8.5   Conclusions

When switching times are no longer dominated by the plasma formation time, such as for photoconductive switching, electrodynamic details of the switching process determine the rise time and pulse shape of the switched pulse. We used an electrodynamic model to optimize the spark gap geometry for our photoconductively switched high-voltage spark gap, to get an output signal with a sharp rise time and no significant oscillations. The model simulates three-dimensional electromagnetic-field propagation in time and is able to determine the output signal of a switched spark gap. We started the optimization procedure from the literature where, by a lumped element and transmission line approach, a biconical spark gap is suggested to be the most optimal spark gap configuration. We showed that for photoconductive switching time scales (ps) and our dimensions (mm) this is not correct, because it is based on a zero or one-dimensional approach, neglecting important electric field-propagation in three dimensions. The initial electromagnetic-field disturbance in the gap reflects at the outer conductor and interferes with the initial field again. The amount of reflection and interference is essential for the output. We propose an optimization procedure, which consists of two steps:
Vary the sharpness of the inner conductor until the output signal is almost critically damped. The sharpness controls the influence of the reflected field and thus the shape of the output signal. Some over- or under-damping is allowed.
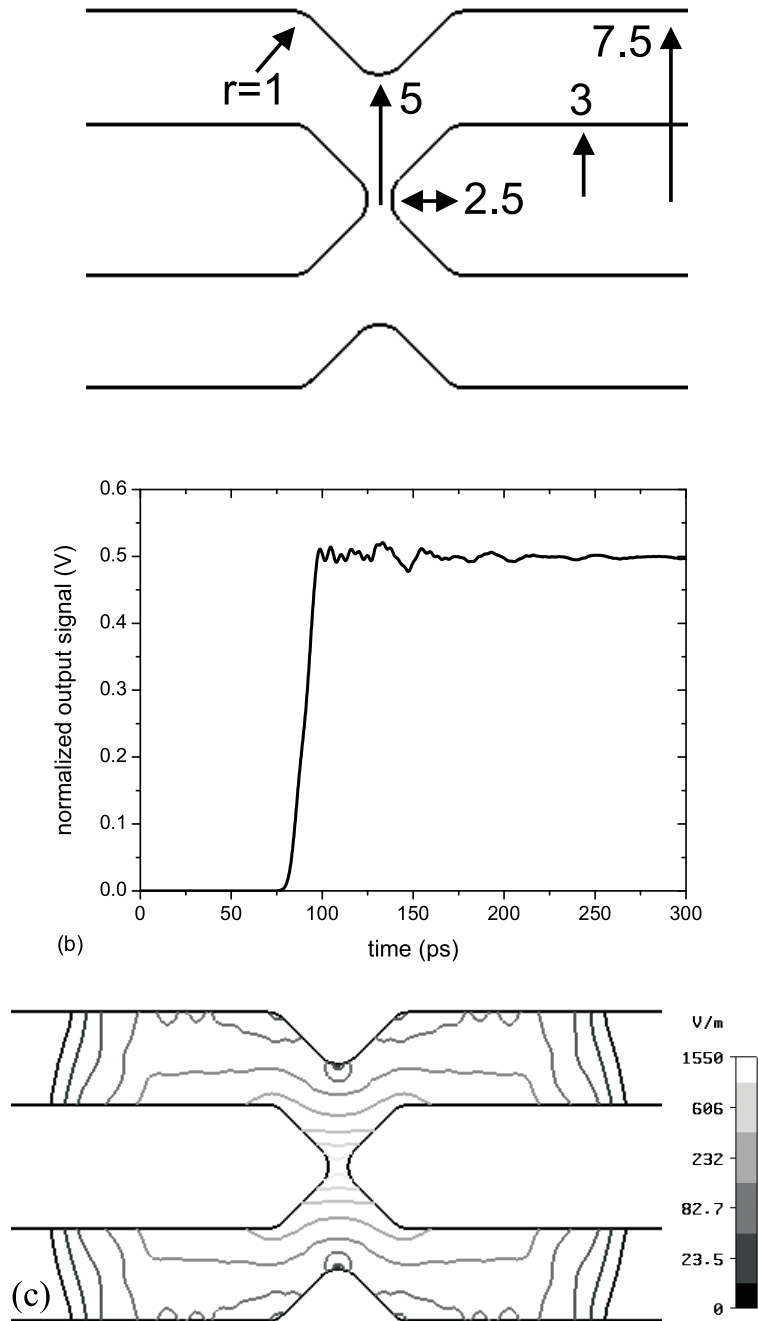
Figure 8.9. *Optimal spark gap configuration with its dimensions (in mm) (a) together with its TEM output signal (b) and the electric field strength distribution at t = 55 ps (c).*

Vary the constriction of the outer conductor. This parameter shifts the moment of reflection at the outer conductor slightly and can be used to fine-tune the signal to a critically damped signal without significant oscillations.

Finally, we proposed an optimal spark gap geometry that gives the best output signal at photoconductive switching.

8.6 Acknowledgments

References

[1] A.H. Guenther and J.R. Bettis, J. Phys. D, 11 (11) p. 1577 (1978)

[2] J.R. Woodworth, P.J. Hargis, Jr., L.C. Pitchford and R.A. Hamil, J. Appl. Phys. 56, 1382 (1984).

[3] L. Ya. Polonskiy, A. Yu. Goltsov and A.V. Morozov, Phys. Plasmas, 3, 2781 (1996)

[4] S. Soubacq, P. Pignolet and S. Mendonca, J. Phys. D, 35, 1955 (2002)

[5] B.M. Luther, L. Furfaro, A. Klix and J.J. Rocca, Appl. Phys. Lett., 79 (20) p. 3248 (2001)

[6] P.F. Williams and A.H. Guenther, Advances in pulsed power technology, vol. 2: Gas discharge closing switches, ed G. Schaefer , M. Kristiansen and A. Guenther (New York: Plenum Press) p. 145 (1990)

[7] W.D. Kimura, M.J. Kushner, E.A. Crawford and S.R. Byron, IEEE Trans. Plasma Sci., 14, 246 (1986)

[8] R. Najafzadeh, E.E. Bergmann and R.J. Emrich, J. Appl. Phys., 62, 2261 (1987)

[9] G.J.H. Brussaard and J. Hendriks, Appl. Phys. Lett., 86, 081503 (2005)

[10] J. Hendriks, B.H.P. Broks, J.J.A.M. van der Mullen and G.J.H. Brussaard, J. Appl. Phys., 98, 043309 (2005)

[11] J. Hendriks, S.B. van der Geer and G.J.H. Brussaard, J. Phys. D: Appl. Phys., 38, 2798 (2005)

[12] CST Microwave Studio Version 5, CST GmbH, Germany (2003)

[13] S. Levinson, E.E. Kunhardt, M. Kristiansen and A.H. Guenther, Proc. 2nd IEEE Pulsed Power Conference, Lubbock, Texas, USA, p. 433 (1979)

[14] J.M. Lehr, C.E. Baum, W.D. Prather and R.J. Torres in ultra-wideband, short pulse electromagnetics 4, E. Heyman, Ed. New York: Kluwer Academic/Plenum Publishers, p. 11. (1999)

[15] J.W. Spears, H. Krompholz and L.L. Hatfield, Proc. 14th IEEE Int. Pulsed Power Conf. (Dallas, TX, 2003) p. 1347 (2003)

Chapter 9

General discussion

9.1 Introduction

The goal of the research described in this thesis was to develop a new type of high-voltage switch which can sharpen high-voltage pulses, with an amplitude in the MV range and a pulse length of the order of ns, to pulses with a rise time as short as (a few) ps and no time jitter. This study was performed to investigate the feasibility of a new type of electron accelerator, a multistage pulsed DC electron accelerator. This accelerator is able to create acceleration gradients which are an order of magnitude higher than conventional RF accelerators. While studying the (experimental) principle of photoconductive switching in gas, we found that existing theoretical models to predict the rise time in laser-triggered spark gaps were no longer sufficient for predicting the switching behavior of our switch. To fill this gap an electrodynamic model was developed to predict the rise time of the photoconductively switched spark gap and to try to optimize the spark gap configuration to get an even better rise time. Finally, feasibility studies were done on two diagnostics. One to monitor the switching-plasma evolution to get a better insight in the switching behavior. The other to be able to resolve the ps rise time of the switched high-voltage pulse.

This concluding chapter links the former chapters. It gives a short overview of the obtained results and while discussing them an outlook is given for future research.

9.2 Conclusions and future research

With our spark gap setup we proved the principle of photoconductive high-voltage switching in air and nitrogen by using a high-power femtosecond laser. We showed a clear transition from laser-triggered switching to photoconductive switching when the laser power is increased. The photoconductive switching regime is characterized by a saturation level where more laser power has no significant influence on the switched pulse anymore. The time jitter dropped dramatically when going from the laser-triggered regime to the photoconductive switching regime. Stochastic breakdown processes that dominate the switching behavior in the triggering regime are passed over at photoconductive switching. Photoconductive switching makes it possible to use the same spark gap to switch voltages as low as 10% of the self-breakdown voltage, whereas laser-triggered spark gaps can only switch voltages down to 80%.

When voltages down to 10% of the self-breakdown voltage were switched, a significant part of the applied voltage was lost over the gap. The observed voltage drop depends on the applied voltage and, therefore, on the current. This means that, next to the laser created plasma, also the current of the pulse to be switched is an important factor for the switching behavior. Two possible causes of the observed voltage drop were investigated, the cathode fall of the switching plasma and the resistance of the plasma. We found that the cathode fall of the switching plasma has no significant influence on the observed voltage drop. The resistance of the switching plasma, however, depends on the current that runs through the plasma while switching. If the current is too low, not enough dissipation takes place in the plasma to lower its resistance significantly. Due to the relatively high net resistance a significant part of the voltage is lost over the gap. This was the case at lower voltages. This also means that we were not able to fully ionize the switching plasma with the laser, because then the resistance of the plasma would be low enough to avoid a measurable voltage drop over the gap at any applied voltage. This was confirmed experimentally with the interferometer. In the current configuration, no plasma was visible which means that the ionization degree is below 10%. From an application point of view, the following conclusions can be drawn. First, a fully ionized plasma is not an absolute requirement for switching a spark gap photoconductively and to create high-voltage pulses with a rise time of 10s of ps and no measurable time jitter. Secondly, voltages down to 10% of the self-breakdown voltage can be switched photoconductively. Thirdly, when the applied voltage is comparable to the voltage range of a laser-triggered spark gap, 80-100% of the self-breakdown voltage, the full applied voltage is switched. At lower voltages (10-80% of the self-breakdown voltage) a part of the applied voltage is lost over the gap, making the switching process less efficient but still possible. Finally, voltages down to 10% of the self-breakdown voltage can only be switched without a significant voltage drop if the

switching plasma is made larger to decrease the resistance of the plasma. This requires more laser power.

It will be interesting to switch with even more laser power. The switching plasma can then be made visible on the interferometer and the evolution of this plasma can be followed with fs resolution. This way, the plasma simulation results can be confirmed experimentally. Also switching at lower applied voltages without significant dissipation will be possible. In order to do all this, the Ti:Sapphire laser system has to be upgraded to the TW-power-level. Then, however, the cylindrical lenses that are used to create the cylindrical switching plasma have almost certainly to be replaced by reflective optics. The power density on these lenses will be so high that the lenses will probably be damaged.

A drawback for widespread application of the photoconductively switched spark gap is the price of a Ti:Sapphire laser system. A TW system costs around one million Euro. Since the invention of chirped pulse amplification in 1985 and the development of the Ti:Sapphire Kerr lens modelocked laser in 1990 [1–3], table-top Ti:Sapphire laser development took a flight. Nowadays, commercial 100 TW systems are available and in several labs PetaWatt (PW) Ti:Sapphire laser systems are being built. Since ("low" power) Ti:Sapphire lasers are used for many purposes, including ultrafast spectroscopy and other analysis techniques, the price of such systems will certainly drop. Also, large facilities like Z at Sandia National Laboratory, NIF at Livermore and large accelerator laboratories either already have a high-power Ti:Sapphire laser system available for other purposes or have budgets in which the cost of such a system is not prohibitive to improve high-voltage synchronization. From this can be concluded that a widespread application of the photoconductively switched spark gap is certainly possible in the near future.

The measured rise time and time jitter of the photoconductively switched pulses were limited by the resolution of the oscilloscope. The shape of the rising edge of the pulse could not be resolved. A feasibility study on electro-optic pulse detection with ps time resolution did not give a positive result. It was not possible to apply this method to our photoconductively switched high-voltage pulses. In order to get an insight in the pulse characteristics we needed a model that was able to simulate the photoconductively switched pulses in the spark gap. Conventional lumped element and transmission line approximation-theories were no longer accurate, because of the extremely short time scales at photoconductive switching. Also geometrical discontinuities could not be taken into account by these conventional models. From a modelling point of view, the benefit of photoconductive switching is that plasma processes take place on a time scale negligible compared to the rise time of the switched pulse and do not have to be taken into account. We developed a three-dimensional model in a commercially available, user-friendly electromagnetic simulation

program (CST Microwave Studio) that does not require any additional programming. Different geometries can be implemented and electric and magnetic field movies give a clear insight in the field evolution. The simulations showed that the rise time of a switched pulse is the time needed for the electromagnetic field to develop into a stable TEM mode in the gap region. This time is determined by the geometry of the gap region, in approximation equal to the time it takes an electromagnetic wave to cover the distance from the center of the gap to the outer conductor. Conventional optimization models for pulse shape enhancement of pulses out of the spark gap are, again, based on lumped element and transmission line theory. These models suggest an optimal spark gap configuration which is not optimal at all for photoconductive switching. Our three-dimensional electrodynamic model has proven its suitability for optimizing the geometry of our photoconductive switch such that switched pulses have a nice rising edge and a flat top without oscillations.

A high-voltage pulse detection system is essential for fully resolving the rise time and time jitter of the switched pulses and to verify the electrodynamic model experimentally. An oscilloscope with sub-ps time resolution is not a realistic option. We showed that the electro-optic measurement setup, which is often used for measuring the length of electron bunches [4], can not be copied straightforwardly into an atmospheric coaxial high-voltage setup. A good alternative could be to build an isolated electro-optic setup or to develop a measurement setup based on the Kerr-effect where an insulating medium is used [5].

9.3   Applicability for electron acceleration

As mentioned in the introduction chapter of this thesis, one of the final purposes for the photoconductive switching project is to build a multistage pulsed DC accelerator. This requires switching of 2 MV, 1 ns high-voltage pulses within a ps. Because we were primarily interested in the principle of photoconductive switching, we only switched easy-to-handle voltages up to 5 kV here. However, the spark gap configuration was designed such that if the gap would be 3 mm, it can sustain a 2 MV, 1 ns pulse without self-breakdown of the gap [6]. Based on the findings in this thesis, we can conclude that photoconductive switching of the 2 MV, 1 ns pulses can be done if additional laser power is available to "fill" a gap which is three times larger than the one investigated here. The necessary laser power would then be approximately 0.6 TW. On the other hand however, spark gap optimization simulations showed that the rise time of the switched pulse is not enhanced, but only the shape of the output pulse. This means that switching 2 MV, 1 ns pulses within a ps is not possible in this setup and therefore the multistage pulsed DC accelerator, as described in [7], can not reach an average acceleration gradient of 1 GV/m. However, photoconductive switching

can still be used for acceleration purposes. A single 2 MV pulsed DC acceleration stage can be coupled onto a conventional RF accelerator as described in [8, 9]. Photoconductive switching of the 2 MV, 1 ns pulse is essential for synchronization with the RF accelerator. In this setup the initial acceleration gradient will be 1 GV/m resulting in high-brightness electron bunches as short as 100 fs.

References

[1] S. Backus, C.G. Durfee III, M.M. Murnane and H.C. Kapteyn, Rev. Sci. Instrum., 69 (3) 1207 (1998)

[2] G.A. Mourou and D. Umstadter, Sci. Am., 286 (5) 80 (2002)

[3] U. Keller, Nature, 424, 831 (2003)

[4] F.B. Kiewiet, PhD thesis Eindhoven University of Technology and references herein, Eindhoven, The Netherlands (2003)

[5] D.A. Vyuga, PhD thesis Eindhoven University of Technology, Eindhoven, The Netherlands (2006)

[6] G.J.H. Brussaard and D.A. Vyuga, IEEE Trans. Plasma Sci., 32 (5) 1993 (2004)

[7] S.B. van der Geer, M.J. de Loos, G.J.H. Brussaard, O.J. Luiten and M.J. van der Wiel, Proc. Eur. Particle Accelerator Conf. Paris, France, June 3-7, 2002, 989 (2002)

[8] F.B. Kiewiet, O.J. Luiten, G.J.H. Brussaard, J.I.M. Botman and M.J. van der Wiel, Proc. Eur. Particle Accelerator Conf. Vienna, Austria, June 26-30, 2000, 1660 (2000)

[9] M.J. de Loos, S.B. van der Geer, F.B. Kiewiet, O.J. Luiten and M.J. van der Wiel, Proc. Eur. Particle Accelerator Conf. Paris, France, June 3-7, 2002, 1831 (2002)

Summary

Photoconductive switching of an atmospheric, air-filled spark gap by a high-power femtosecond laser is a novel approach for switching high voltages into pulses with a very fast rise time (order ps) and almost no shot-to-shot time variation (jitter). Such a switch makes it possible to synchronize high-voltage pulses more accurately than presently possible. The goal of this research was to create ultrafast high-voltage pulses in order to develop a new type of electron accelerator and its diagnostics. An interesting future application of photoconductively switched ultrashort pulses is the creation of broadband, high-intensity terahertz radiation, which is a harmless alternative to X-rays for a number of medical and security purposes.

Photoconductive spark gap switching in air combines the benefits of two fields of high-voltage switching: First, laser-triggered spark gap switching where the switching medium is either gas or liquid and a laser is used to initiate the breakdown of the gap. Secondly, photoconductive switching where the switching medium is a semiconductor device, which is completely illuminated by a short pulsed laser. If a complete (gas-filled) gap is sufficiently ionized by a femtosecond, high-power laser, stochastic breakdown processes (dominating in the laser-triggered switch) no longer determine the actual breakdown-behavior of the gap. The rise time of the photoconductively switched pulse is then determined by the geometry of the gap. The time jitter is limited only by the jitter of the switching laser (as in the semiconductor switch) and, because the switching medium is a gas, high currents can be switched.

The principle of photoconductive switching was demonstrated in air and in nitrogen (*Chapter 3 and 4*). A femtosecond Ti:Sapphire laser was cylindrically focused in a 1 mm spark gap biased at 4.5 kV. When sufficient laser power was used (> 0.1 TW) the spark gap switched photoconductively. The measured rise time and jitter of the switched pulses were both below the resolution of the measurement equipment, i.e., better than 100 ps and 15 ps, respectively. Measurements at lower applied voltages but with the same gap distance showed that it was possible to switch voltages as low as 10% of the self-breakdown voltage. However, a voltage drop over the gap was observed, which became more pronounced

when switching lower voltages. Transient-plasma simulations (*Chapter 6*) explained this behavior by showing that the conductivity of the plasma is a function of the current that runs through the plasma. Together with an interferometric study of the switching plasma (*Chapter 5*), the simulations also revealed that photoconductive switching does not require full ionization of the switching plasma. The voltage drop can be reduced when more laser power is used to create a switching plasma column that has the same initial electron density but a larger diameter.

A three-dimensional electrodynamic model to simulate a photoconductively switched high-voltage spark gap was developed (*Chapter 7*). This model describes and monitors the electromagnetic field-propagation in a coaxial spark gap setup after switching. It reveals also the influence of discontinuities, such as viewing ports, on the pulse shape and the rise time. The rise time is determined by the time it takes for a stable TEM mode to build up in the gap region. Commonly used zero-dimensional lumped element and one-dimensional transmission line models for laser-triggered spark gap optimization are shown to be insufficient for optimizing the geometry of the photoconductive switch, because the electromagnetic field-propagation in three dimensions is neglected. We developed an optimization procedure for spark gap geometries based on our fully three-dimensional electrodynamic simulations (*Chapter 8*).

In conclusion, we proved the principle of photoconductive switching of high voltages in air. The shot-to-shot time stability and the voltage working range of a spark gap are greatly enhanced, compared to conventional laser triggering, and high-voltage pulses with a very fast rise time can be made and modelled. New possibilities for compact pulsed DC electron acceleration are opened up by photoconductive switching, as well as numerous applications in other areas of research.

Samenvatting

Hoogspanning is niet meer weg te denken uit de moderne maatschappij. Het meest bekend zijn waarschijnlijk de hoogspanningsleidingen die via de hoogspanningsmasten het Nederlandse landschap doorkruisen, de bovenleidingen van de spoorwegen en natuurlijk de hoogspanning die ervoor zorgt dat we tv kunnen kijken. Hoogspanning wordt echter op nog veel meer plaatsen gebruikt en zeker in het wetenschappelijk onderzoek heeft het een voorname rol. Een paar voorbeelden hiervan zijn het bliksem-onderzoek dat gedaan wordt met hoogspanning, deeltjesversnellers die op hoogspanning werken en kernfusie-experimenten die niet gedaan zouden kunnen worden zonder hoogspanning.

De bovengenoemde "wetenschappelijke" hoogspanningen zijn allemaal gepulste hoogspanningen. Dit wil zeggen dat er ergens een schakelaar moet zitten die van een gelijk- of wissel-hoogspanning een puls kan maken. De schakelaar die hiervoor nodig is, is niet te vergelijken met de mechanische schakelaar van de verlichting thuis. Zo'n lichtschakelaar is niet geschikt voor het schakelen van hoogspanningen en al zou hij dat zijn, dan zou de schakelaar niet snel genoeg zijn, want vaak zijn snelle hoogspanningspulsen nodig. Er is een grote variatie aan hoogspanningsschakelaars bedacht. We zullen hier beginnen met de "spark gap", ook wel vonk brug genoemd. Een spark gap bestaat uit twee metalen geleiders die gescheiden zijn door lucht of een ander gas (de "gap"). Als nu op een van de geleiders een hoogspanning gezet wordt die hoog genoeg is, dan zal er een vonk ("spark") overspringen van de ene (opgeladen) geleider naar de andere (niet-opgeladen) geleider. Deze vonk is vergelijkbaar met een bliksemflits of een lasboog en wordt een plasma genoemd. Zo'n plasma (een geïoniseerd gas) heeft de eigenschap dat het elektrisch geleidend is. Het zorgt er hier voor dat er een stroom kan gaan lopen van de ene naar de andere geleider. Het plasma ontstaat als volgt: Ergens in de tijd ontstaat er een vrij elektron, veelal door kosmische straling. Dit elektron wordt versneld in het elektrisch veld dat tussen de twee geleiders in de gap staat en wint zo energie. Het elektron zal, na een zekere weg afgelegd te hebben, botsen met een ander deeltje. Als zijn energie hoog genoeg geworden is, dan wordt uit het botsende deeltje ook een elektron weggeslagen en zo blijven er twee elektronen over. Deze worden weer versneld in het elektrisch veld en botsen weer met twee andere deeltjes waarna er dus vier elektronen overblijven. Deze worden weer versneld etc.,

en uiteindelijk ontstaat uit deze lawine van elektronen het plasma tussen de geleiders. Het nadeel van dit plasma-ontstaan-proces is dat het een stochastisch proces is. Bij herhaling zal het plasma niet op precies hetzelfde tijdstip aanwezig zijn tussen de geleiders, maar hier zit een tijdvariatie in (jitter). Om deze jitter te verkleinen moet het plasma proces versneld worden. Dit kan door een laser te gebruiken die in de gap gefocusseerd wordt (laser-getriggerde spark gap). Doordat het laserlicht in het focus zo intens is, worden in de gap in een groter gebied meerdere vrije elektronen gemaakt. Deze vrije elektronen hoeven dus minder nieuwe elektronen vrij te maken voordat het plasma ontstaat. Dit maakt het proces beter tijd-gedefinieerd en de jitter wordt kleiner. Ook kunnen op deze manier spanningen lager dan de doorslag-spanning geschakeld worden. Nadeel is echter dat dit type schakelaar relatief langzame pulsen genereert (stijgtijd in de orde nanoseconde) en dat er toch nog steeds jitter aanwezig is.

Een ander soort schakelaar, de fotogeleidende halfgeleider schakelaar, heeft dit nadeel niet. Deze bestaat wederom uit twee geleiders die nu gescheiden zijn door een stukje halfgeleider materiaal. Door nu met een korte laserpuls dit stukje halfgeleider volledig te belichten, ontstaan in de halfgeleider vrije ladingsdragers die ervoor zorgen dat er vrijwel instantaan een stroom gaat lopen van de ene (opgeladen) geleider naar de andere (niet-opgeladen) geleider. Het voordeel is dat er geen stochastische processen meespelen, dus geen jitter, en dat deze schakelaar heel snel is. Het nadeel is echter dat het halfgeleider materiaal breekt als de stromen die erdoorheen moeten te groot worden. Hierdoor kunnen niet al te hoge spanningen geschakeld worden.

Wij hebben nu een schakelprincipe ontwikkeld dat de voordelen van beide schakelaars combineert. Door een hoogvermogen, femtoseconde laser te gebruiken in een lucht gevulde spark gap en hiermee de hele gap in één keer voldoende te ioniseren worden de stochastische ionisatie-processen overgeslagen en wordt bijna instantaan een plasma gecreëerd. De jitter zal vergelijkbaar zijn met die van een halfgeleider schakelaar, maar de stromen die geschakeld kunnen worden zullen vergelijkbaar zijn met die van de laser-getriggerde spark gap.

Het principe van fotogeleidend schakelen hebben we gedemonstreerd in zowel atmosferische lucht als stikstof (*Chapter 3 en 4*) door een femtoseconde Ti:Sapphire laser cilindrisch te focusseren in een spark gap van 1 mm waar een spanning van 4.5 kV overheen staat. De gemeten stijgtijd en jitter van de geschakelde pulsen waren beide beter dan de tijdresolutie van de meetapparatuur (100 en 15 picoseconde respectievelijk). Metingen met een lagere spanning maar met dezelfde gap-grootte en laser energie toonden aan dat het mogelijk was spanningen tot 10% van de doorslag-spanning te schakelen. Bij lagere spanningen werd er echter een spanningsval over de gap geconstateerd. Deze spanningsval nam toe naarmate

de geschakelde spanning lager werd. Tijdopgeloste plasma simulaties (*Chapter 6*) lieten zien dat de geleidbaarheid van het schakelplasma afhangt van de spanning (en dus de stroom) van de te schakelen puls. Samen met een interferometer-studie (*Chapter 5*) werd duidelijk dat het schakelplasma niet volledig geïoniseerd hoeft te zijn om fotogeleidend te kunnen schakelen. De spanningsval kan gereduceerd worden door meer laser vermogen te gebruiken om een initieel schakelplasma te maken met dezelfde elektronen dichtheid, maar met een grotere diameter.

We hebben een volledig drie-dimensionaal elektrodynamisch model ontwikkeld om het gedrag van de fotogeleidende, gasgevulde hoogspanningsschakelaar te simuleren (*Chapter 7*). Dit model beschrijft en volgt de elektromagnetische veld uitbreiding in een coaxiale spark gap opstelling. De stijgtijd van de geschakelde puls kan bepaald worden en de invloed van discontinuïteiten, zoals laser-poorten, op de stijgtijd en de vorm van de puls wordt in kaart gebracht. De tijd die nodig is om een stabiele TEM-mode in de gap-regio op te bouwen bepaald de stijdtijd van de geschakelde puls. Voor de optimalisatie van laser-getriggerde schakelaars worden vaak nul- en één-dimensionale "lumped-element" en trans-missielijn modellen gebruikt. Deze blijken niet langer voldoende te zijn om de geometrie van de fotogeleidende gasgevulde hoogspanningsschakelaar te optimaliseren, omdat elektromagnetische veld propagatie in drie dimensies hierin verwaarloosd worden. We hebben, gebaseerd op het drie-dimensionaal elektromagnetisch model, een optimalisatie procedure ontwikkeld voor de geometrie van de fotogeleidende schakelaar (*Chapter 8*).

Uit dit onderzoek kan geconcludeerd worden dat het principe van fotogeleidend schakelen van hoogspanningen in lucht door gebruik van een hoogvermogen femtoseconde laser in een cilindrisch focus werkt. De voordelen van de reeds bestaande fotogeleidende halfgeleider schakelaar en de laser-getriggerde schakelaar zijn in deze nieuwe schakelaar gecombineerd. Zo is de stabiliteit in de tijd tussen verschillende schoten en het voltage-bereik ten opzichte van de laser-getriggerde schakelaar aanzienlijk verbeterd en is het mogelijk om op deze manier hoogspanningspulsen met een hele snelle stijgtijd te genereren. Voor toekomstige toepassingen kan met dit schakelprincipe de synchronisatie tussen verschillende hoogspanningspulsen aanzienlijk worden verbeterd. Met de steile hoogspanningspulsen zou ook breedbandige, hoog-intense Terahertz (THz) straling opgewekt kunnen worden dat een onschadelijk alternatief is voor Röntgen-straling in een aantal medische- en beveiligingstoepassingen. Tevens kunnen elektronen-versnellers nog beter en compacter gemaakt worden door het principe van gepulste DC-hoogspanningsversnelling toe te passen.

Publications

The publications associated with this thesis are:

Papers

- G.J.H. Brussaard and J. Hendriks, Photoconductive switching of a high-voltage spark gap, *Appl. Phys. Lett.* **86** 081503 2005
- J. Hendriks, S.B. van der Geer and G.J.H. Brussaard, Electrodynamic simulations of a photoconductively switched high-voltage spark gap, *J. Phys. D: Appl. Phys.*, **38** 2798 2005
- J. Hendriks, B.H.P. Broks, J.J.A.M. van der Mullen and G.J.H. Brussaard, Experimental investigation of an atmospheric photoconductively switched high-voltage spark gap, *J. Appl. Phys.*, **98** 043309 2005
- J. Hendriks, S.B. van der Geer and G.J.H. Brussaard, Spark gap optimization by electrodynamic simulations, *J. Phys. D: Appl. Phys.*, **39** 274 2006
- B.H.P. Broks, J. Hendriks, W.J.M. Brok, G.J.H. Brussaard and J.J.A.M. van der Mullen, Theoretical investigation of a photoconductively switched high-voltage spark gap, *accepted for publication in J. Appl. Phys.* 2006

Conference proceedings

- J. Hendriks and G.J.H. Brussaard, Picosecond high-voltage switching of a pressurized spark gap, *Proc. 14th IEEE Int. Pulsed Power Conf. (PPC)*, Dallas, Texas, United States, 587-590 (2003) (Oral presentation)
- J. Hendriks and G.J.H. Brussaard, Picosecond high-voltage switching for pulsed DC acceleration, *Proc. 9th Eur. Particle Accelerator. Conf. (EPAC)*, Luzern, Switzerland, 722 (2004) (Poster presentation)
- B.H.P. Broks, J. Hendriks, W.J.M. Brok, G.J.H. Brussaard and J.J.A.M. van der Mullen, Plasma physical model of the photoconductively switched spark gap, *Proc. 27th Int. Conf. on Phenomena in Ionized Gases (ICPIG)*, Eindhoven, The Netherlands, 17-376 (2005) (Poster presentation)

Conference abstracts

- DPG-NNV Spring meeting on plasma physics and short time-scale physics, 24-28 March 2003, Aachen, Germany, Jimi Hendriks and Seth Brussaard, Picosecond high-voltage triggering of a pressurized spark gap (Poster presentation)

- Int. WE-Heraeus Summer School on Low Temperature Plasma Physics: Basics and Applications, 2126 September 2003, Bad Honnef, Germany, Jimi Hendriks and Seth Brussaard, Femtosecond diagnostics of a laser switched high-voltage spark gap (Poster Presentation)

- 16th NNV-CPS Symposium on Plasma Physics and Radiation Technology, 16-17 March 2004, Lunteren, The Netherlands
  - J. Hendriks and G.J.H. Brussaard, Towards picosecond high-voltage switching (Oral presentation)
  - J. Hendriks and G.J.H. Brussaard, Towards picosecond high-voltage switching (Poster presentation, Winner best poster prize)

- Int. Conf. on High Power Particle Beams (BEAMS), 18-23 July 2004, St. Petersburg, Russia, G.J.H. Brussaard, J. Hendriks and M.J. van der Wiel, Picosecond high-voltage switching for multistage DC electron acceleration

- 17th NNV-CPS Symposium on Plasma Physics and Radiation Technology, 1-2 March 2005, Lunteren, The Netherlands
  - J. Hendriks and G.J.H. Brussaard, Photoconductive switching of a high-voltage spark gap (Oral presentation)
  - J. Hendriks, S.B. van der Geer and G.J.H. Brussaard, Electrodynamic simulations of a photoconductively switched high-voltage spark gap (Poster presentation)
  - B.H.P. Broks, W.J.M. Brok, J. Hendriks, G.J.H. Brussaard and J.J.A.M. van der Mullen, Preliminary investigation of a photoconductively switched spark gap plasma

- 32nd IEEE Int. Conf. on Plasma Science (ICOPS), 20-23 June 2005, Monterey, California, United States, J. Hendriks, B.H.P. Broks and G.J.H. Brussaard, Photoconductive switching of a high-voltage spark gap (Poster presentation)

- 8th Euregional WELT PP Workshop on the Exploration of Low Temperature Plasma Physics, 24-25 November 2005, Kerkrade, The Netherlands, B.H.P. Broks, J. Hendriks, W.J.M. Brok, G.J.H. Brussaard and J.J.A.M. van der Mullen, Model of the plasma in a photoconductive switched spark gap

- 18th NNV-CPS Symposium on Plasma Physics and Radiation Technology, 22-23 March 2006, Lunteren, The Netherlands, J. Hendriks and G.J.H. Brussaard, Photoconductive spark gap switch: Pushing the frontiers of high-voltage switching (Poster presentation)

Dankwoord

Dit proefschrift is het resultaat van samenwerking met vele enthousiaste mensen. Ik wil daarom ook graag de laatste pagina's gebruiken om deze mensen te bedanken voor hun bijdrage aan de totstandkoming van dit proefschrift. Allereerst natuurlijk Seth Brussaard. Als directe begeleider heb ik veel van je geleerd over hoog-vermogen lasers, vooral ook omdat je regelmatig zelf in het lab te vinden was. Mede door jouw enthousiasme hebben we de schakelaar toch mooi aan de praat gekregen. Onze discussies waren soms pittig maar zeker nuttig. Bedankt voor het nakijken van al die bergen papier die ik geproduceerd heb. Marnix van der Wiel, mijn 1^e promotor, jouw kijk op zowel de details als het grote geheel waren erg bruikbaar. Ik heb veel geleerd van je input tijdens presentaties. De vrijheid om mijn onderzoek zelf in te richten en conferenties te bezoeken heb ik zeer gewaardeerd.

De volgende mensen wil ik ook zeker bedanken voor hun hulp tijdens mijn promotie:
Bas van der Geer, voor de bruikbare tips over de elektrodynamische simulaties en de discussies over de resultaten hiervan.
Bart Broks, Wouter Brok en Joost van der Mullen voor de fijne, plasma-fysische samenwerking. Bart, door jouw plasma simulaties en uitleg heb ik een goed beeld gekregen van het plasma-fysische gedrag van de schakelaar.
I want to thank the members of my core committee, prof. Blom, prof. Roth, prof. Boller and prof. Ebert for reading my thesis and for their useful suggestions.
Eddy Rietman, Ad Kemper, Harry van Doorn, Wim Kemper, Frits van Hirtum en Eric van der Eerden. Jullie technische ondersteuning was onmisbaar voor dit project.
Traineeship students Willem-Jan van Harskamp and Pawan Tiwari, thank you for your help with the experiments on the FROG and the interferometer.
Guus Pemen, Peter Wouters, Dorota Pawelek en Keping Yan van de Electrical Power Systems groep. Bedankt voor jullie elektrotechnische input.

Speciaal wil ik nog mijn collega's van de groep FTV noemen. Ik heb het erg naar mijn zin gehad in het cyclotrongebouw, de afgelopen vier jaar. De koffie- en lunchpauzes waren erg gezellig. Ik zal de kerstborrels met de eigen wijnproeverij, de groepsuitjes en de etentjes missen. Christian Leewis, Charlotte Kjellander, An Prenen en Ruben Roijers bedankt voor

jullie gezelschap in kamer 2.12.

Als laatste natuurlijk Ingrid, mijn familie en goede vrienden. Dankjewel voor al jullie steun!

Jimi Hendriks
21 maart 2006

Curriculum Vitae

October 14, 1976
Born in Hoensbroek, The Netherlands

1989-1995
Gymnasium at Sintermeerten College Heerlen

1995-2002
M.Sc. in Applied Physics at Eindhoven University of Technology

Traineeship in the group Low Temperature Physics (prof. dr. A.T.A.M. de Waele)
Thermo-acoustic cooler

Traineeship at the Micro Analytical Research Centre (Assoc. prof. D.N. Jamieson PhD), University of Melbourne, Australia
Nuclear microprobe analysis of structure and composition of high temperature superconductors

Graduation project in the group Physics of Surfaces and Interfaces (prof. dr. H.H. Brongersma and dr. R.G. van Welzenis)
Preparation and surface analysis of ScSZ Fuel Cell Electrolyte Material

1997-1998
Treasurer of the student union of Applied Physics SVTN J.D. van der Waals, Eindhoven University of Technology

2002-2006
Ph.D. at the group Physics and Applications of Accelerators of the Department of Applied Physics at Eindhoven University of Technology (prof. dr. M.J. van der Wiel)
The physics of photoconductive spark gap switching: Pushing the frontiers